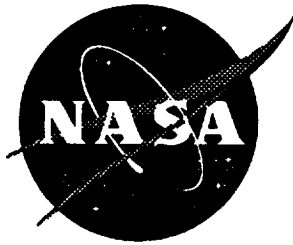NASA Contractor Report 201601

A Method for Landing Gear Modeling and Simulation With Experimental Validation

James N. Daniels
George Washington University
Joint Institute for the Advancement of Flight Sciences
NASA Langley Research Center, Hampton, Virginia

National Aeronautics and
Space Administration
Langley Research Center
Hampton, Virginia 23681-0001

Abstract

An approach for modeling and simulating landing gear systems is presented. Specifically, a nonlinear model of an A-6 Intruder Main Gear is developed, simulated, and validated against static and dynamic test data. This model includes nonlinear effects such as a polytropic gas law, velocity squared damping, a geometry governed model for the discharge coefficients, stick-slip friction effects and a nonlinear tire spring and damping model. An Adams-Moulton predictor corrector was used to integrate the equations of motion until a discontinuity caused by a stick-slip friction model was reached, at which point, a Runga-Kutta routine integrated past the discontinuity and returned the problem solution back to the predictor corrector. Run times of this software are around 2 minutes per 1 second of simulation under dynamic circumstances. To validate the model, engineers at the Aircraft Landing Dynamics facilities at NASA Langley Research Center installed one A-6 main gear on a drop carriage and used a hydraulic shaker table to provide simulated runway inputs to the gear. Model parameters were tuned to match one dynamic case. Other cases were then run with the updated parameters and the results were in excellent agreement with the test data.

Table of Contents

iv

Nomenclature

A_s ....Generic area for one snubber orifice (ft^2)

C_d ....Discharge coefficient of a flow through an orifice

$C_{dS}^{\ C}$ ....Discharge coefficient of a snubber orifice during compression

$C_{dS}^{\ E}$ ....Discharge coefficient of a snubber orifice during extension

C_t ....Tire damping coefficient (lbf*sec/ft)

$C_{1/3}$ ....Redefinition of damping coefficient (lbf*sec^2/ft)

$C_{2/4}$ ....Redefinition of damping coefficient (lbf*sec^2/ft)

D_i, A_i ....Diameter (ft) and area (ft^2) of flow at point (i)

D_L, A_L ....Diameter (ft) and area (ft^2) of lower chamber

d_o, A_o ....Variable diameter (ft) and area (ft^2) of main orifice

D_{op} ....Fixed diameter of orifice plate (ft)

D_{pi} ....Diameter of piston shaft (ft)

D_{pin} ....Variable diameter of the metering pin (ft)

D_R, A_R ....Diameter (ft) and area (ft^2) of rebound (or snubber) chamber

$d_s^{\ C}, A_s^{\ C}$ ....Diameter (ft) and area (ft^2) of one snubber orifice during compression

$d_s^{\ E}, A_s^{\ E}$ ....Diameter (ft) and area (ft^2) of one snubber orifice during extension

D_u, A_u ....Diameter (ft) and area (ft^2) of upper chamber

E_1, E_2, E_3, E_4 ....Redefinition of nonpressure terms in flow equations (ft^8/(sec^2*lbf))

f ....All friction in gear (lbf)

F_i ....External force on body (i) (lbf)

F_{ow} ....Variable friction due to moment created by offset wheel (lbf)

F_{peak} ....Maximum sticking friction between two bodies (lbf)

F_r ....Relative force between bodies one and two (lbf)

f_{seal} ....Constant friction due to seal tightness (lbf)

F_{stick} ....The force to stick the two bodies together (lbf)

F_t ....Force transmitted through tire (lbf)

g ....Gravitational acceleration (ft/sec^2)

K_t ....Tire stiffness (lbf/ft)

$K_{1/3}$ ....Redefinition of spring stiffness term (lbf*ft$^\gamma$)

$K_{2/4}$ ....Redefinition of spring stiffness term (lbf*ft$^\gamma$)

L ....Lift function on wing (lbf)

ma ....Moment arm of tire force acting on piston (ft)

M_i ....Mass of body (i) (slug)

M_L ....Piston Mass and Wheel/Tire Mass (slug)

M_o ....Moments about point O (lbf*ft)

M_u ....Portion of Airplane Mass and Cylinder Mass (slug)

N ....Normal reactant force of cylinder wall on side of piston head (lbf)

P ....Pressure of a fluid at a point (psi)

P_i ....Pressure at point (i) in a fluid (psi)

P_L ....Hydraulic pressure in lower chamber (psi)

P_s ....Hydraulic pressure in snubber chamber (psi)

P_{si} ....Pressure to which upper chamber is initially charged (psi)

P_u ....Pneumatic pressure in upper chamber (psi)

Q ....Volumetric flow rate of a fluid (ft^3/sec)

Q_{ideal} ....Ideal flow through an orifice (ft^3/sec)

Q_o ....Flow through the main orifice (ft^3/sec)

Q_{real} ....Real flow through an orifice (ft^3/sec)

Q_s^C ....Flow through a snubber orifice during compression (ft^3/sec)

Q_s^E ....Flow through a snubber orifice during extension (ft^3/sec)

stp ....Minimum separation between bearings when fully extended (ft)

U, $\dot{U}$ ....Input position (ft) and velocity (ft/sec) from ground

V ....Velocity of a fluid at a point (ft/sec)

V_i ....Velocity at point (i) in a fluid (ft/sec)

V_i ....Velocity of body (i) (ft/sec)

V_r ....Relative velocity (ft/sec) between bodies one and two

$\dot{V}_r$ ....Time derivative of relative velocity (ft/sec^2)

W_i ....Momentum of body (i) (slug*ft/sec)

$\dot{W}_i$ ....Time derivative of momentum of body (i) (lbf)

X_a, $\dot{X}_a$, $\ddot{X}_a$ ....Wheel axle position (ft), velocity (ft/sec), and acceleration (ft/sec^2)

X_s ....Stroke remaining in strut (ft)

$\dot{X}_s$ ....Stroking rate (ft/sec)

X_{si} ....Stroke position at which upper chamber is charged (ft)

X_{smax} ....Fully extended stroke value (ft)

X_{wg}, $\dot{X}_{wg}$, $\ddot{X}_{wg}$ .....Wing/Gear position (ft), velocity (ft/sec), and acceleration (ft/sec^2)

Z ....Height of a point in a fluid from some reference (ft)

Z_i ....Height at point (i) in a fluid (ft)

1/3 ....Subscripts associated with compression

2/4 ....Subscripts associated with extension

Greek Symbols

β ....The ratio of orifice area over flow from area (ft/ft)

δ ....Velocity deadband near zero (ft/sec)

γ ....Polytropic gas constant

μ ....Coefficient of friction between piston head and cylinder wall

ν ....Specific weight of a fluid (slug/(ft*sec^2))

ρ ....Density of a fluid (slug/ft^3)

List of Figures

List of Tables

Chapter 1: Introduction

1.1 Background

In recent years, NASA and many aerospace companies have increased their research focus on the High Speed Civil Transport (HSCT). The concept is to fly a supersonic (mach 2.4) airplane to various places on the globe at an economical price for both carrier and passenger use. Its overall appearance will be similar to that of the Concorde, a current, expensive supersonic carrier.

To make the HSCT more cost effective, much effort is being expended in the design stage. One major problem encountered in its development is the trade-off between structural rigidity and total weight. To this point, the structure of the fuselage and wings has been designed for aerodynamic performance. In the early stages of design, however, landing gear location and dynamic performance are rarely considered. Since the fuselage on the HSCT is very long and slender, it is very sensitive to external, low frequency disturbances, or vibrations. Therefore, a goal of the landing gear design is to reduce disturbance transmission from the ground to the fuselage.

Computer simulations are being developed to study this disturbance transmission problem. The task is to take information concerning gear dynamics, fuselage dynamics, runway profile, and taxi speed, to develop a simulator for predicting aircraft ground response. Simulation of landing gear dynamics has been the subject of much research for many years. The military has long been interested in simulating gear response to repaired, bomb-damaged runways. A great deal of effort has been applied to the problem of determining how well to repair a runway to prevent landing gear failures. This effort did not focus on changing the gear (i.e. to control the force transmission), but rather on changing the runway repair specifications. Active control concepts may render landing gears less sensitive to rough runways, decreasing the time needed to repair damaged runways, and thus allowing quicker response of military missions.

1

1.2 Objective

This document will present an approach for modeling and simulating landing gear systems. Specifically, a nonlinear model of an A-6 Intruder Main Gear is developed, simulated, and validated against test data. This model includes nonlinear effects such as a polytropic gas model, velocity squared damping, a geometry governed model for the discharge coefficients, stick-slip friction effects and a nonlinear tire spring and damping model. To validate the model, engineers at the Aircraft Landing Dynamics Facility at NASA Langley Research Center installed one A-6 main gear on a drop carriage and used a hydraulic shaker table to provide simulated runway inputs to the gear. Model validation used both quasi-static and dynamic tests. In summary, then, this research presents a comprehensive mathematical formulation of landing gear systems, verifies the modeling techniques with tests, and discusses approaches for further model correlation using the test results.

1.3 Literature Survey

Concurrent and past work of this kind have been generally to predict taxi loads of military aircraft over repaired, bomb-damaged runways. This work has led to extensive modeling of military aircraft with the goal of determining minimum repair procedures to runways to prevent gear failure on rollout. One major accomplishment of this research is the HAVE BOUNCE[1] simulation program. Using this program, the USAF has simulated the dynamic response of many military aircraft over bomb damaged runways. These simulations are validated with test data and are used to identify component weaknesses and operational limits. Validation of these simulations is usually achieved through the use of the Aircraft Ground Induced Loads Excitation (AGILE)[2] test facility at Wright-Patterson Air Force Base. Simulations usually combine nonlinear coupled differential equations of the landing gear with linear techniques describing the fuselage structure to generate the total aircraft response. Each of these simulations is usually very good, but each is also very tailored for the plane in question. In addition, the military is concerned mainly with the problem of traversing repaired sections sequentially on a runway. They have, therefore, limited the inputs to their models mainly to the various classes of repairs.

2

Another approach discussed in the literature uses data from tests to determine parameters of a state space model for the landing gear and fuselage[3]. These parameters are included in a quasi-linear formulation through look-up tables. Depending on the exact form of the model and the measurement capability, the results of this type of formulation are fair to good in comparison to actual test data. This approach is good when test data is easily accessible for parameter determination, and simulation computation time is limited. Freymann[4] revisited an experiment by Ross and Edson[5] in which an actively controlled servovalve is connected to a landing gear to augment damping in the system. Ross and Edson[5] described an electronic controller and an actively controlled landing gear which was found to significantly reduce forces sustained by an aircraft during takeoff, landing impact and rollout. The results were obtained analytically through the use of a linearized model of the equations of motion and confirmed experimentally. The servo-controller was designed to maintain a certain command force level by porting flow into and out of the landing gear. This approach to active control, however, is very expensive in terms of weight and complexity. There, also, was no recourse developed in case of servo failure. Their model included a linear tire spring, no tire damping, no metering pin and no rebound chamber. However, they did include friction and velocity squared fluid damping. Freymann extended this research by implementing this active control scheme on a fighter aircraft and testing this aircraft's response to various frequency inputs. The control system performed well in attenuating aircraft motions.

Much effort has been exerted by Stirling Dynamics[6,7] in the field of simulation and control. Their main simulation program includes many highly detailed models of the various components of several types of landing gear. The program allows part selection for individual gear types and outputs landing gear dynamic responses in terms of positions, velocities, accelerations and angular equivalents for any part of the gear or fuselage which is selected as a node. Other outputs were subsystem force interactions. Extensive validation has proven this to be a very accurate simulation tool. The complexity of the model generally captured most dynamic effects seen in test data. This same program was used to test an active orifice concept applied to the nose gear of a typical transport plane. These results showed reduction of peak and root mean square values of normal acceleration, especially in the nose and tail section of the plane. An active orifice mechanism was not detailed, only an assumed behavior. This is a very good program for

3

landing gear design and testing of existing gear configurations. However, a simpler model would allow the physics of the strut, only, to be scrutinized, leading perhaps to a clearer understanding of landing gear behavior.

Research into the behavior of a supersonic carrier during ground operations was performed by C. G. Mitchell[8]. His theoretical analysis and test experience with the Concorde has shown that the supersonic transport is more sensitive to uneven runways than the subsonic transport. Results reported in [8] show that much care must be taken to minimize undercarriage stiffness and friction if problems of cockpit vibrations and airframe and undercarriage fatigue were to be avoided.

Ramamoorthy[9] performed a parameter study on his model of an articulated landing gear and found that changes in the discharge coefficient could alter the results dramatically. No quantitative conclusions were made and no validation of the model was performed. However, Wahi[10] found that the coefficient can alter forces transmitted to the fuselage by as much as 25% and that proper estimation of this parameter needs to be based on both the Reynolds number and orifice geometry. A semi-empirical model developed by Bell, Schlichting, Knudsen et. al. was used for this parameter. With this model for the discharge coefficient, Wahi[10] developed a landing gear model with two degrees of freedom to investigate the optimization of the metering pin shape. The results of this model compared well to flight and drop tests. Optimization of the metering pin, for this particular case, showed some improvement in the force reduction. Once a metering pin shape has been defined, it cannot change. An active orifice concept would allow the damping characteristics of the gear to be continuously changed in reaction to any input to reduce vibration transmission.

An optimization of many strut characteristics was performed by Li, Gou-zhu, and Qing-zhi[11]. This paper described an optimization approach for landing gear design using as design variables the initial pressure, initial air volume, and an artificial oil damping coefficient (which in reality, is a function of the hydraulic and pneumatic areas as well as the discharge coefficient and oil density). The objective function was the mean square value of the fatigue power spectral density. Constraints were in the form of landing impact energy, static compression ratio, maximum compression ratio and limits on the damping coefficient. The results show a significant reduction in the accumulated fatigue on the simulated Boeing 707. What the results fail to show, however, is whether the

upper and lower limits on the damping coefficients are physically achievable. The limits did not include considerations of geometry and realistic discharge coefficient values.

Doyle[12] provides an excellent literature survey on aircraft ground dynamic simulation techniques. His report contains a brief summary of the computer programs written to predict the dynamic displacements and forces resulting from nonflight aircraft operations. The capabilities of each program and their limitations and numerical techniques are cited.

1.4 Research Significance

The significance of the material treated in this research is that it brings together in one place a comprehensive development of the theory of telescoping gear. This document contains the development of the equations of motion and details the more standard practices of expressing them in terms of physically measurable quantities. The model has only two degrees of freedom, both in the vertical direction. In the investigation of loads transmitted into the fuselage, though, this is the most important direction. The model is fully nonlinear and includes such effects as a polytropic gas model, a velocity squared damping term, which includes a discharge coefficient that is a function of orifice geometry, extension damping, stick-slip friction in the gear, and nonlinear tire model. All parameters such as polytropic gas constant, orifice geometry, frictional quantities, etc. appear explicitly in the equations, and can be used in a sensitivity analysis. Also, optimization of gear geometry and initial charge pressures and volumes is easily accomplished using this model. In the end, control concepts can be linked to this model for investigation of force transmission reduction.

This research also treats the subject of numerical integration of the equations of motion. The stiff, nonlinear, and discontinuous behavior of these equations make this a difficult problem to solve numerically, and many considerations were made to make it easier. Also, this document details a series of tests and procedures by which to validate the model. This validation is both static and dynamic. A frequency response method was used to update the parameters in the model and other types of cases to validate the simulation.

1.5 Document Outline

This document is divided into six chapters. After the introduction in Chapter 1, Chapter 2, discusses the theoretical and mathematical development of the equations of motion of a landing gear. Chapter 3 details the method in which these equations were numerically implemented and some of the problems that were encountered. Chapter 4 discusses the equipment used in the experimental validation effort. The next chapter describes the test procedures that were implemented to validate this simulation and some statements about error control. Finally, Chapter 6 will discuss some future research and experimental plans and presents some concluding remarks. Also included, in Appendix A, is the FORTRAN program used to obtain the simulation results shown in this document.

Chapter 2: Problem Formulation

2.1 Initial Landing Gear Investigation

This chapter is intended to familiarize the reader with landing gear terminology and to demonstrate a mathematical development of the equations of motion for a telescoping landing gear. Figure 2-1 is intended to acquaint the reader with basic landing gear components. It shows the simplified components of a telescoping, main landing gear (as opposed to a nose gear).

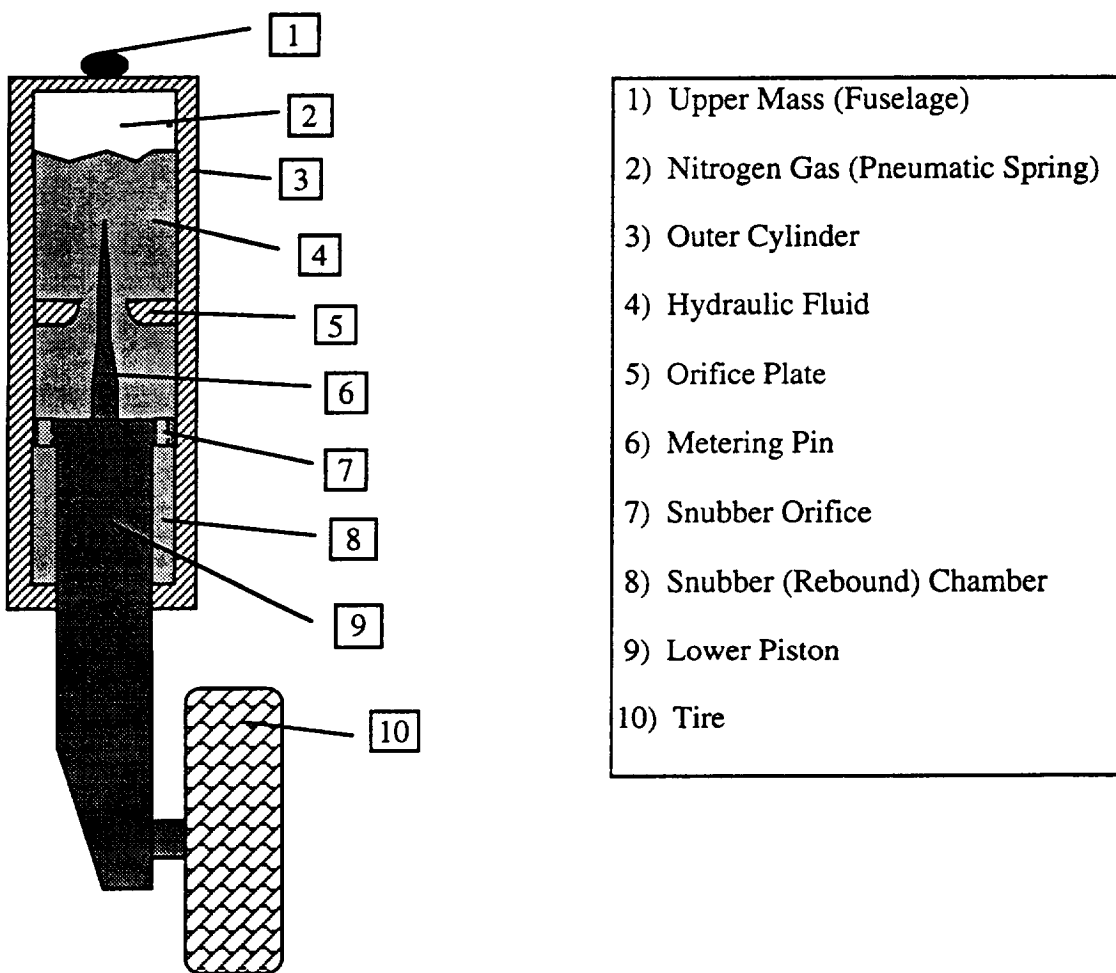|	
1)	Upper Mass (Fuselage)
2)	Nitrogen Gas (Pneumatic Spring)
3)	Outer Cylinder
4)	Hydraulic Fluid
5)	Orifice Plate
6)	Metering Pin
7)	Snubber Orifice
8)	Snubber (Rebound) Chamber
9)	Lower Piston
10)	Tire

Figure 2-1: Schematic of typical telescoping main landing gear.

Point 1 on the figure is a rigid body representation of the aircraft fuselage that the gear carries and is the interface between the plane and the gear. Point 2 is a chamber containing compressed nitrogen which serves as a spring that carries the weight of the plane in ground operations. Point 3 refers to the main, upper cylinder which houses the compressed gas, hydraulic fluid, and within which the piston slides. The hydraulic fluid is represented by the shaded area located by point 4. Point 5 is the orifice plate. It is essentially a circular plate with a hole in the center through which the hydraulic fluid flows when the strut is stroking. It, along with the metering pin, point 6, controls the damping characteristics of the gear. The metering pin is rigidly fixed to the piston head. As the strut strokes, the changing size of the metering pin passes through the constant hole in the orifice plate, causing a variable effective orifice diameter, i.e. variable fluid damping. Nose gear on most planes have no metering pin. Point 7 locates one of many rebound or snubber orifices (usually around 12, depending on the gear). These holes lead into a small volume on the backside of the piston head (point 8) called the rebound or snubber chamber. The purpose of the snubber is to provide damping when the strut extends. The snubber orifices are variable in that they are dependent upon a slip ring that either allows a large orifice in the compression stage or a smaller orifice in the extension stage. Point 9 is the piston. It houses the metering pin and is also the rigid connection of the wheel axle. Finally, point 10 is the tire. This element of the gear adds both spring and damping characteristics to the overall performance of the gear, and is selected carefully for various applications.

A study by Ross and Edson[5] of Hydraulic Research provided the initial information for this research. They developed nonlinear equations for a simplified telescoping landing gear. They then linearized the equations about the ground equilibrium point and studied the effect of an active damping control scheme. The model they developed did not include a metering pin or a rebound chamber. However, their model included a servovalve to port fluid from one chamber (upper or lower) to the other to control the gear damping response, precluding the usefulness of the snubber or metering pin. This method of control requires high hydraulic pressures and large pumps and plumbing to accomplish the task, making it difficult to implement. The report, however, did conclude that active control gear can reduce the ground loads transmitted to the fuselage. Their simulation was validated using experimental equipment and facilities of

Hydraulic Research. The linearized model did not allow explicit investigation of orifice diameters and other parameters critical in understanding the landing gear's dynamic behavior. But, these studies were considered investigative in nature and led to a more complete understanding of some of the complex dynamics of landing gear.

2.2 Nonlinear Model Development

To extend the work by Ross and Edson[5], this research discusses an independent development of a mathematical model of a main landing gear with all the relevant physical parameters included. The nonlinear equations of motion are developed for a telescoping main gear. The analytical model used is a representation of an A-6 Intruder main gear. This gear was chosen because facilities exist to test and characterize an A-6 gear for simulation validation. Specific details of the gear were taken from the technical drawings supplied by the Grumman Company.

An initial model was developed that only included the air-spring above the fluid, fluid dynamics through a fixed orifice, and a linear tire spring term. This simple model allowed some trend comparison between the results of this model and the early results of the linearized gear of Edson and Ross[5]. A metering pin was then added to change the main orifice effective diameter as a function of stroke. Another variation from Edson and Ross was the addition of a snubber, or rebound chamber. This feature provides damping while the gear is extending. Since this new model is to be validated with test data, some attempt to quantify frictional effects was also made. The model includes constant seal friction as well as a variable friction that is a function of stroke. In a further effort to be realistic, a nonlinear tire model was added. This tire model has a spring rate that is a function of tire deflection and damping proportional to compression rate. In the equations developed below, the spring and damping coefficient are used as if they were constant. The nonlinear characteristics of each of these terms is included in the equations of motion that are actually integrated.

Figure 2-2 is a schematic of the gear used in the development of the equations of motion. This schematic is representative of a general telescoping-type main landing gear. It includes the aerodynamic lift on the plane, Lift, the upper mass (of the plane's fuselage) and the mass of the main cylinder lumped together as a rigid mass, M_u and the mass of the piston and the mass of the tire, also lumped together as M_L. The inertial coordinate of

9

the upper mass is X_{wg}. The zero value for X_{wg} is when the gear is fully extended with the tire just touching the ground. From this same gear configuration, X_a, the coordinate of the lower mass, is taken as zero at the axle of the tire. Therefore, when the gear is in some compressed state, X_a measures the deflection of the tire when the ground input, U(t), is zero. In the compressed nitrogen chamber (upper cylinder) with cross sectional area of A_u, the pressure is P_u. Likewise, in the lower chamber with cross sectional area of A_L, there is a pressure of P_L. In the snubber chamber, with annulus area of A_R, the pressure is defined to be P_s. The orifice plate has a hole of diameter D_{op} through which the metering pin, with variable diameter D_{pin} moves. Fluid reaches the snubber chamber through the orifices d_S^C and d_S^E, where the superscripts represent either the compression mode or extension mode respectively. The diameter of the piston, D_{pi}, is used to calculate A_R. Simply subtract the area of the piston shaft from that of the lower cylinder to get A_R. The tire is also shown in Figure 2-2 with a distinction of pointing out that the tire spring and damping coefficients, K_t, and C_t are nonlinear and contribute to the calculation of the tire force F_t.

Lift

Upper Mass/ Cylinder M_u

P_u, A_u

$+X_{wg}$

g

Oil

D_{pin}

D_{op}

Slip Ring Snubber
d_s^C Large
   (Compression)
d_s^E Small
   (Extension)

P_L, A_L

P_s, A_R

K_t, $C_t \Rightarrow F_t$
Nonlinear

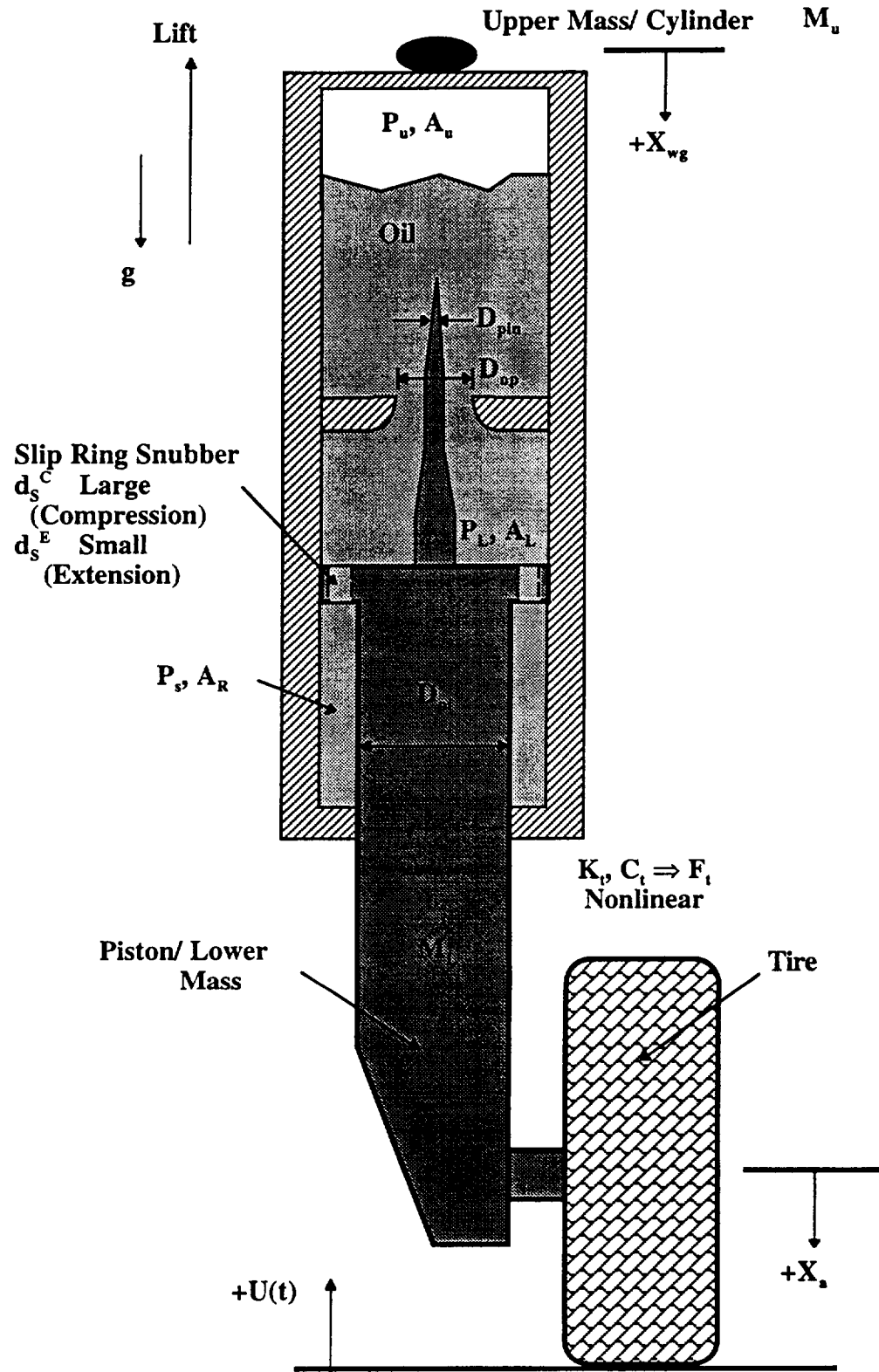Piston/ Lower
Mass

Tire

$+X_a$

$+U(t)$

Figure 2-2: Schematic of a telescoping main landing gear.
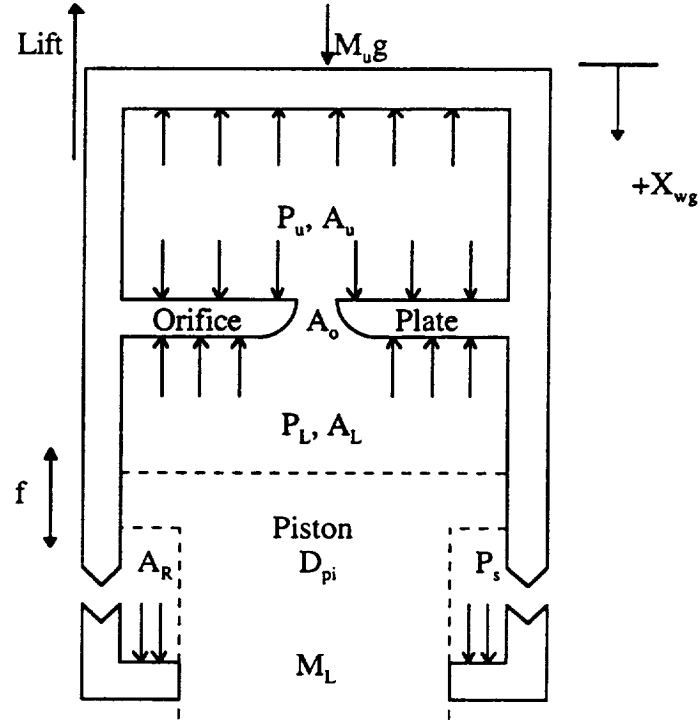
Figure 2-3: Schematic of upper mass and main cylinder

Figure 2-3 shows the forces acting on the upper mass. Balancing the forces on the upper mass gives the following equation:

$$M_u \ddot{X}_{wg} = M_u g - L - P_u A_o - P_L(A_L - A_o) + P_s A_R \mp f \qquad (2.1)$$

The term on the left hand side of Eq. (2.1) is the inertial motion term, g is the gravitational acceleration, f is the friction present in the gear, and all other terms are as described previously. This equation assumes that the fluid pressure in the upper cylinder is identical to the pneumatic pressure. In this development, the variable A_o, the main orifice area, reflects the fact that the metering pin is included, i.e. it is a variable cross-sectional area depending on stroke.
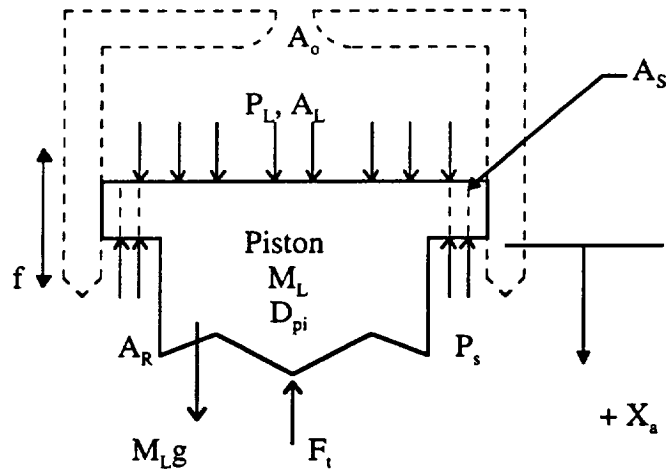
Figure 2-4: Schematic of lower mass.

Figure 2-4 shows the forces acting on the piston. Summing the forces on the lower mass (piston) the force balance equation is:

$$M_t \ddot{X}_a = M_t g + P_L (A_L - A_S) - P_s (A_R - A_S) - F_t \pm f \tag{2.2}$$

where the left hand side of Eq. (2.2) is the inertial motion of the lower mass and A_s is the area of the snubber orifice. F_t is the force that is transmitted through the tire from the ground and has the form:

$$F_t = K_t (X_a + U) + C_t (\dot{X}_a + \dot{U})$$

where the tire force is a function of a nonlinear tire stiffness and a damping force that is composed of a damping coefficient that is proportional to the tire stiffness and the time rate of change of the tire deflection.

2.3 Relation of Pressures to Stroke Position and Stroke Rate

The pressure terms in Eqs. (2.1) and (2.2) are as yet unknown and need to be related to the positional variables X_{wg} and X_a or their derivatives. The pressure of the compressed nitrogen in the upper cylinder can be described by the polytropic gas law for a closed system as:

$$P_u = P_{si} \left(\frac{X_{si}}{X_{s \, max} - X_s} \right)^{\gamma}$$ (2.3)

where X_s is the stroke *available*, given by:

$$X_s = X_{wg} - X_a$$ (2.4)

with X_{si} as some initial length, P_{si}, the charge pressure at X_{si}, and γ, the polytropic gas constant. X_{smax} is the maximum value to which the gear can be extended. This form of representation of the pressure change is assumed to happen as a quasi-equilibrium process[13]. The significance of the polytropic gas constant is that it describes the type of process that occurs. For example, if $\gamma = 0$, the process would be isobaric, or constant pressure. However, for an ideal gas, $\gamma = 1$, corresponding to an isothermal (constant-temperature) process. If γ is equal to the ratio of the specific heats of a gas, the process is isentropic, or constant entropy. These cases are idealizations of particular processes. In real situations though, the polytropic gas constant is not constant at all and is usually calculated from pressure-stroke data. An average value is usually sufficient in application.

Equation (2.3) was defined in such a manner that P_u will become very large when X_s is near X_{smax}, i.e. the gear is nearly completely collapsed. This is a suitable representation of the process, with only the polytropic gas constant γ as an unknown.

The pressures (P_L and P_s) of the fluid in the lower cylinder and in the snubber are related to the flow rates of the fluid into and out of those regions. The volumetric flow rates through the orifice plate hole, Q_o, and the snubber orifices, Q_S, can be determined by combining the continuity equation and Bernoulli's equation for fluids[14]. Flow is always from the higher pressure to the lower pressure. Bernoulli's equation for an incompressible fluid states that along a streamline[14],

$$P/\upsilon + (1/2g)V^2 + Z = \text{Constant}$$ (2.5)

where P is the pressure at some point, g is the gravitational acceleration, V is the velocity of the flow, υ is the specific weight of the fluid which is equal to the fluid density (ρ) multiplied by the gravitational acceleration (g), and Z is the height difference from some zero reference. This equation assumes that the viscous effects within the fluid are negligible, the flow to be steady and incompressible, and that the equation is applicable along a streamline.

Equating Bernoulli's equation (Eq. (2.5)) at two points in the flow along the same streamline yields:

$$P_1/\upsilon + (1/2g)V_1{}^2 + Z_1 = P_2/\upsilon + (1/2g)V_2{}^2 + Z_2 \qquad (2.6)$$

In the case of a landing gear, the potential distance between Z_1 and Z_2 can be neglected as the distances involved are very small compared to the other terms. Equation (2.6) with the continuity equation for incompressible fluids which states $Q = A_1V_1 = A_2V_2$ allows for the solution of this equation in terms of one of the velocities. Assuming that $P_1 > P_2$, i.e. the flow is from P_1 to P_2, then solve for V_1 from the continuity equation as:

$$V_1 = \frac{D_2^2}{D_1^2} V_2$$

and substitute this velocity into Eq. (2.6) and solve for V_2:

$$V_2 = \pm \sqrt{\frac{2(P_1 - P_2)}{\rho\left(1 - \dfrac{D_2{}^4}{D_1{}^4}\right)}} \qquad (2.7)$$

When the flow reverses, i.e. $P_1 < P_2$, then the velocity at point 2 is described by the above equation with the pressure terms switched and a negative sign on the square root. The ideal volumetric flowrate (Q_{ideal}) for an incompressible fluid can be expressed as $Q_{ideal} = A*V$. In a realistic flow situation though, there is a loss due to the Vena Contracta effect. This loss is empirically quantified by a discharge coefficient (C_d), which represents the percentage of the ideal flow that actually occurs. This coefficient, when multiplied by the ideal flow, yields Q_{real} as:

$$Q_{real} = C_d Q_{ideal} = AC_d V \qquad (2.8)$$

Substituting Eq. (2.7) into Eq. (2.8) for velocity:

$$Q_{real} = AC_d \sqrt{\frac{2}{\rho\left(1 - \left(\dfrac{D_1}{D_2}\right)^4\right)}} \sqrt{P_1 - P_2} \rightarrow P_1 > P_2 \qquad (2.9)$$

For the landing gear shown in Fig. 2-2, there are two flows that are of concern, the flow through the orifice plate and the flow into and out of the snubber chamber. Define $Q_S{}^C$ as the flow rate into the snubber chamber in the compression mode, where the snubber orifice area (A_S) becomes $A_S{}^C$, which allows larger flow. The flow rate through the snubber orifice during the extension mode is defined as $Q_S{}^E$, and the area A_S becomes $A_S{}^E$, which

15

only allows small, restricted flow. In both cases, the flow through the main orifice plate is Q_o.
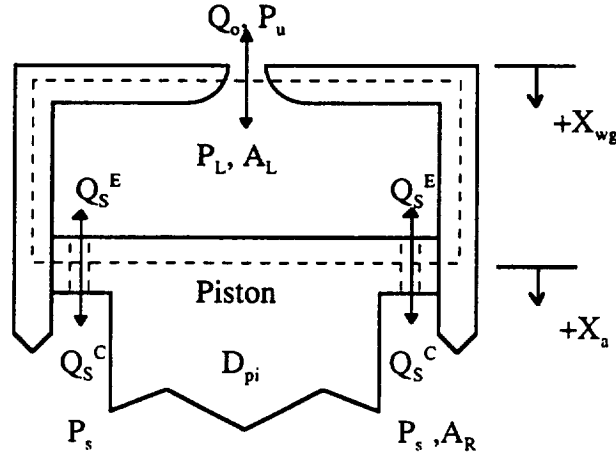

Figure 2-5: Control volume between piston and orifice plate.

Figure 2-5 shows the direction of fluid flow into and out of a control volume in the lower chamber as a function of stroke mode (extension or compression). In relating the flow rates to the pressures, defining a control volume as shown by the dashed line in Figure 2-5 is necessary. The stroke rate is defined as:

$$\dot{X}_s = \dot{X}_{wg} - \dot{X}_a \tag{2.10}$$

where the compression mode is given by $\dot{X}_s > 0.0$, and the extension mode by $\dot{X}_s < 0.0$. The flow is assumed to be negative leaving the control volume, and is positive entering it. For an incompressible fluid, the volumetric flow rates for compression and extension can be written as:

$$Q_o + Q_S^C + A_L \dot{X}_s = 0.0 \tag{2.11}$$

during the compression mode, and:

$$Q_o + Q_S^E + A_L \dot{X}_s = 0.0 \tag{2.12}$$

during the extension mode. Equation (2.9) defined the general form of the equation for a flow rate. Substituting the appropriate pressures, areas, and diameters into Eq. (2.9), the flow rate through the orifice plate during the compression mode (when flow is out of the control volume and $P_L > P_u$ and P_s) can be written as:

16

$$Q_o = -A_o C_d \sqrt{\frac{2}{\rho\left(1-\left(\dfrac{d_o}{D_L}\right)^4\right)}}\sqrt{P_L - P_u} \quad \text{for } P_L > P_u \qquad (2.13)$$

where d_o is the effective diameter of the main orifice, D_L is the diameter of the lower chamber, and C_d is the discharge coefficient of the main orifice. The flow through the snubber orifices during this mode is described by:

$$Q_S^C = -A_S^C C_{dS}^C \sqrt{\frac{2}{\rho\left(1-\left(\dfrac{d_S^C}{D_L}\right)^4\right)}}\sqrt{P_L - P_s} \quad \text{for } P_L > P_s \qquad (2.14)$$

with d_S^C as the diameter of a snubber orifice, D_L as described above, C_{dS}^C is the discharge coefficient of the snubber orifice and A_S^C is the effective area of the snubber orifice. Similarly, for the extension mode, where flow is into the control volume ($P_L < P_u$ and P_s):

$$Q_o = A_o C_d \sqrt{\frac{2}{\rho\left(1-\left(\dfrac{d_o}{D_L}\right)^4\right)}}\sqrt{P_u - P_L} \quad \text{for } P_u > P_L \qquad (2.15)$$

where the difference between this equation and Eq. (2.13) is that the pressure terms have exchanged positions and the whole term is now positive. The flow rate through the snubber orifices during the extension mode is given by:

$$Q_S^E = A_S^E C_{dS}^E \sqrt{\frac{2}{\rho\left(1-\left(\dfrac{d_S^E}{D_R}\right)^4\right)}}\sqrt{P_s - P_L} \quad \text{for } P_s > P_L \qquad (2.16)$$

where D_R is the effective diameter of the annulus snubber chamber, d_S^E is the diameter of a snubber orifice, A_S^E is the effective area of the snubber orifices and C_{dS}^E is the discharge coefficient of the snubber orifices in the extension mode. To simplify Eqs. (2.13), (2.14), (2.15), and (2.16), let the non-pressure terms be redefined as:

$$E_1 = A_o C_d \sqrt{\dfrac{2}{\rho\left(1-\left(\dfrac{d_o}{D_L}\right)^4\right)}},$$

$$E_2 = A_S^C C_{ds}^C \sqrt{\dfrac{2}{\rho\left(1-\left(\dfrac{d_S^C}{D_L}\right)^4\right)}},$$

$$E_3 = E_1,$$

$$E_4 = A_S^E C_{ds}^E \sqrt{\dfrac{2}{\rho\left(1-\left(\dfrac{d_S^E}{D_R}\right)^4\right)}}$$

respectively. Substituting Eqs. (2.13) and (2.14) into Eq. (2.11) and Eqs. (2.15) and (2.16) into Eq. (2.12) using this new notation, rewrite Eqs. (2.11) and (2.12) as:

$$-E_1\sqrt{P_L - P_u} - E_2\sqrt{P_L - P_s} + A_L \dot{X}_s = 0.0 \quad \text{for } \dot{X}_s > 0.0 \tag{2.11a}$$

$$E_3\sqrt{P_u - P_L} + E_4\sqrt{P_s - P_L} + A_L \dot{X}_s = 0.0 \quad \text{for } \dot{X}_s < 0.0 \tag{2.12a}$$
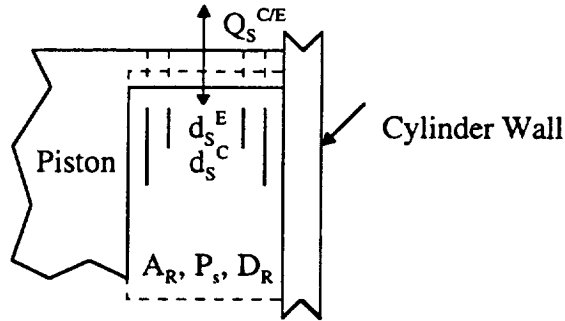
Figure 2-6: Control volume for the snubber chamber.

Additional information about the flow rate-pressure relationship can be gained by studying a control volume in the snubber chamber as shown by the dashed line in Figure 2-6. The variables A_R and D_R in Fig. 2-6 are the rebound chamber annulus area and

18

effective diameter respectively. P_s is the pressure in the rebound chamber and $d_s{}^C$ and $d_s{}^E$ are the diameters of the snubber orifices in the compression mode and extension mode respectively. In the case of compression, where $\dot{X}_s > 0.0$ and $P_L > P_s$,

$$Q_S^C + A_R \dot{X}_s = 0.0 \qquad (2.17)$$

Substituting the flow rate $Q_S{}^C$ of Eq. (2.14) into Eq. (2.17) yields:

$$-A_S^C C_{ds}^C \sqrt{\dfrac{2}{\rho\left(1-\left(\dfrac{d_S^C}{D_L}\right)^4\right)}} \sqrt{P_L - P_s} + A_R \dot{X}_s = 0.0 \qquad (2.17)$$

From previous notation of E_i, this expression becomes:

$$-E_2\sqrt{P_L - P_s} + A_R \dot{X}_s = 0.0 \qquad (2.18)$$

Rearrange Eq. (2.18) to get an expression for the pressures in terms of the stroke rate as:

$$\sqrt{P_L - P_s} = +\frac{A_R}{E_2}\dot{X}_s \qquad (2.19)$$

Substitute Eq. (2.19) into Eq. (2.11a) and solve for the variable P_L as:

$$P_L = P_u + \left(\frac{A_L - A_R}{E_1}\right)^2 \dot{X}_s{}^2 \qquad (2.20)$$

where P_u is given in Eq. (2.3). Square both sides of Eq. (2.19) and solve for P_s as:

$$P_s = P_L - \left(\frac{A_R}{E_2}\right)^2 \dot{X}_s{}^2 \qquad (2.21)$$

Similarly, for the extension case with $\dot{X}_s < 0.0$:

$$P_L = P_u - \left(\frac{A_L - A_R}{E_3}\right)^2 \dot{X}_s{}^2 \qquad (2.22)$$

$$P_s = P_L + \left(\frac{A_R}{E_4}\right)^2 \dot{X}_s{}^2 \qquad (2.23)$$

These known pressures [Eqs. (2.3), (2.20), (2.21), (2.22), (2.23)] can now be substituted into Eqs. (2.1) and (2.2). Algebraic simplification of these equations leads to the compression and extension cases in terms of readily measurable quantities as:

$$M_u \ddot{X}_{wg} = M_u g - L + (A_R - A_L)P_{si}\left(\frac{X_{si}}{X_s}\right)^\gamma +$$

$$\left\{\left[\left(\frac{A_L - A_R}{E_1}\right)^2 - \left(\frac{A_R}{E_2}\right)^2\right]A_R - \left(\frac{A_L - A_R}{E_1}\right)^2(A_L - A_o)\right\}\dot{X}_s^2 + f \qquad (2.1a)$$

$$M_L \ddot{X}_a = M_L g + (A_L - A_R)P_{si}\left(\frac{X_{si}}{X_s}\right)^\gamma +$$

$$\left\{\left[\left(\frac{A_R}{E_2}\right)^2 - \left(\frac{A_L - A_R}{E_1}\right)^2\right](A_R - A_S^C) + \left(\frac{A_L - A_R}{E_1}\right)^2(A_L - A_S^C)\right\}\dot{X}_s^2 - F_t - f \qquad (2.2a)$$

for the compression case, and:

$$M_u \ddot{X}_{wg} = M_u g - L + (A_R - A_L)P_{si}\left(\frac{X_{si}}{X_s}\right)^\gamma +$$

$$\left\{\left(\frac{A_L - A_R}{E_3}\right)^2(A_L - A_o) - \left[\left(\frac{A_L - A_R}{E_3}\right)^2 - \left(\frac{A_R}{E_4}\right)^2\right]A_R\right\}\dot{X}_s^2 - f \qquad (2.1b)$$

$$M_L \ddot{X}_a = M_L g + (A_L - A_R)P_{si}\left(\frac{X_{si}}{X_s}\right)^\gamma +$$

$$\left\{\left[\left(\frac{A_L - A_R}{E_3}\right)^2 - \left(\frac{A_R}{E_4}\right)^2\right](A_R - A_S^E) - \left(\frac{A_L - A_R}{E_3}\right)^2(A_L - A_S^E)\right\}\dot{X}_s^2 - F_t + f \qquad (2.2b)$$

for the extension case. Introduce a new notation using subscripts to simplify the above equations: "1" and "2" will be associated with compression (equation set (a)), and "3" and "4" with extension (set (b)). With this change, the equations can be written in the form:

$$M_u \ddot{X}_{wg} = M_u g - L + C_{1/3}\dot{X}_s^2 + K_{1/3}X_s^{-\gamma} \pm f \qquad (2.1c)$$

$$M_L \ddot{X}_a = M_L g + C_{2/4}\dot{X}_s^2 + K_{2/4}X_s^{-\gamma} - F_t \mp f \qquad (2.2c)$$

where the coefficients of the stroke rate squared term are assigned the C_i's, and the coefficients of the stroke position term are the K_i's.

20

The only unknown term left in these equations is friction. As mentioned previously, friction in this gear comes mainly from two sources, friction due to tightness of the seal and friction due to the offset wheel (moment). The seal friction is assumed to be a maximum value statically and some function of velocity in the dynamic state. The functional relationship between frictional force level and velocity could be determined through testing. The friction due to the offset wheel is the result of the moment produced by the nonaxially loaded piston within the cylinder.
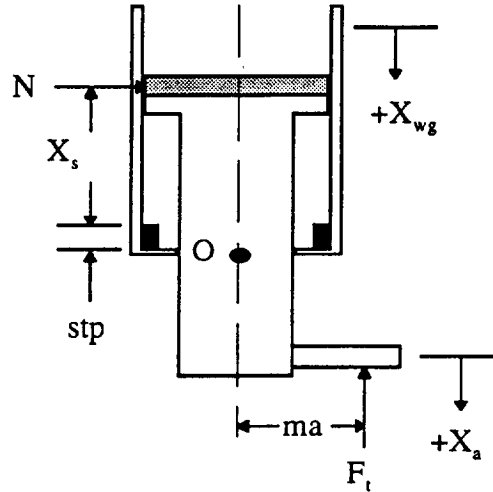
Figure 2-7: Schematic of gear for friction model development.

It can be seen from Figure 2-7 that the force between the piston head and the cylinder, N, is a result of the tire force, F_t, applied at moment arm, ma, from the centerline of the piston. The frictional force due to the offset wheel (F_{ow}) is assumed to be of the form (refer to Figure 2-7):

$$F_{ow} = \mu N \tag{2.24}$$

Where N is the normal force of the cylinder wall resisting the side of the piston head, and μ is the coefficient of friction between the two parts. To find the unknown force N, sum the moments about point O to zero to get:

$$\Sigma M_o : \quad F_t ma - N(X_s + stp) = 0 \tag{2.25}$$

Where stp is the minimum distance between the piston head and the lower seal when the gear is fully extended. Rearrange Eq. (2.25) by isolating N, and then substitute N into Eq. (2.24) to get an explicit form of F_{ow}:

21

$$N = \frac{ma * F_t}{X_{wg} - X_a + stp}$$

$$F_{ow} = \mu \left(\frac{ma * F_t}{X_{wg} - X_a + stp} \right)$$

The total friction in the landing gear, f, in equations (2.1c) and (2.2c) is now assumed to be:

$$f = F_{seal} + F_{ow} \qquad (2.26)$$

This development assumes that a proportionate part of the fuselage (half of the 80% of the total weight that rests upon the main gear) is treated as a lump mass centered at the centerline of the main upper cylinder. Also, this model takes into account only vertical loads on the strut. The tire is modeled as a nonlinear spring and damper. This tire model does not take into account spinning stiffness (because the test tire does not spin) or spin-up drag. The fluid is assumed to be incompressible and all structural members are assumed to be rigid, with each having only a vertical degree of freedom. These assumptions are good only for straight-line taxiing over runway profiles and landing impact (spin-up drag on the tire does not significantly effect the vertical loads on the strut). Any braking or turning maneuvers are not covered in the development. The equations developed here are the basis for a "rollout" simulation.

2.4 Summary

In this chapter, the nonlinear equations of motion were developed for a general, telescoping main landing gear. These equations contain a pneumatic spring that is determined based on the polytropic gas compression law, a hydraulic damping that is proportional to the stroke rate squared, gravitational forces, lift, inputs from a runway, and finally friction, which is composed of both a constant seal friction and a variable bearing friction. These equations explicitly contain the empirical parameters of polytropic gas constant, discharge coefficients for both the main orifice and the snubber orifices, and the friction levels in the gear. These parameters are the only variables that appear in equations (2.1) and (2.2) that cannot be directly measured.

Equations (2.1) and (2.2) are highly nonlinear and are discontinuous due to the differing values of friction and discharge coefficient as a function of extension and compression. Chapter 3 will discuss more about the nature of these equations and present a method of solving these equations for gear displacements and velocities.

Chapter 3: Numerical Analysis

3.1 Introduction

In Chapter 1, a brief history was given in regard to past and concurrent landing gear research. In Chapter 2, the terminology associated with a landing gear was defined and the equations of motion were developed. As seen in Chapter 2, the equations of motion of the landing gear system are nonlinear, due to velocity squared damping, polytropic spring rate, and friction. Many numerical routines exist to integrate nonlinear equations. However, those given by Eqs. (2.1) and (2.2) require some special consideration in that they are nonlinear, and discontinuous due mainly to friction, and under some conditions, stiff. This chapter will discuss the problem of stiff equations and discontinuities. It will detail the process undertaken to numerically integrate these types of equations and present a final scheme that successfully solves the problem.

3.2 Model Integration

The linearized model as presented by Edson and Ross[5] indicated that landing gear systems are stiff. In a system of two or more bodies, one type of "stiffness" in the equations is a result of the difference in time scales of the dynamics between the various bodies, or, in other words, there is at least one body whose solution time scale is much smaller or larger than the others[15]. The problem this causes for a numerical routine is that the time steps attempted must be small enough to accurately track the progress of the short time scale solution. These time steps can be orders of magnitude smaller than the time step required to accurately predict the solution of the other masses. The integration routine is therefore spending a lot of time tracking this fast solution while carrying other, slower solutions along. Most common integration routines are based on forward Euler schemes, known also as explicit integration routines. The problem of taking large time steps with an explicit Euler integration routine, when a fast time scale is present in the solution, is that the total solution may become unstable. However, a different type of routine, called an implicit (or backward) Euler routine, is able to take larger time steps when a fast time scale is present. These implicit routines are what are used to solve stiff equations. The main difference between the two is that the explicit routine uses derivative

information at the previous step to make the next step, whereas the implicit routine uses derivative information at the attempted step to reach that step. This assures that the implicit routine is stable, even for very large time steps, whereas the explicit routine is not.

The equations of motion of the landing gear, as developed in Chapter 2 are numerically stiff. The numerical stiffness in the landing gear case comes from a couple of sources. Part of the stiffness is a consequence of the difference in time scales (about 30 times difference) between the lower mass, which, because of its smaller mass compared to the upper mass, experiences very high accelerations, and the upper mass, which is very large and has much lower accelerations. The other source of numerical stiffness is introduced from the sliding friction model (Eq. 2.26). In the mathematical model, as velocity changes sign, the friction essentially *steps* from one large value to the negative of that value. In the original simulation, this was modeled as a discontinuous process, assigning a negative sign to friction as velocity passed through zero. To allieviate this discontinuity, a hyperbolic tangent was used as a continuous function to cause friction to change sign. It has been specified that the sliding friction will go from one value to the negative of that value in a velocity band around zero of about +/- 1 in/sec. This is a fix to the discontinuity problem, but introduces a new stiffness problem. The rise time of this function is taken to reduce numerical stiffness while maintaining a friction model that approaches reality.

Many numerical routines were investigated in an attempt to solve this problem of stiff differential equations. It was found that a Runga-Kutta routine, with strict tolerances could solve the problem, but the time of solution was unacceptable. After further investigation, it was found that Eqs. (2.1) and (2.2), could be solved much more efficiently with an implicit predictor corrector routine. A predictor corrector routine uses a polynomial based on previous solution points to first extrapolate the solution to the next time step (predictor) and then uses correction iterations to drive the error between the predicted solution and the solution which satisfies the differential equation to within some tolerance[16]. It should be noticed that the predictor corrector routine needs some initial, one-step integration method to accumulate the first few points upon which to build the initial polynomial. For this landing gear case, a modified Adams-Moulton method was used. The routine, DDRIV2.f, was written at the Los Alamos National Laboratory (by

D. Kahaner and C. Sutherland, 9/24/85, available at http://gams.nist.gov/). The routine is designed to solve n first order ordinary differential equations in state space form given the initial conditions. The program also has options to allow the solution of both stiff and non-stiff differential equations, as well as an option to allow a dynamic selection of stiffness. For stiff equations, it uses a fifth order predictor-corrector and for non-stiff equations, it uses a twelfth order predictor-corrector. The routine is very flexible and contains checks to ensure proper usage. This program also has many input parameters that need to be selected with care, depending upon the problem to be solved. These parameters include the maximum time step attempted by the routine, defined by the difference between the initail time and the requested final time (0.00025 is used), a value of the requested relative accuracy in all solution components (1e-6 for this problem), the smallest physically meaningful value for the solution (1e-15), and the mode of stiffness solution (dynamic selection). The parameters in the current simulation have been set to values that seem to most efficiently solve the problem.

As mentioned earlier, the problem at hand is also discontinuous. Two reasons exist for this discontinuity. The first occurs in the damping coefficients, C_i's as presented in Eqs. (2.1c) and (2.2c). The damping coefficient is a function of fluid density, ρ, gear areas and discharge coefficients, C_d's, only. The discharge coefficients are assumed to be functions of orifice geometry (diameter) only. This model assumes that the flow through the orifice will be laminar (below a certain Reynolds number). A representative equation for the discharge equations is given[17] to be:

$$C_d = 0.8\beta^2 - 0.4813\beta + 0.8448$$

In this model, β is the ratio of the orifice diameter over the diameter of the chamber from which the fluid is flowing. This model is for circular holes with rounded edges and was selected as a first approximation to the actual, unknown, discharge coefficient. If the gear is going from an extension to a compression mode, or vice versa, the value of the diameter of the rebound chamber inlets change nearly instantaneously. This is due to a slip ring in the physical gear that responds to the flow of the fluid and either chokes the flow (extension) or slides to a position that allows easier flow (compression). The model of this process is discontinuous. For compression, one value is used, and for extension, another value of discharge coefficient is used. Even though this is a discontinuity, it is a minor one. Since this discontinuity effects the calculation of a fluid damping coefficient

25

that gets multiplied by a velocity squared (see Eqs. (2.1c) and (2.2c)) term, and this discontinuity occurs at zero velocity, the effect of this discontinuity on the solution is small, and no further steps were taken to smooth the transition.

The second discontinuity comes from the event of strut sticking or breaking loose. The event of stiction, or the sticking together of the two parts to move as a rigid body, is modeled in this simulation. The method for implementing stiction friction, as used in the simulation, was developed by Karnopp[18]. This model treats near zero relative velocity stick friction in a manner that does not introduce further numerical stiffness and does not require reformulation of the equations of motion.

3.3 Karnopp Friction Model[18]

This section deals with the manner in which a numerical integrator can handle the task of integrating a model that includes a frictional model that allows sticking. Figure 3-1 shows a two mass system in which W_1, V_1, M_1, F_1 are the momentum, velocity, mass and applied force to the first mass. The same holds for the second mass. F_r and V_r are the relative force and velocity between the two bodies.
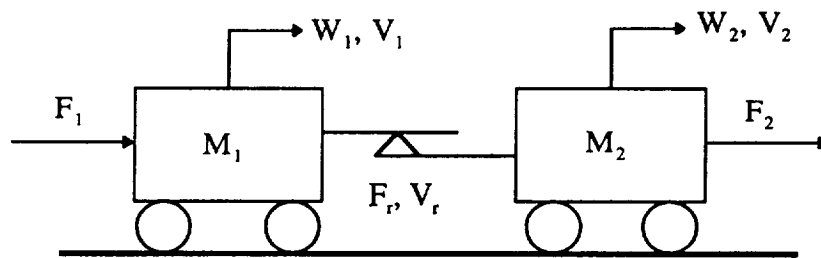

Figure 3-1: Simple two mass system with stick-slip friction.

For this two mass system, take the momentum (W_i) of each mass as the state vectors. The state equations are then given as:

$$\dot{W}_1 = F_1 - F_r \tag{3.1}$$

$$\dot{W}_2 = F_2 + F_r \tag{3.2}$$

and the velocities can be solved from the momentum to be:

26

$$V_1 = \frac{W_1}{M_1} \tag{3.3}$$

$$V_2 = \frac{W_2}{M_2} \tag{3.4}$$

with $V_r = V_1 - V_2$. When the two masses are stuck together there should be no relative velocity. Let $F_r = F_{stick}$, the force required to keep $V_r = 0$. For the two masses to display no relative motion through time, the time derivative of the relative velocity also needs to be zero. This derivative is taken as:

$$\dot{V_r} = \frac{\dot{W_1}}{M_1} - \frac{\dot{W_2}}{M_2} \tag{3.5}$$

Substitute Eqs. (3.1) and (3.2) into Eq. (3.5) to get:

$$\dot{V_r} = \frac{(F_1 - F_r)}{M_1} - \frac{(F_2 + F_r)}{M_2} \tag{3.6}$$

Setting the Eq. (3.6) to zero and solving the resulting expression for F_r, or F_{stick}, gives:

$$F_{stick} = \frac{M_2}{M_1 + M_2} F_1 - \frac{M_1}{M_1 + M_2} F_2 \tag{3.7}$$

The logic of Karnopp's model states that if the absolute value of the relative velocity, $|V_r|$, is smaller than some defined quantity, δ, and if the absolute value of the difference between applied forces, $|F_1 - F_2|$, is less than the peak, sticking frictional force, F_{peak}, then the masses will stick together. Otherwise, slippage occurs and there is relative velocity between the two masses, and friction can be any arbitrary function. For the case of a landing gear, the equations of motion can be cast into a form in which momentum is the state vector as:

$$\dot{W_1} = M_u \ddot{X}_{wg} = M_u g - L + C_1 \dot{X}_s^2 - K_{1/3} X_s^{-\gamma} - F_r \tag{2.1}$$

$$\dot{W_2} = M_l \ddot{X}_a = M_l g + C_2 \dot{X}_s^2 + K_{2/4} X_s^{-\gamma} - F_l + F_r \tag{2.2}$$

where, $F_r = +/- f$. To use Karnopp's model, let:

$$F_1 = M_u g - L + C_1 \dot{X}_s^2 + K_{1/3} X_s^{-\gamma}$$

$$F_2 = M_l g + C_2 \dot{X}_s^2 + K_{2/4} X_s^{-\gamma} - F_l$$

This reassignment allows the Equations (2.1) and (2.2) to be written in the form:

$$\begin{aligned} \dot{W_1} &= F_1 - F_r \\ \dot{W_2} &= F_2 + F_r \end{aligned} ,$$

after which the same logic as above can be applied.

This model uses the relative velocity and the relative force as the decision factors for sticking. If the velocity is very close to zero and the relative force is below a preselected sticking frictional force, then the logic is to assign the frictional force such that the relative acceleration is zero. This implies that the relative velocity remains constant, at some small value, δ, which is unwanted. An addition to this model was to damp out this small velocity. Coulomb damping was used to decrease the remaining velocity to zero after the sticking condition is active. When slipping, the friction can be any arbitrary function.

In considering how to model friction, two other models were also investigated[19]. One was called the "bristle model" in which a number of bristles, or springs, are defined between the two relative surfaces. Each bristle has a stiffness and can be broken after a certain amount of relative force has built up. As some bristles break, others are established. The number of bristles established is a function of velocity. This model will capture the effect of sticking, but is numerically inefficient. The other model is called the "reset integrator model". This model is similar to the bristle model except that there is only a single bond between the relative surfaces. Its advantage is that it also has a mechanism for the frictional energy to damp out when the two bodies are sticking. This model is much more efficient than the bristle model and compares well to the Karnopp model. The Karnopp model was chosen because of its ease of implementation, its realism in capturing the slip-stick phenomenon, and its numerical efficiency.

3.4 Treatment of Discontinuities

For the reasons due mainly to stick-slip friction, the simulation contains discontinuities that need special treatment. The Adams-Moulton integration routine incorporates a system of warnings and errors that allows the user to become aware of some of the problems that the routine is having. One such warning to the user indicates when DDRIV2 is attempting too many iterations, or reductions of time step, to get to the next output time with the specified accuracy. This warning has been used to determine when a discontinuity, either sticking or breaking-free, has been encountered. The predictor-corrector routine is trying to fit the next point of at least a fifth order polynomial to a corner in the solution history (the discontinuity). The calling program has been

28

modified so that when this warning is activated, the main program switches to an error control, variable-step fourth order Runga-Kutta integration routine, RKF4.f (by S. Baudendistel and G. Haigler, 4/1/83, available at http://gams.nist.gov/). This routine is an explicit-type one step integrator and is based on Fehlberg's formulas. This program was used to get past the discontinuity, at which point, the main program directs the predictor corrector to continue the solution. The variable step feature of this R-K routine is useful in error control. When passing the solutions from Adams-Moulton to R-K, and back again, it was found that the error tolerance of each program needs to be near the same order. Numerical errors in the form of instabilities were encountered when different tolerances were used. The solution is unstable for a difference in specified tolerance of three orders of magnitude, i.e. R-K tol. = 1e-3 and A/M tol. = 1e-6. For error tolerances within two orders of magnitude, the over all solution was stable, but there were many areas of local numerical instability. Finally, for R-K tolerances of 1e-5 and A/M tolerances of 1e-6, the solution is well behaved, with only a few numerical problems under stick-slip conditions. It was found that decreasing the R-K or A/M tolerance to 1e-7 was a bad trade off between the time it takes to complete the run and the incremental increase in numerical stability. When the gear breaks loose, the predictor corrector will generally call Runga-Kutta once or twice, depending on how quickly the break-loose is. The faster the break loose, the less it calls R-K. Adams-Moulton seems to have the most problem when the gear goes from a relative motion state to the stuck state. This condition will almost always trigger the R-K. When the gear experiences forces and velocities very near the break-free point, i.e., it is in a continuous state of sticking and slipping, the run times can become longer, as Rung-Kutta does more of the integration. Under the current set of parameters, the run times for a fully dynamic case (no sticking) is about 25 seconds real time per 1 second simulated time. When sticking and slipping are involved, the run times are longer, about 2 minutes real time per 1 second simulated time.

3.5 Summary

In an effort to maintain model fidelity, the equations were left in their nonlinear form rather than linearized. Such considerations as the stiffening effect of sliding friction and the discontinuous behavior of stick-slip friction and discharge coefficients were also factors in this decision. Therefore, numerical routines were found to handle this problem.

A modified Adams-Moulton routine integrates the stiff, nonlinear equations until a discontinuity is encountered, as detected by the routine attempting to reduce the time step too many times without getting to the next step, at which point, a variable step, error control Runga-Kutta integrates past the discontinuity, and then the Adams-Moulton continues the solution. Adjustment of the control parameters to the integration routine has led to a more stable solution as well as reasonable run times. The next task is to verify the model parameters with experimental data. Chapter 4 will detail the facility and equipment used in the tests and Chapter 5 will present experimental results and discuss their significance and usefulness in the validation process of the simulation, as well as present dynamic comparisons between the updated model and test data.

Chapter 4: Experimental Facility

4.1 Introduction

The equations of motion as developed in Chapter 2 are nonlinear, due to the velocity squared damping term and the polytropic gas law assumption, and stiff and discontinuous due to friction. As discussed in Chapter 3, however, a number of numerical integration schemes were evaluated for use in this simulation. The final method uses a predictor corrector and a Runga-Kutta scheme to solve the problem. This chapter describes the experimental facility and equipment used to validate the simulation with experimental data.

The objective of the testing was to determine the physical characteristics of the A-6 gear and to use that information to adjust parameters and/or models in the simulation. Quasi-static tests determined such quantities as masses, maximum static frictional forces, load-stroke curve for the nitrogen spring, and tire load-deflection curve. Dynamic tests were used to find dynamic levels of friction and values of orifice discharge coefficients. Initial tests to validate the simulation software were performed at NASA Langley Research Center. The particular equipment used was an instrumented A-6 main landing gear and a mobile data acquisition system. The gear is mounted on a truss-like drop carriage, which is constrained for vertical motion within a main, translational carriage. The tire of the gear rests on a hydraulic shaker table which is controllable via computer.

4.2 Test Equipment

As stated previously, an A-6 main landing gear was selected for these tests. This gear was chosen for its availability. It and four other main gears were scrapped by the Navy as part of the phasing out of the A-6 Intruder fleet. The landing gears are still in operational condition and were acquired from NAVICP-PHILA, a Naval surplus yard, as a gift toward research. The gear and a GoodYear USA 36X11 Type VII tire inflated to 120 psi was installed on the drop carriage so that it would be in the standard vertical position, as shown if Figure 4-1. A connecting plate was fabricated to allow the normal mounting of the gear to the plate, and the plate was then rigidly connected to the drop carriage. The drop carriage is a truss-structure that weighs about 4.5 tons and allows the

gear to be raised and lowered. The translational carriage weighs about 55 tons and rides on horizontal tracks. It can be moved such that the landing gear tire is over concrete only (for drop tests) or over the shaker table (for some static and many dynamic tests). The mass of the drop carriage rests upon the landing gear. This mass simulates the rigid portion of the aircraft mass carried by the gear. Once the gear is loaded, the shaker table is used to input forces into the gear. Hydraulic lift cylinders, powered by a hydraulic mule, are used to lift the drop carriage and unload the gear. Once the gear has been lifted, the ability exists to lock the gear in that position with hydraulic valves.
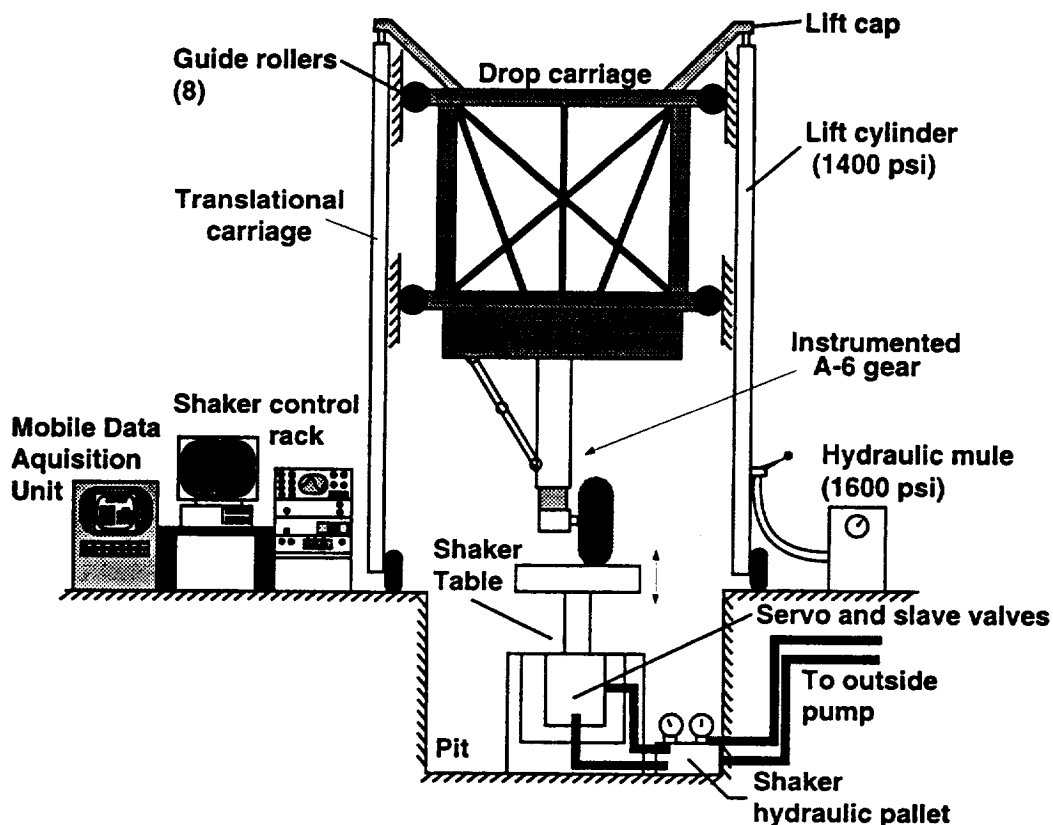
Figure 4-1: Schematic of experimental set-up.

The hydraulic shaker table was built specifically for the task of examining the A-6 landing gear. It was built by TEAM Corporation to the specifications of NASA LaRC. These specifications included the capability to perform a step bump of one inch in no longer than 2 ms while bearing 12,000 lbm. The shaker is also capable of simulating

32

wave functions at user-selected frequencies with amplitudes of about 3.5 inches, at a dynamic force level of at least 10,000 lbf., and for a duration of at least two cycles within no more than a ten second period. The wave functions include: (1-cos), sine, a trapezoidal bump with user-selected rise time, and a saw-tooth wave form. The shaker can also be driven by a file containing runway elevation versus time data and, through positional feedback to the controller, internally adjust the inputs to the shaker to accomplish the input profile. The shaker is also capable of supporting variable static loads of at least 12,000 lbf and allows actuator movement of 6 inches. This shaker package included a digital servo control system that operates from a PC computer. This controller provides for user-selectable displacement, velocity, or acceleration actuation of the shaker head. It is also capable of controlling the shaker to accomplish all of the built-in waveforms and user selected profiles. This software also provides plots to show the user-selected runway profiles/simulations versus the accomplished runway profile/simulation.

The gear was instrumented to provide the necessary information for model validation (see Fig. 4-2). There are two accelerometers, one placed at the upper mass and the second one at the lower mass. Two potentiometers are also used, one to locate the upper mass with respect to a fixed position on the translational carriage and one to measure the relative position between the upper and lower masses of the gear. Two pressure transducers are included in the instrumentation as a check of some of the basic assumptions of the simulation (mainly that the fluid and the gas do not mix to any significant degree after initial shaking). One is located just outside the charge port of the upper cylinder, and the other is embedded in the piston head. Finally, there is a strain gage on the wheel axle of the gear. This gage is calibrated to read the vertical load through the strut and the bending moments induced by the tire.

Table 4-1 shows the instrument sensitivity and other detailed sensory information. These instruments were selected to allow direct comparisons to the simulation results developed from the equations of motion obtained in Chapter 2.
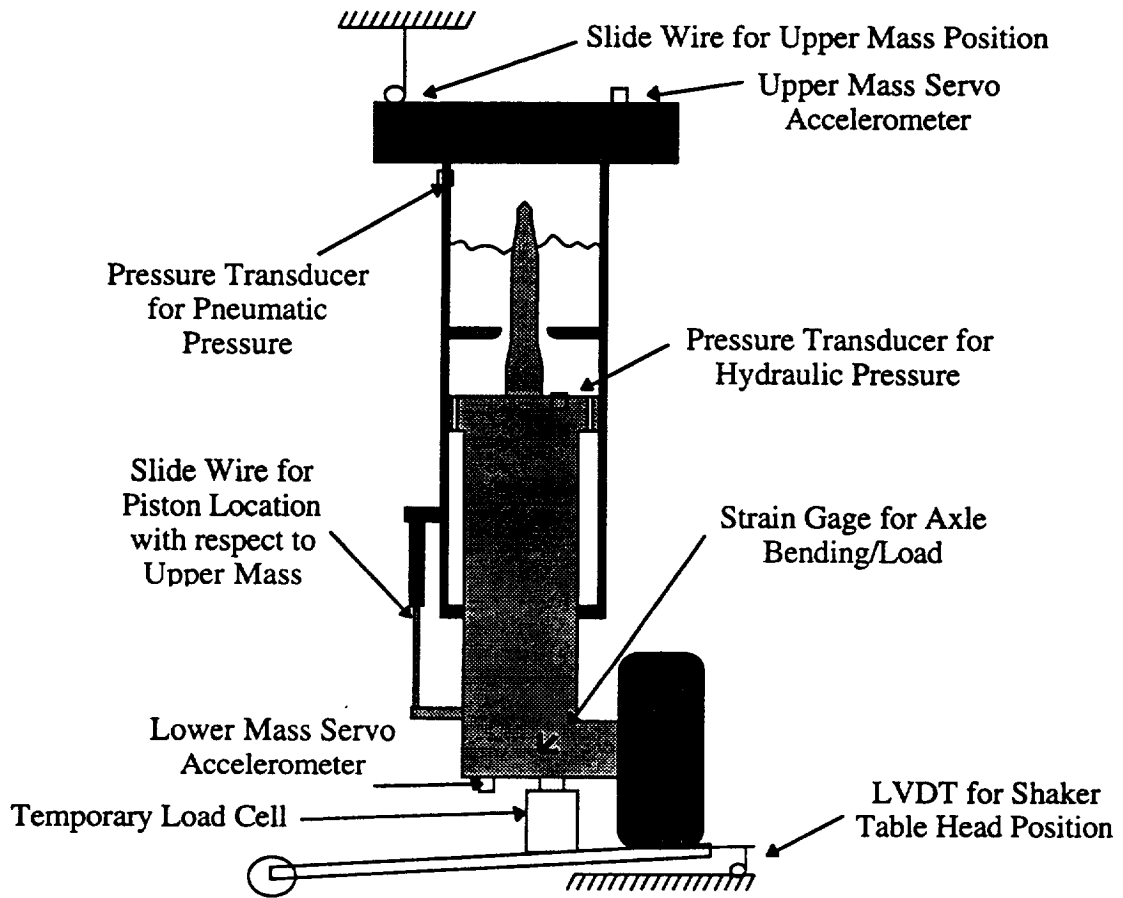
33

Figure 4-2: Instrumented A-6 landing gear.

NAME	Type	Range	Offset	Sensitivity
***	***	***	Co	C1
Upper Mass Position	Slide Pot Wire, TCC	40 in.	28 in	-10.48 in/volt
Strut Piston Position	Slide Pot, Bourns	16 in.	-1.94 in	4.04 in/volt
Lower Chamber Press.	Pressure Transducer, Kulite	2 ksi.	-115.4 psi	865.75 psi/volt
Upper Chamber Press.	Pressure Transducer, Kulite	2 ksi.	-92.7 psi	834.80 psi/volt
Upper Mass Accel.	Accelerometer, Kistler	(+/-) 12 g's	0	2.41 g/volt
Lower Mass Accel.	Accelerometer, Kistler	(+/-) 12 g's	0	2.40 g/volt
Axle Load (bending)	Wire Strain Gage, MMT	162.2 klbs.	1050 lb	6488.0 lb/mvolt
Temp. Load Cell	BLH 20 klbs	20 klbs.	16 lb	3999.20 lb/volt
Shaker Head Position	LVDT, TEAM	(+/-) 3.89 in.	0	0.77 in/volt

Engineering Units (EU) = Co + C1*Voltage Reading

Table 4-1: Instrument guide on A-6 test specimen.

A mobile data acquisition system has been developed to gather, manipulate, plot and store data taken from the tests. This system is a roll-around rack that allows 16 channels (expandable) of input and incorporates a LABVIEW interface. Data from two channels can be plotted in real time. At post test, up to 16 channels can be plotted versus time simultaneously, or any selected channel can be plotted against any other channel. The system has a user defined acquisition rate of between 1 Hz and 3000 Hz and has built-in user selected digital data filters. Finally, this system allows manipulation of the data and will store the data in a Microsoft EXCEL worksheet format.

4.3 Summary

The object of the tests, again, is to determine the physical characteristics of the A-6 test gear and use that information to update the simulation. These tests to validate the simulation software were performed at the Aircraft Landing Dynamics Facility in building 1262 at NASA Langley Research Center. An instrumented A-6 main landing gear is mounted on a truss-like drop carriage, which is constrained to vertical motion within a main, translational carriage. The tire of the gear rests on a hydraulic shaker table which is controllable via computer. A mobile data acquisition system records and manipulates the data incoming from the test set-up. Chapter 5 will explain the procedures of each test and present the results, as well as explain how the results of each test are to be incorporated into the model.

Chapter 5:   A-6   Experimental Parameter Determination

5.1 Introduction

The previous chapters have defined the theoretical basis for modeling the landing gear, the numerical analysis involved in solving the equations of motion, and finally the test equipment used to determine some of the unknown parameters of the model. This chapter is divided into two sections. The first section describes the procedures and results of the tests to determine static values of some parameters like system masses, static frictional levels, pressure-stroke curve, and tire load-deflection curve. The second section describes the procedures for determining dynamic parameters in terms of discharge coefficients and dynamic frictional levels, and tire damping. Adjustments to the statically updated model are made using dynamic data and the final model is compared in frequency space to test data.

5.2 Determination of Static Parameters

The first set of quasi-static tests were designed to define the masses of the system and some static frictional loads. It was recognized early on that there may be external forces acting on the upper mass due to the friction in the bearings of guide rollers on the drop carriage. The first test was designed to measure the total system mass and to measure the frictional level of the bearings. This test was a quasi-static test and was performed as follows. The upper and lower mass were locked together to prevent relative motion and the drop carriage was raised by the lift cylinders until the tire lost contact with the shaker head. A load cell was then placed under the jack lug of the gear, shown in Figure 5-1, and the drop carriage was lowered until the entire mass rested on the load cell. Very slowly, the shaker head was manually raised and lowered for just over one cycle for a total displacement of about six inches. During this time, load cell reading and upper mass position were being recorded. The expected result was a hysteresis loop centered around the weight of the system with the loop defining the positive and negative range of maximum sticking friction in the carriage bearings. The test results are shown in Figure 5-2. The horizontal lines describing the means of friction and weight on the plot were found by first, summing the entire load array and dividing by the number of points, thus

36

getting an estimate of value of the center of the loop (some of the data was repeated as the return stroke overlapped previous distance traveled and so the average is weighted toward the lower bound). Then, the data set was divided along this value into those values higher than the average and those lower. A mean was then found for each of these data arrays, defining the frictional upper and lower limits. These two values were then summed and the average taken to find the average total system weight to be 9465 lbs. Compared to the total weight of the system, the static frictional level of the guide rollers of 117.7 lb. is only 1.25% of the load felt through the gear. Under dynamic conditions, this frictional level will decrease, having an even smaller effect on the dynamics. For this reason, this external force is neglected in the simulation. It's addition would complicate the Karnopp model of friction and add only a very small increase of fidelity.
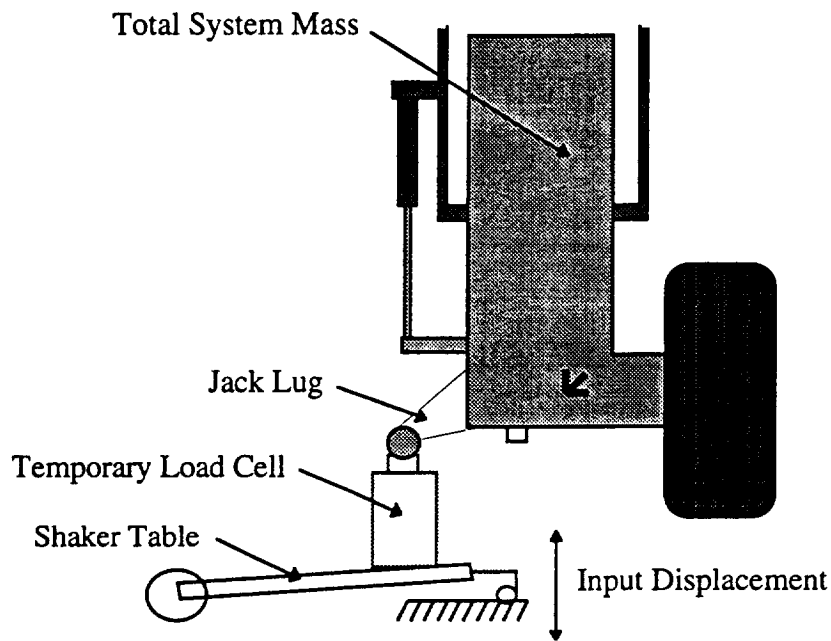

Figure 5-1: Load cell under jack lug to measure system mass and friction.
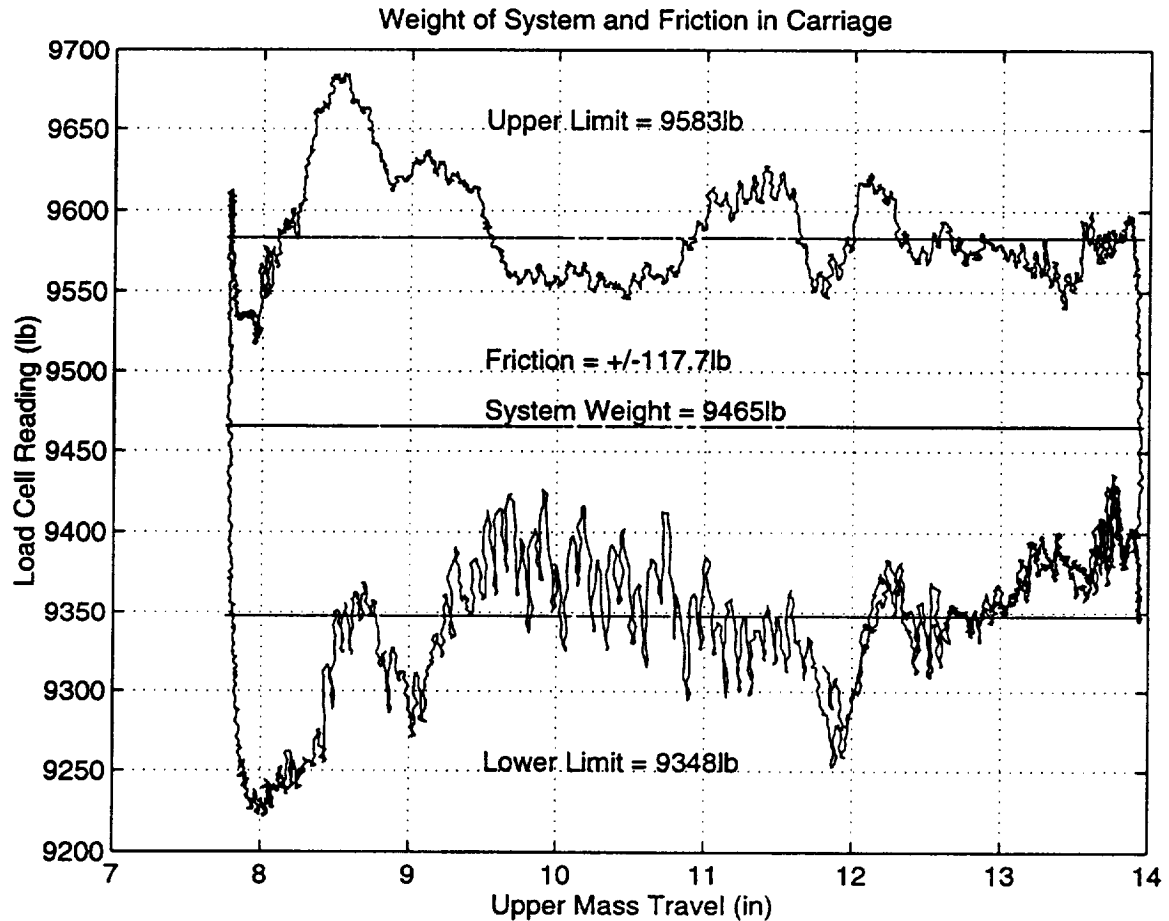
Figure 5-2: Total weight of the system and frictional hysteresis loop.

The next test dealt with finding the mass of the piston, the wheel and tire, and the fluid inside the piston. For this test, the upper chamber was vented to the atmosphere so that the air spring was taken from consideration. The load cell was under the jack lug as in the first test and the gear started from the fully compressed position. The lift cylinders were used to slowly raise the upper mass through about twelve inches of the gear's stroke and returned it to the fully compressed state very slowly. The expected result of this test was another hysteresis loop as found in the first test. However, the center of this loop would be the lower mass weight and the boundaries would be the constant seal static friction. Figure 5-3 displays the test results as measured in the lab, showing the weight to be 318.4 lbs. and a frictional band of +/-115.7 lbs. The lines indicating the mean weight and the mean values of friction were obtained in the same way as in the first test. A check of the test accuracy was also performed. The wheel and piston of one of the

extra gears and a gallon and a half of fluid were measured on a scale. The total lower mass as measured by the scale was 320 lbs. This agrees very well with the data found in the quasi-static test.
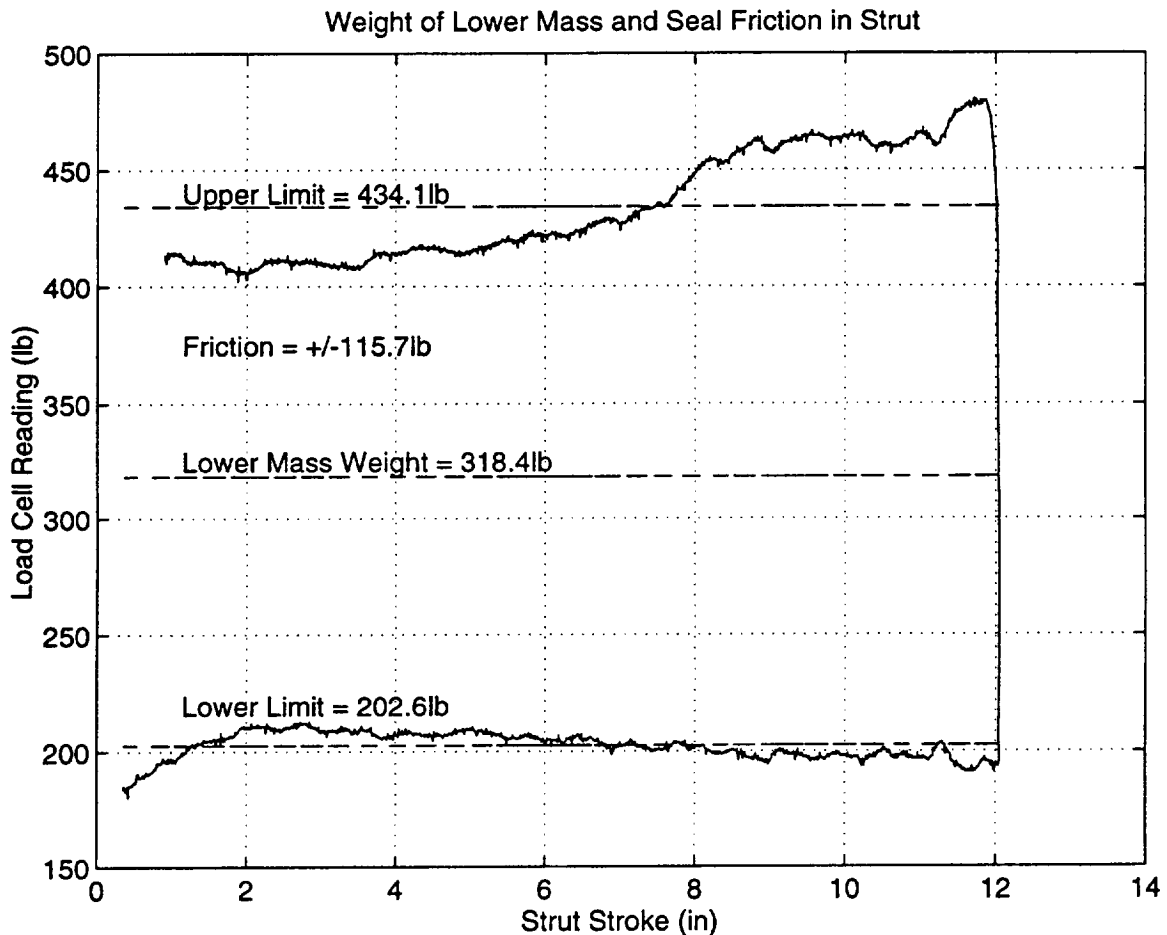
Figure 5-3: Weight of lower mass and frictional hysteresis loop.

The third experiment was also a quasi-static test. The goal of this test was to obtain data concerning the tire load-deflection relationship. The gear was serviced by checking the fluid amount and adding nitrogen to the upper chamber to get a static stroke of about 2 inches above what is desired. The strut was then exercised through vigorous shaking via input from the shaker table. A steady state was reached between the fluid and the compressed gas, i.e. some of the gas volume was lost due to being dissolved into the fluid, and the gear settled to near the desired static stroke. A procedure was developed along these lines to try to predict what charge pressure to inject to a fully extended gear that has not yet been shaken. It was found that if the goal of static stroke was 3.5 inches,

for example, friction could cause the gear to stick at a static stroke value as high as 6.5 inches. With a little shaking, the gear could be settled again to 3.5 inches, indicating that friction will significantly affect procedures in the quasi-static regime. The test started with the gear fully extended and the tire above a platen which rested on the load cell. The lift cylinders were used to slowly lower the gear until it came to equilibrium and then to raise the gear again. As a means to get more data, the drop carriage was locked in position to allow no upper mass displacement and the shaker head was used to further deflect the tire. Two points of data were taken from this test. After some initial deflection, aircraft tire spring behavior becomes essentially linear. The data set found from the continuous test was combined with these two points. A third order polynomial was used to represent the data to capture both the nonlinear behavior at initial compression and the linear behavior around the operating point at 1.6 inches. Figure 5-4 shows the data and the cubic fit.

Fit of Tire Load-Deflection Data

Tire Spring Force (F_{tk})

$$F_{tk} = -252(X_a + U)^3 + 1397(X_a + U)^2 + 4267(X_a + U) + 130$$

Tire Inflation Pressure: 120 psi
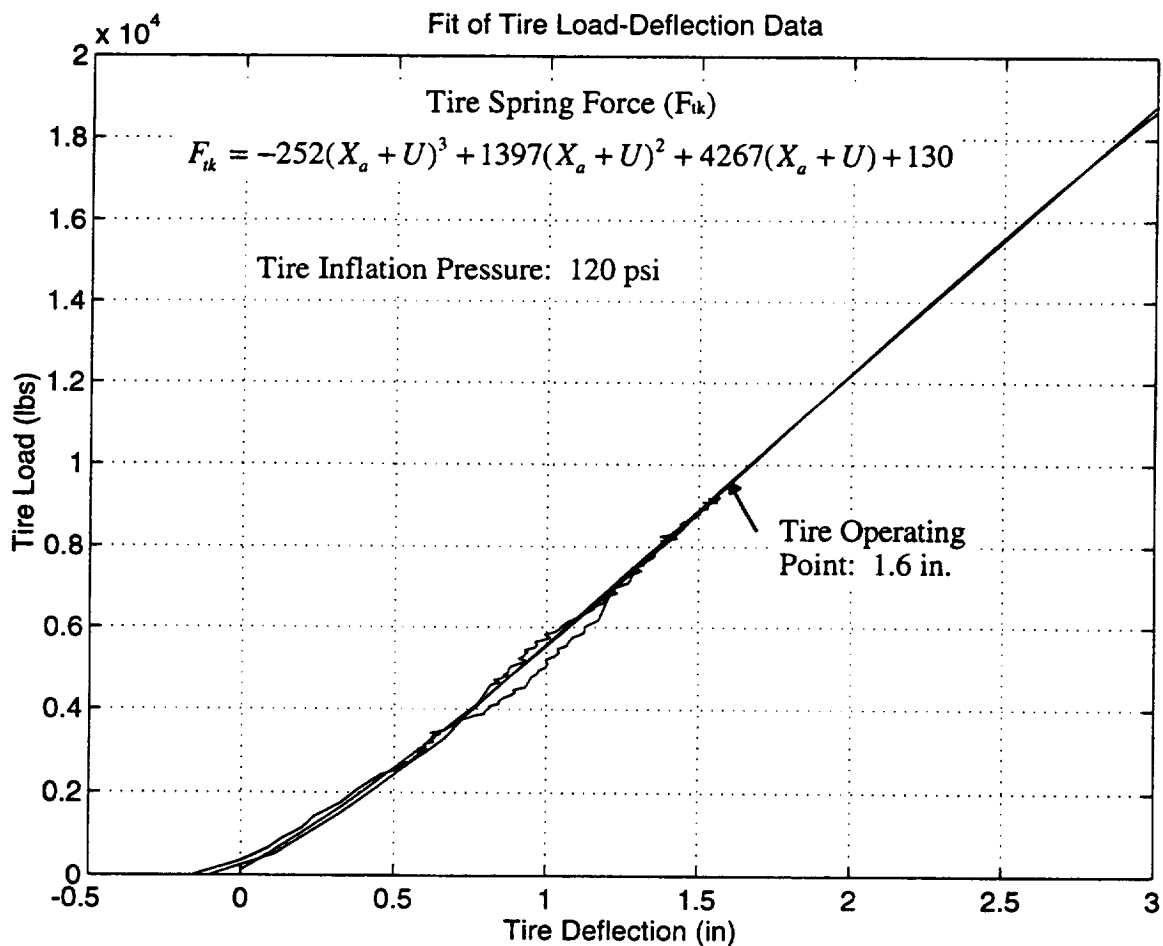
Tire Operating Point: 1.6 in.

Figure 5-4: Experimental tire load-deflection curve.

It may be noticed in Figure 5-4 that the tire load data does not start at zero when tire deflection is zero. The positional data of tire deflection from the continuous data was calculated from measured quantities (Tire deflection = X_{wg} - X_s). The intercept of the data (using an average through the hysteresis) is approximately -0.17 inches. It is thought that combined calibration error of the upper mass (X_{wg}) and strut positional (X_s) measurements, as well as some flexure in the drop carriage may account for this discrepancy.

A final quasi-static test was performed to gather information concerning the pressure-stroke curve and to help correlate the offset wheel friction model. For this test, the upper mass was locked into its equilibrium position by using tie down cables to prevent motion in the upward direction while the lift cylinders prevented motion in the downward direction. The shaker head was then moved from the zero point to the fully retracted position, allowing the gear to stroke about 7.25 inches. Two runs of this test were made. The first controlled the shaker head to move vertically at a slow rate of about 0.084 in/sec till no further stroke was possible with the shaker head (stroke of about 2.8 in left on the gear). The second test used a stroke rate of about 0.725 in/sec. These two tests were performed to determine the effect of nitrogen gas dissolving into the hydraulic fluid and to determine some of the effect velocity has on frictional levels. It was found (see Figure 5-5) that for a faster compression rate, less gas is dissolved into the fluid, leaving more gas in the chamber, causing the air spring to be stiffer. The hysteresis in the pressure measurements represents the amount of volume of gas lost to or gained from the fluid. No plans are made to model this effect. However, the decision as to which pressure curve to use as the model is made with the reasoning that stroke rates that are results of runway inputs will be high. Therefore, the air curve found during the higher-rate test was selected to represent the dynamic response of pressure to stroke. A curve using the form of Eqn. (2.3) was used to fit this data. This calculated curve is also shown on Figure 5-5. Two points in the extrapolated area of this curve were checked against test data. The first point, at about 11.0 inches, agreed to within 1.6% of the test data and the second point, at fully extended stroke, 15.09 inches, agreed to within 9.6%.
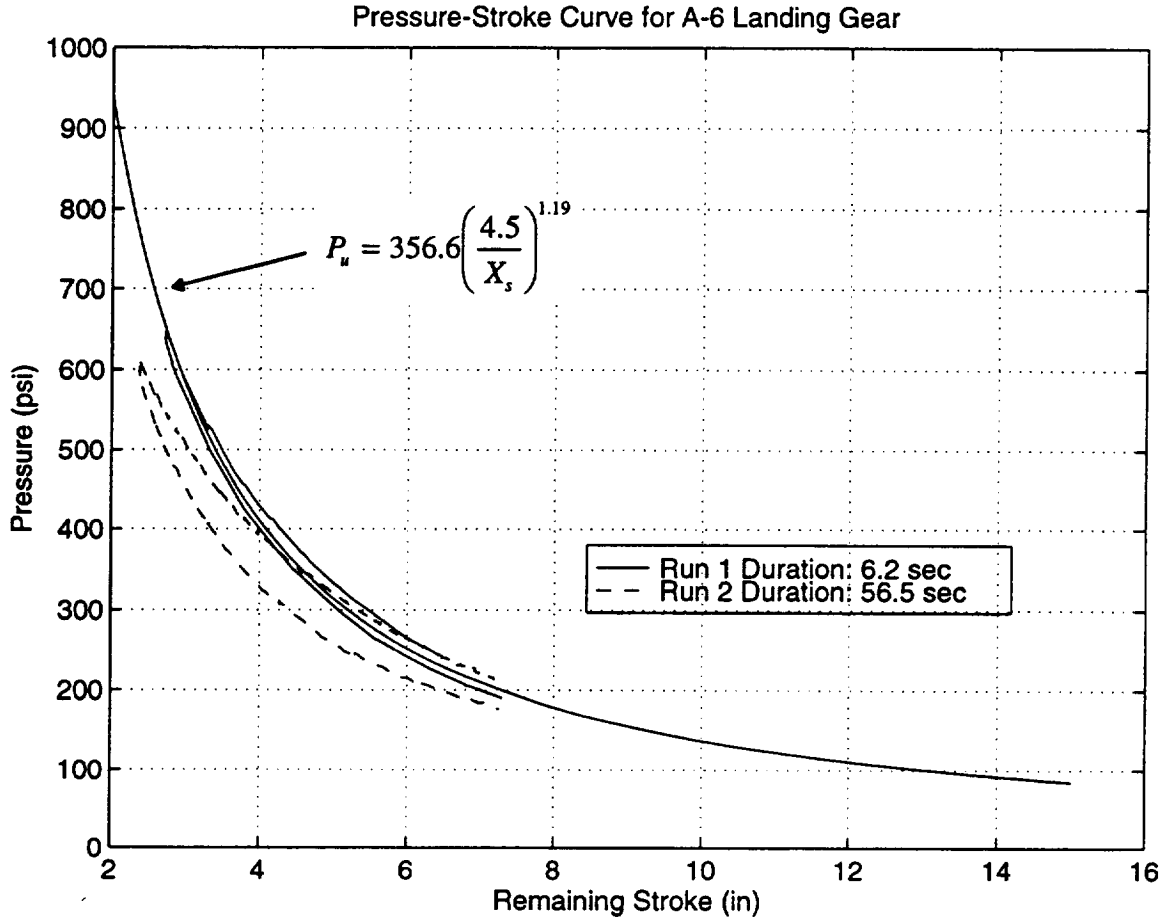
41

Figure 5-5: Pressure-stroke curve and fitted analytical expression.

The folowing procedures were developed in an attempt to statically quantify frictional effects. The result of this method was unclear and the final frictional model was developed using dynamic test data. The approach to finding the analytical expression for friction using static data is to use both the load data measured from the axle strain gage and to calculate the "theoretical" load (or frictionless load) by using the nitrogen pressure times the area it acts on. By subtracting these two data sets, the remaining loads are friction induced. However, as described in the previous section, the pressure does not follow a set rule because of the solubility of the gas into the fluid. It is therefore assumed that the frictional loads should be symmetric with the zero load axis. Figure 5-6 shows the result of subtracting the theoretical "pressure force" from the measured axle load. In this plot, two data sets are represented. The first represents the load measurements that were taken through a slow compression and extension around the 2.2 to 7.5 inch range.

The second represents data that were taken during a faster compression and extension rate through a stroke range from about 5.0 inches to 15.0 inches. There are two major notes to make from this plot. The first is the pressure effect as mentioned above. It is believed that from one time to the next, in a quasi-static regime, the pressure cannot be accurately predicted because of the solubility effect. So, even though the area is constant, the pressure for a given stroke value is very transient unless a long period of time is allowed for the gas and fluid to come to equilibrium, or the process is done so rapidly as to allow no mixing. This transience of pressure can explain why the two data sets in Figure 5-6 are not centered around zero. The next point to notice from the plot is the difference of scale between the two data sets. The set taken at a much slower rate shows a much greater frictional hysteresis loop, whereas in the other set, where the stroke rate was faster, the frictional loop is thinner. This lends credibility to the theory that sliding friction is a function of velocity. Statically, one encounters the maximum amount of friction possible. As velocity decreases, the friction also decreases. Beyond some velocity value, the friction remains essentially constant.
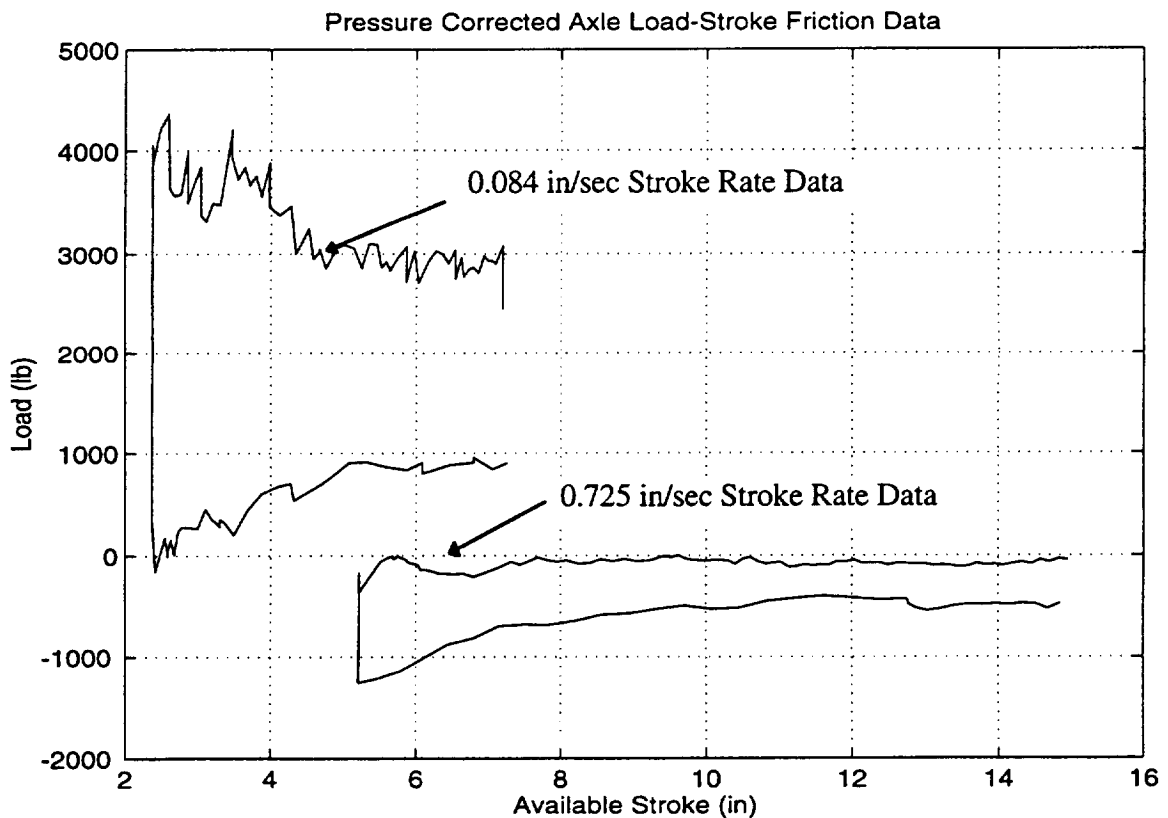
Figure 5-6: Result of "pressure load" subtracted from axle load measurements.

In light of these two points, and the assumption that friction be centered (or symmetric) around zero, a process was developed to center the test data. A rough median value of the two data sets in Figure 5-6 was found and those values were subtracted from their respective data sets, resulting in Figure 5-7.

Corrected Axle Load-Stroke Friction Data
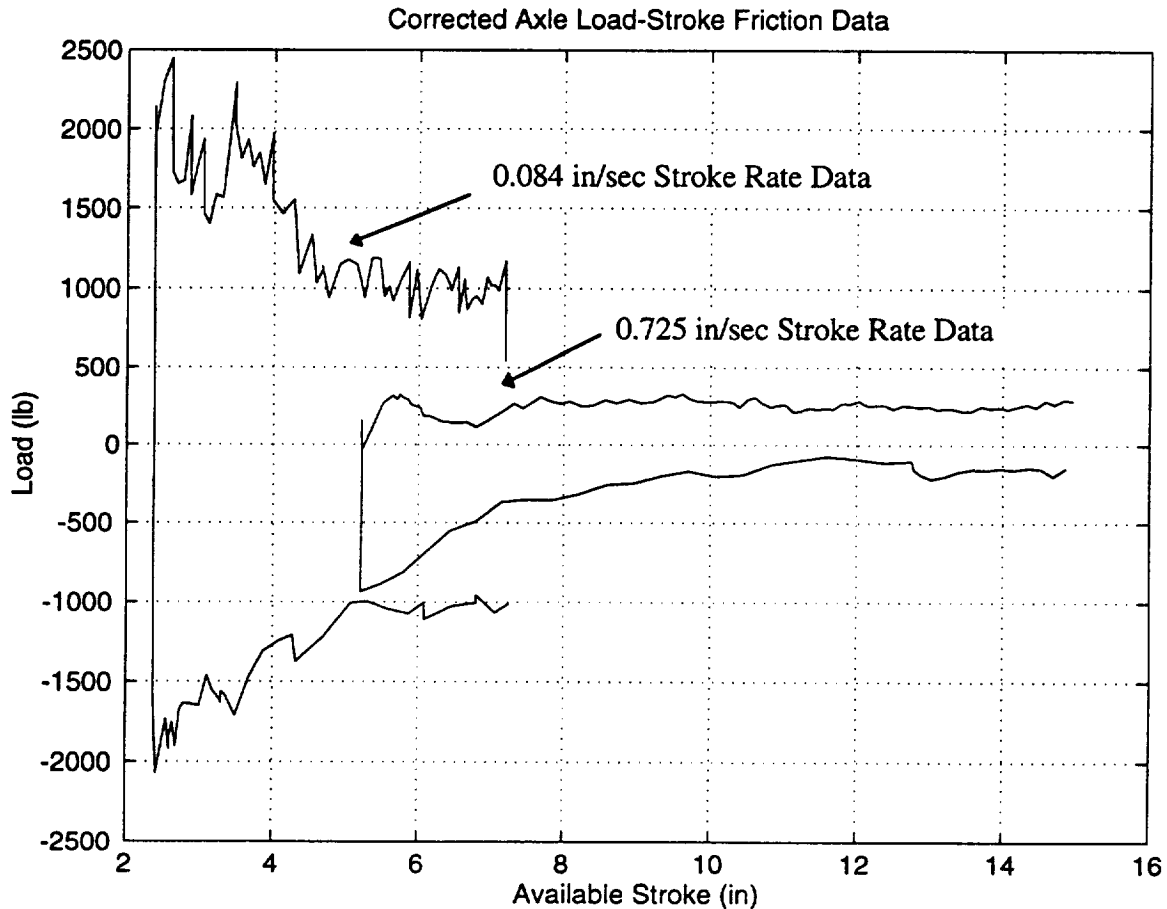
Figure 5-7: Zero centered frictional load data.

The data, as seen in Figure 5-7, may seem to indicate a functional relationship with strut stroke and velocity, but to draw any conclusions from this data, in light of how the pressures are capable of change, would not be useful. In light of the uncertainty associated with this quasistatic frictional information, a working model of friction was developed using dynamic information only. The initial model for comparison against dynamic data will contain the frictional model as developed in Chapter 2, and static friction values of (arbitrarily) 1.3 times that of sliding friction.

44

In summary, the system weight was found to be about 9465 lbs. and the lower mass about 318 lbs., leaving the upper mass to be about 9147 lbs. A frictional level of +/- 117 lbs. was found to exist in the guide rollers of the drop carriage, but in comparison to 9147 lbs., this force is negligible. A static seal friction of roughly 115 lbs. was found to exist in the strut. The friction due to the offset wheel was found possibly to be a function of stroke and gear force, but the data is not clear enough to draw a firm conclusion. The pressure-stroke curve was found to best characterize a rapidly encountered stroke. Finally, the tire load-deflection curve was found to be represented best by a cubic equation to capture both the nonlinear effects at initial compression and the linear spring rate at normal operating deflections. These values and models, except those noted, were implemented for comparison to test data in a dynamic regime.

5.3 Dynamic Testing

Many tests need to be performed to fully validate this landing gear model, such as step bumps, ramp inputs, varying sinusoidal inputs, etc. The remaining unknowns, after the static testing, are the tire damping coefficient, a dynamic polytropic gas constant, the three discharge coefficients, levels of sliding friction, and criteria for when the strut breaks free from the static friction and starts to slide, and when the strut sticks again. A frequency response comparison between the test gear and the simulation of the gear to a sinusoidal sweep from a runway input was used to determine these quantities. This process is only to compare the gain amplitudes and phase shifts of varius parameters given certain, specified inputs to this nonlinear system. This process should not be confused with the typical frequency response used when dealing with linear systems. The purpose of these tests was to make a comparison between the model, which has been updated by the static data, and the test gear. These frequency response tests should demonstrate precisely how the landing gear system responds to a frequency sweep of given amplitudes. The variables under consideration, in comparing the two models, are the gear positional variables and pressure values in both the upper and lower chambers. The maximum, break away friction can also be observed by slowly increasing the frequency of a given amplitude and noting the force levels present in the gear when the strut starts to stroke. These variables considered in the frequency responses comparisons are important to verify because of the intended use of the program. The simulation will

be used to evaluate analytically the effect of various active control concepts that will be applied to the test set-up.

For this frequency sweep test, the gear starts at rest on the shaker head. It is then shaken to allow the fluid and gas to come to equilibrium. The test used as an input a swept sine wave from 0.75 to 3.75 hertz in the course of 40 seconds with an amplitude of about 1.0 inch. The model parameters of sticking friction, sliding friction, tire damping, discharge coefficients, and polytropic gas constant were adjusted such that the predicted frequency response and the test data were within about 10% agreement in the positional and pressure variables over the whole frequency range.

The method for setting the sticking friction was to observe the force level (above the weight of the system) at which the strut started to stroke. This quantity is about 2700 lbs. for the 1.0 inch amplitude case. The predicted slip time, as calculated by the simulation, is very sensitive to this number. The criteria for the break-away friction level may also be function of something other than purely force. From comparison with other runs, such as step bumps and other amplitude sine waves, this number is not consistent and may be a function of how long the strut has been stuck and how fast it was traveling when it stuck, and potential and kinetic energies in the landing gear system. No attempt was made to model these effects, and the constant value of 2690 lbs. was used in the following results.

The tire damping in the model was adjusted such that the tire deflection predicted by the simulation and the data recorded in the test before the strut started stroking matched. The higher frequency tire mode was inspected in this region where only the tire is bouncing and the damping was selected to match the phase of the tire as well as possible.

The other parameters of sliding friction, discharge coefficients and polytropic gas constant are coupled in that they all effect the stroke. The sliding friction and discharge coefficients work to damp the stroke and the polytropic gas constant affects the stroke by changing the curve of pressures as a function of stroke, making the spring stiffer or softer. These parameters were selected by inspecting the dynamic behavior of the variables of upper mass position (X_{wg}), strut stroke position (X_s), upper chamber, or pneumatic pressure (P_u), and lower chamber, or hydraulic pressure (P_L). If, for example, the predicted pressures were much larger than the measured pressures but the positional

variables seemed close, the polytropic gas constant needed to be decreased. However, if both the pressures and the positional data were greater than the measured data, then the damping in the strut, alone, may need to be increased. These parameters were adjusted in an iterative fashion until the frequency responses of each of the above mentioned predicted variables were within about 10% of the measured data. The value used for sliding friction is a constant 400 lbs. This value is somewhat arbitrary and in reality, may indeed be a function of stroke velocity. Further tests need to be run to quantify friction to a larger extent.

The discharge coefficients are still fuctions of orifice geometry, as described in Chapter 3. However, a percentage of each of the three discharge coefficients is taken to help match the data. The model of the discharge coefficients includes only geometry information, no flow velocity information. These models may not be entirely appropriate for this landing gear, but the adjustments as mentioned above improve the results and are taken to be sufficient control on these coefficients. As long as the coefficients do not exceed one, and are greater than about 0.8, arbitrarily, these values are reasonable. The average of the discharge coefficients is about 0.9

The polytropic gas constant was adjusted down to 1.1 from 1.19 as indicated earlier in this chapter. This change reduced the pressure amplitudes for given values of stroke. This change, along with the others mentioned previously, was sufficient to bring the predicted results to within 10% of the measured quantities.

The frequency response comparison of both the measured data and the nonlinear simulation data are presented in Figures 5-8 (a-d). Figure 5-8a shows the gain and phase plots for the strut stroke variable (X_s) as a response to the 1 inch shaker head swept sine input. As can be seen from the figure, the maximum gain predicted by the simulation at natural frequency of about 1.6 Hz. is not as great as that recorded in the experiment by about 13%. This value is greatly affected by the damping in the strut. The parameters of discharge coefficient and sliding friction may still need to be adjusted. The phase of the response agrees very well with that of the test data. Over the rest of the frequency range, the two gains match to within an average of 5%. The "jumps" at the beginning and end of some of the phase plots presented are the usual difficulty in distinguishing between +/- 180 degrees and the fast Fourier transformation routine calculating a response to a nonlinear system where no data exists. The next figure, Figure 5-8b, shows the

frequency response comparison of the upper mass position (X_{wg}) with respect to the shaker input. The gain plot shown here indicates that for higher frequencies, the upper mass, as simulated, moves through larger amplitudes (about 14%) than the test gear. One reason for this may be the frictional and discharge coefficients as mention above. If the strut were allowed to stroke a little further each time, the upper mass amplitudes would not be as large. The suggestion is to reduce the damping, to some small extent, in the strut to accommodate this behavior. The phase of this predicted value is also slightly in error. This may also improve with the suggested changes.

Response of Strut Stroke Position due to Shaker Head (1.0 in.)
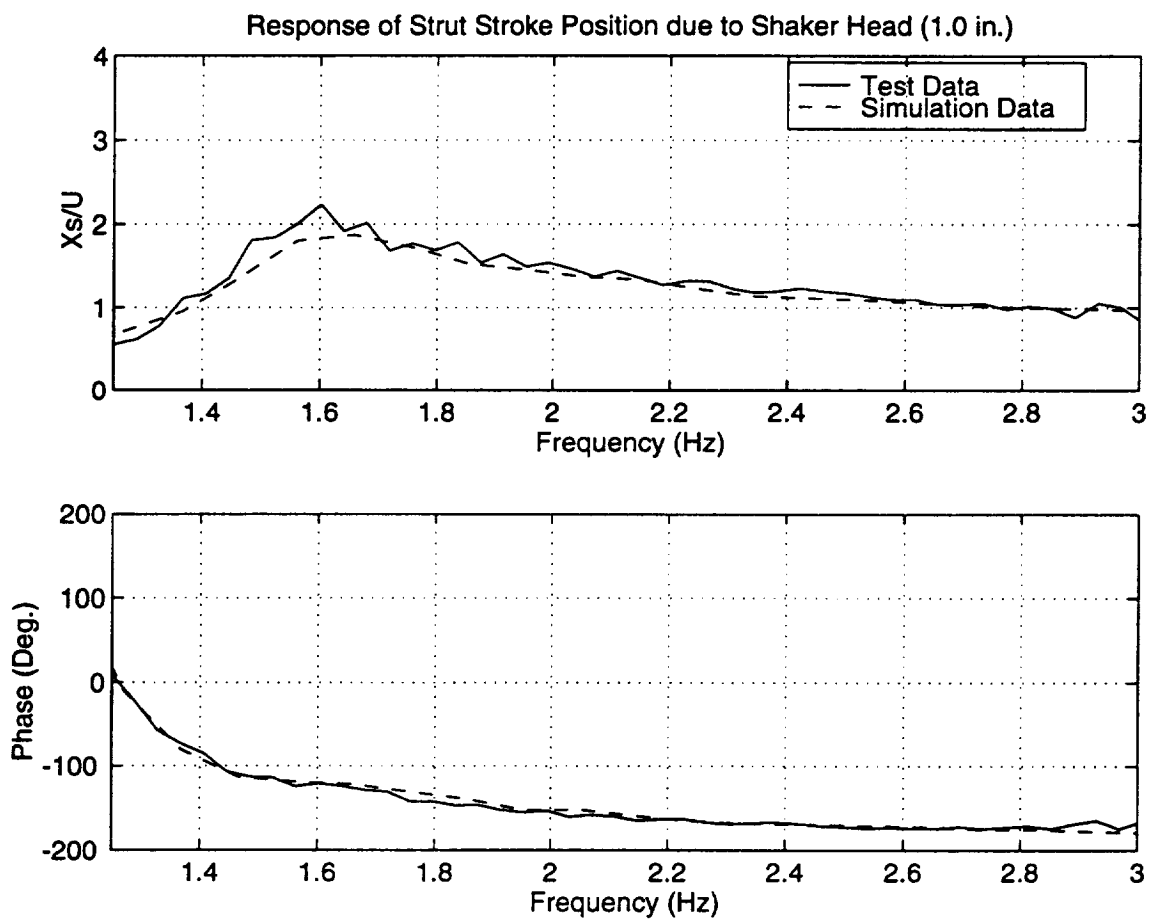
Figure 5-8a: Frequency response comparison of strut stroke to shaker input.

Figure 5-8b: Frequency response comparison of upper mass position to shaker input.

Figure 5-8c shows the frequency response comparison of the pressure in the upper chamber (P_u). For the pressure measurements, it is useful to compare amplitude gains between the model and the actual measurements over a range of frequency inputs. The upper chamber and lower chamber (see Figure 5-8d) pressures are both high by about 10% through all frequency ranges except near 1.6 Hz, the natural frequency of the gear. Again, damping in the strut is the critical component in this comparison. It is noticed that at natural frequency, where the strut would otherwise stroke more, the calculated pressure is not larger than the measured pressure. This lower pressure value corresponds directly to lower stroke values at this frequency. The damping limiting the stroke indicates that the main orifice discharge coefficient may need to be a little larger, to allow more flow through the orifice. This would allow larger stroke rate by decreasing the damping in the

strut. The polytropic gas constant may also need to be decreased slightly to lower the pressure amplitudes over the whole range of frequencies.

Figure 5-8c: Frequency response comparison of upper chamber pressure to shaker input.
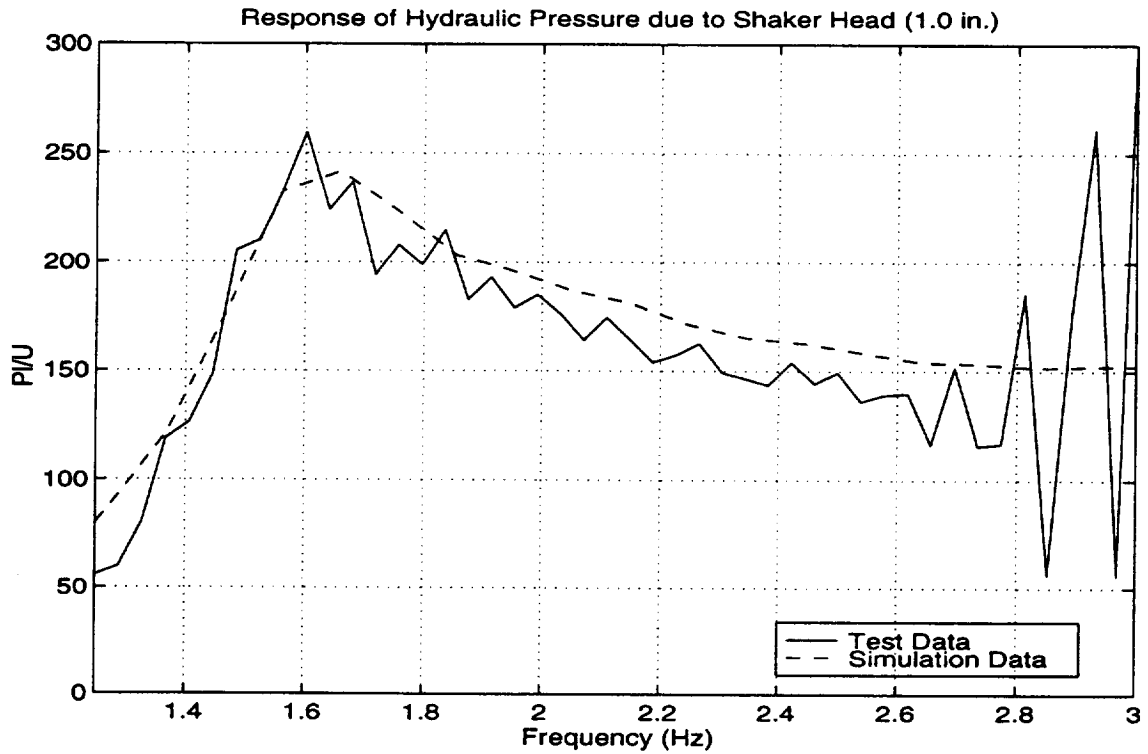
Figure 5-8d: Frequency response comparison of lower chamber pressure to shaker input

Figure 5-8d of the hydraulic pressure shows a response similar to that of the pneumatic pressure. The difference in amplitudes (pressure) between the hydraulic and pneumatic drive the motion of the strut.

5.4 Validation of Updated Model

The swept sine used in Section 5.3 is an extreme case for a landing gear to encounter. The model parameters were selected such that the model predicted certain measured quantities to within 10% for this one case. As a validation to the model updates, several other tests were performed and the results were compared to the predicted data. The first was a swept sine test over the same frequency range and with an amplitude of about 0.5 inches, again over the course of 40 seconds. The results are shown in Figures 5-9 (a-d). The reasons, as discussed in the previous section, to reduce strut damping are apparent when looking at Figure 5-9a. Over the whole range of frequencies, the response as predicted by the simulation is below that of the test data by about 9%. With the exception of this one variable, however, the data and the predicted values agree very well.

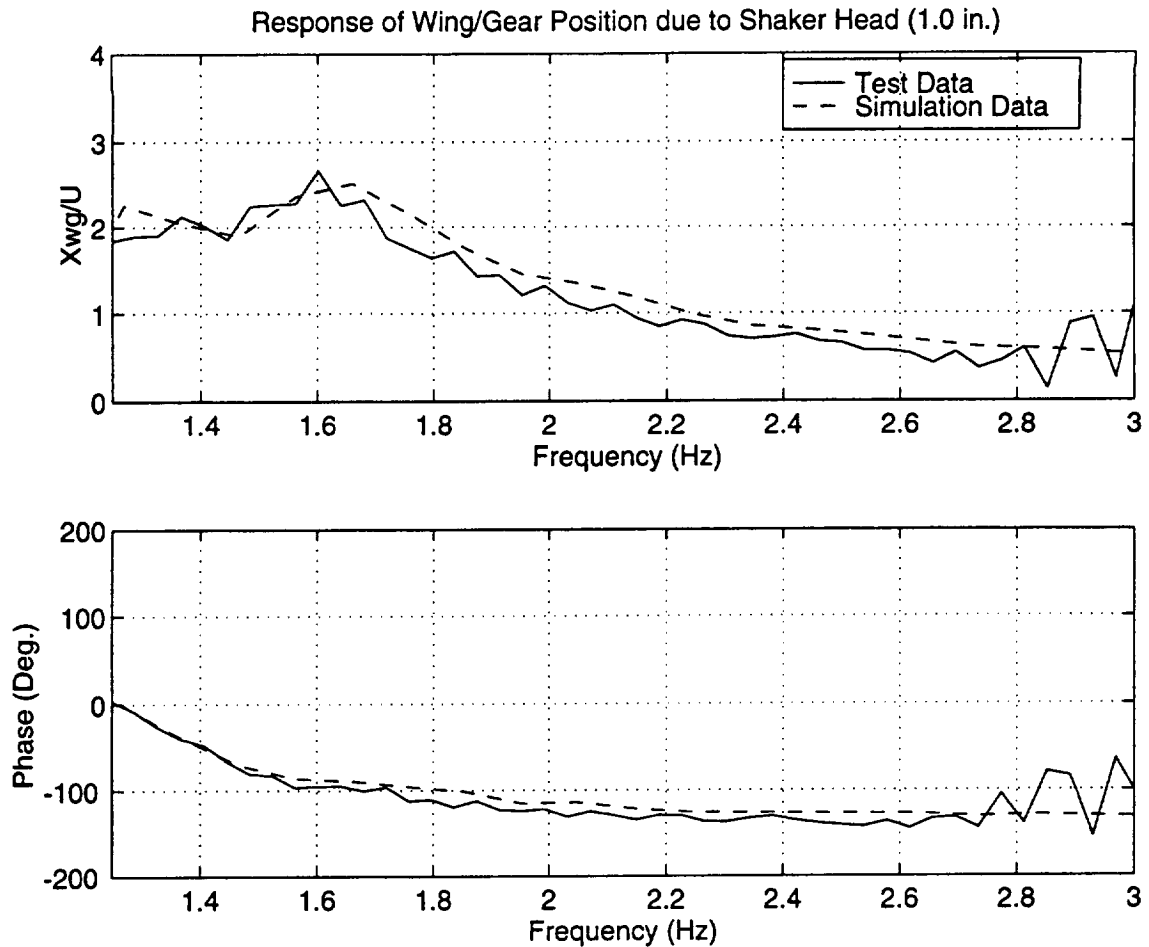**Figure 5-9a:** Frequency response comparison of strut stroke to shaker input.
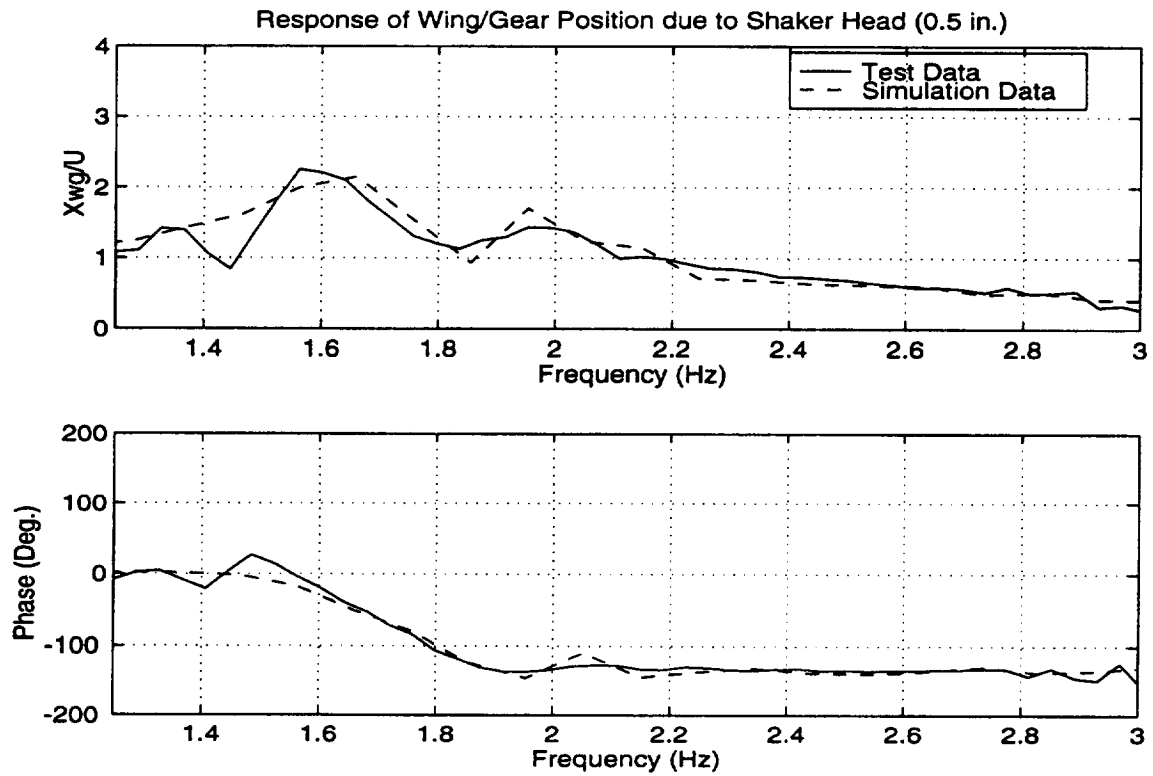
Figure 5-9b: Frequency response comparison of upper mass position to shaker input.
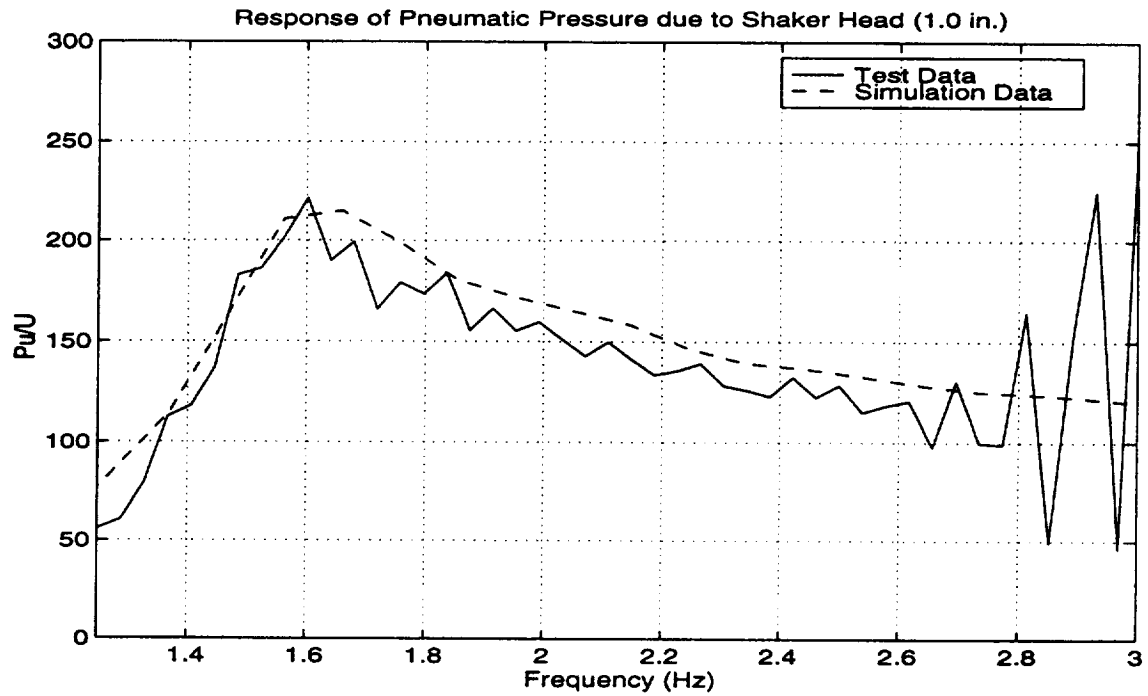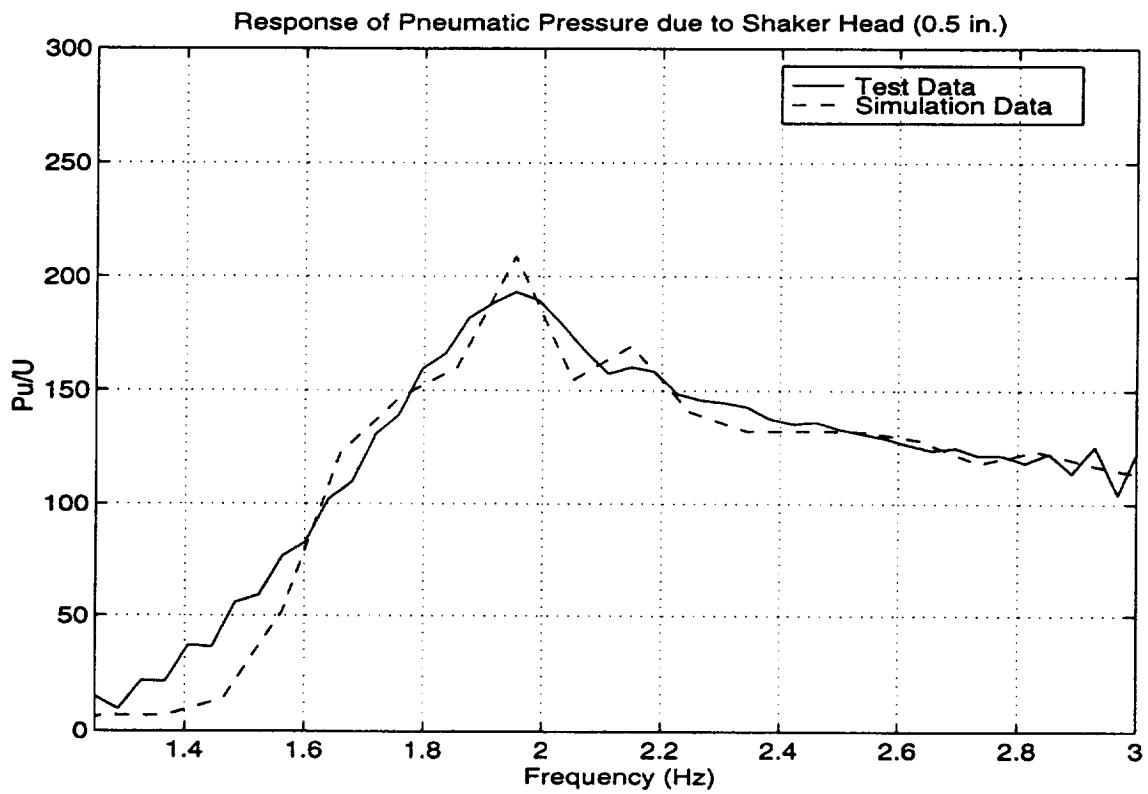

Figure 5-9c: Frequency response comparison of upper chamber pressure to shaker input.
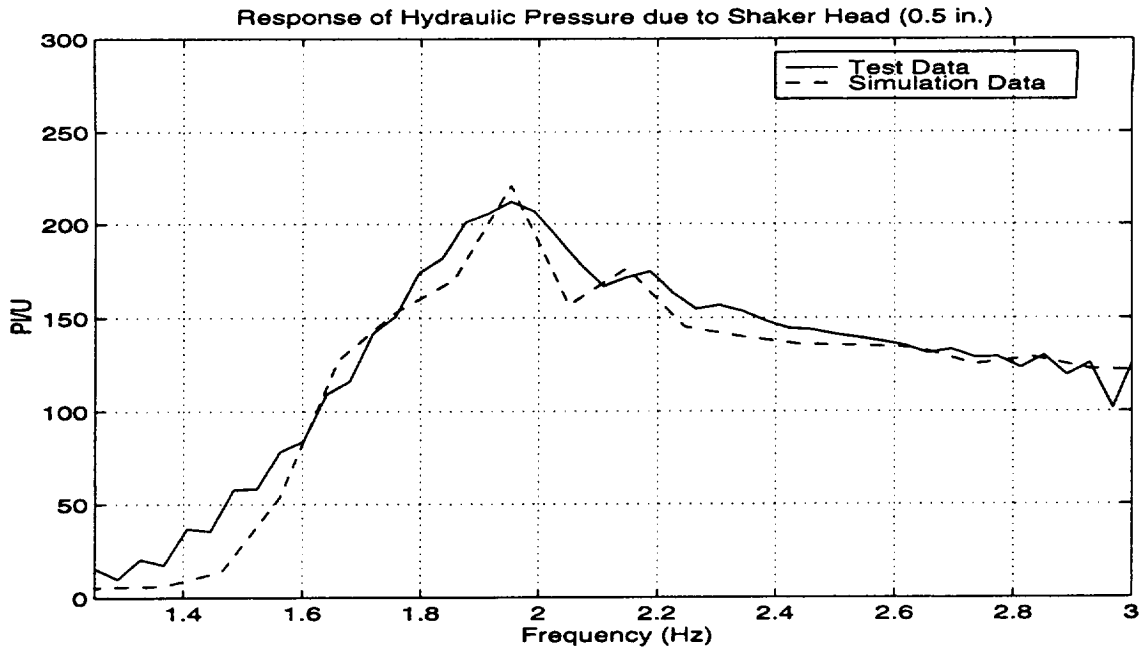
Figure 5-8d: Frequency response comparison of lower chamber pressure to shaker input

The second check was to run a test where the sweep rate of the frequency range was different. This test swept a 1.0 inch amplitude sine wave from 0.75 to 3.75 Hz. over the course of 25 seconds.

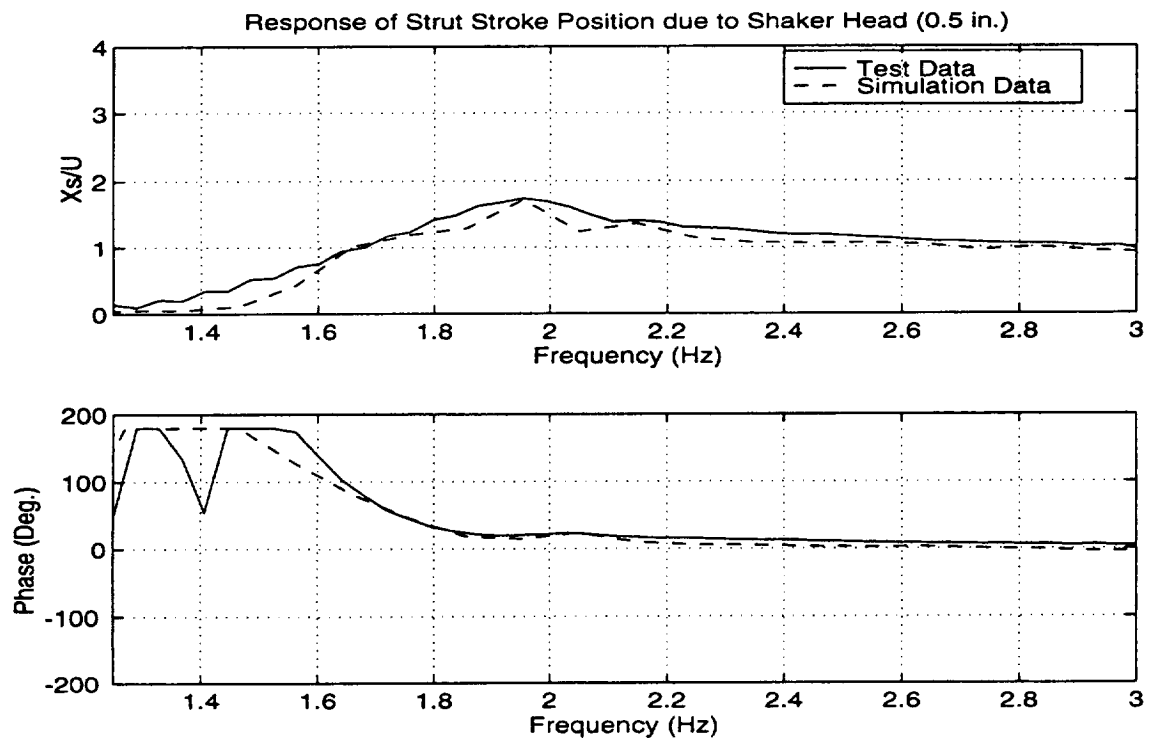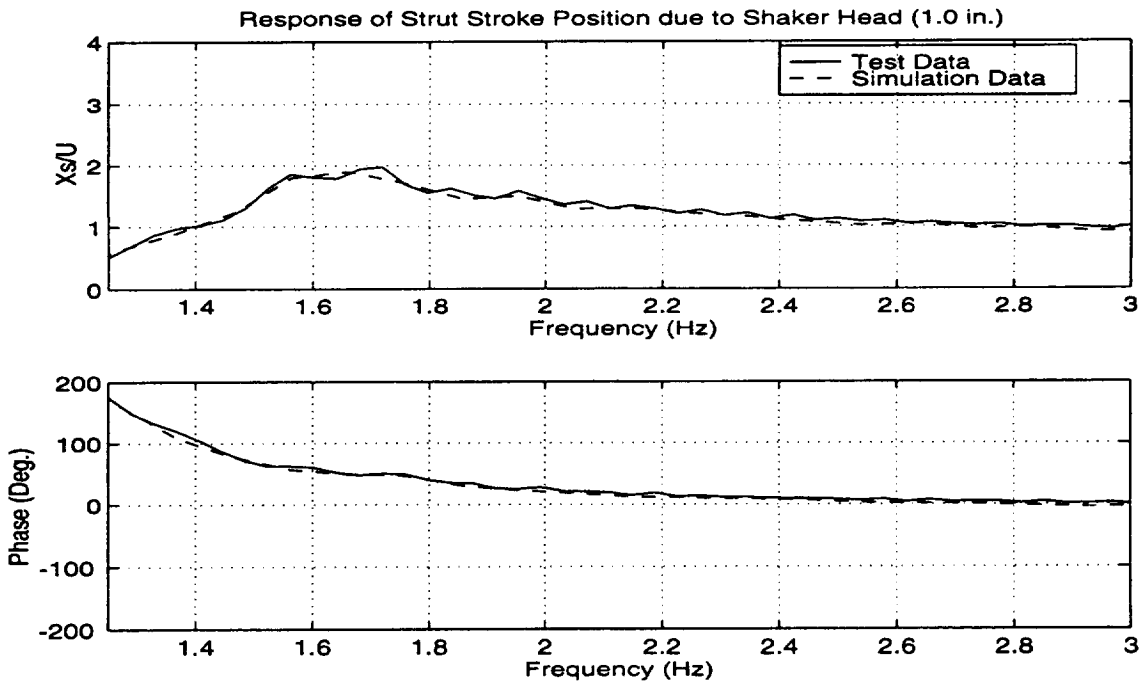**Figure 5-10a:** Frequency response comparison of strut stroke to shaker input.
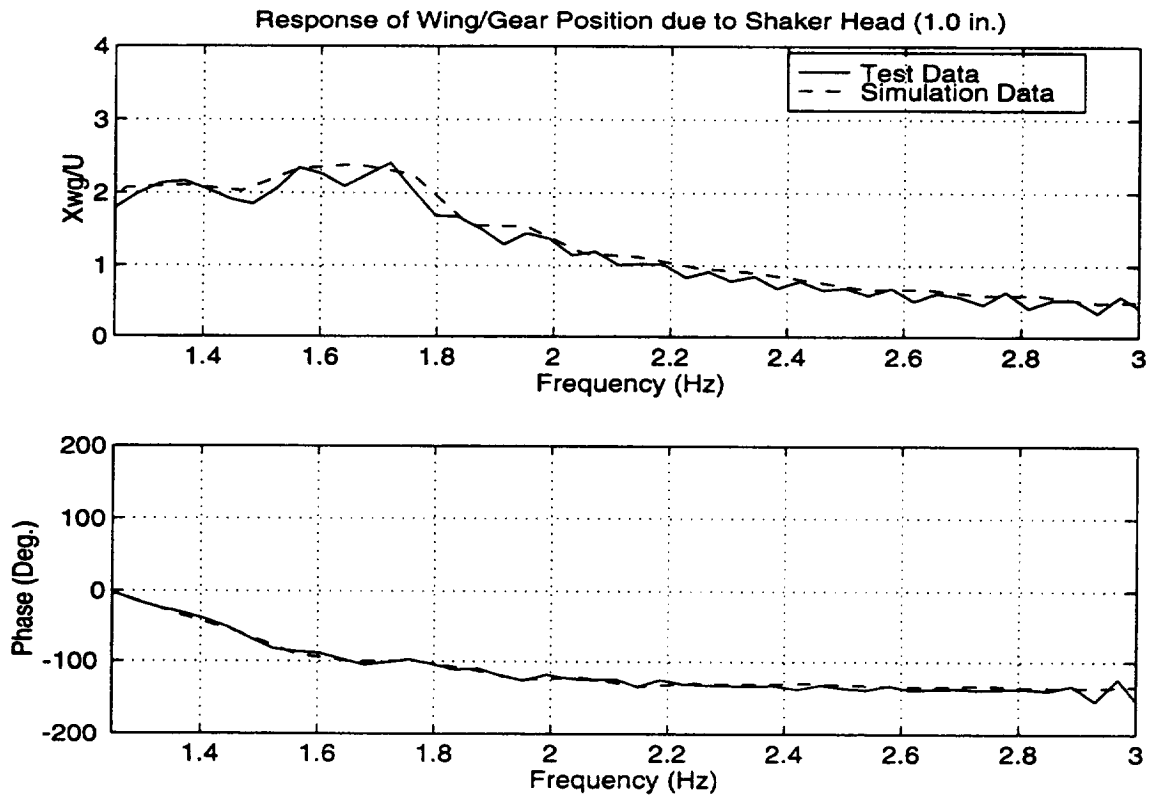
Figure 5-10b: Frequency response comparison of upper mass position to shaker input.
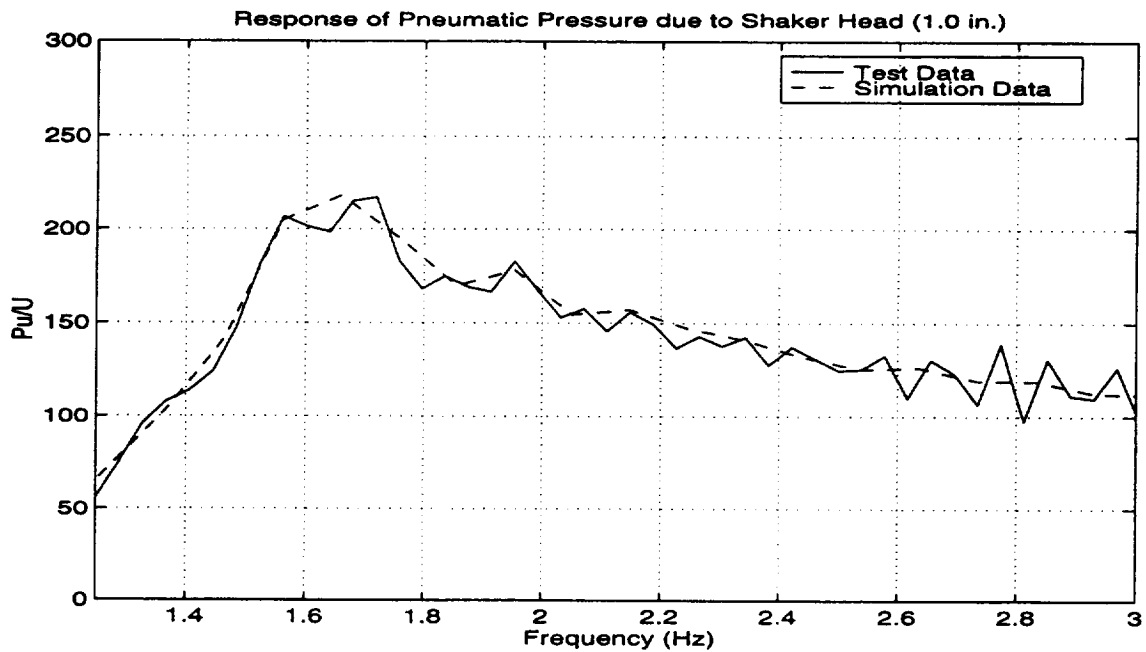
Figure 5-10c: Comparison of responses of upper chamber pressure to shaker input.

54
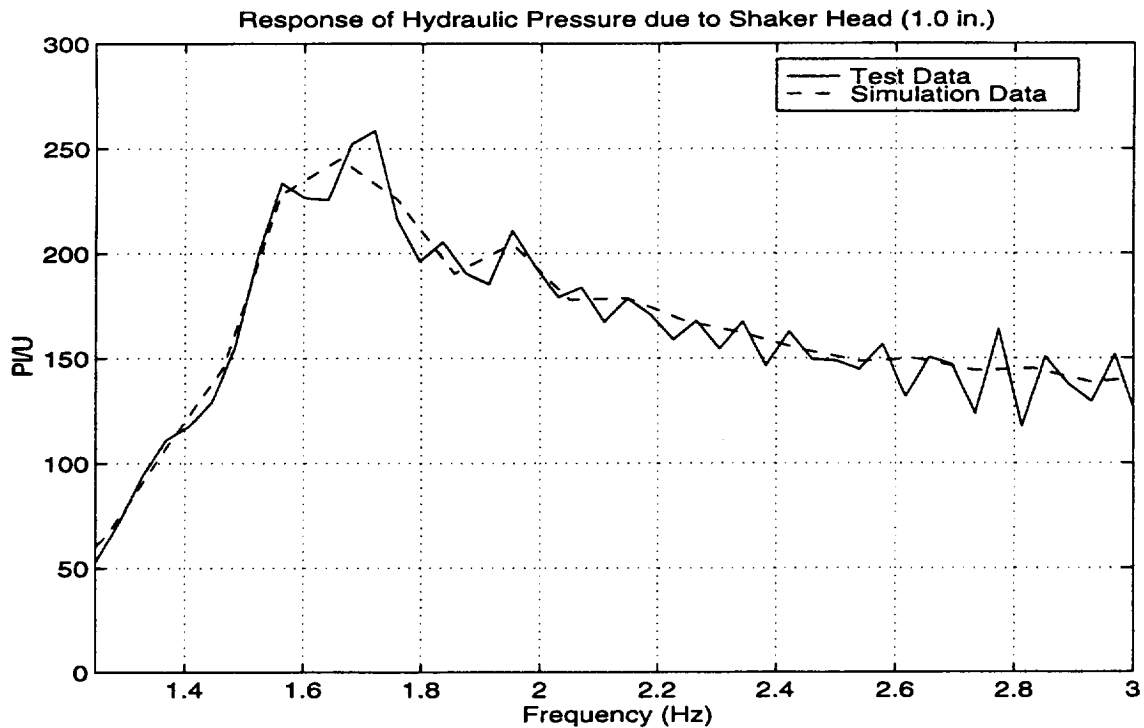
Figure 5-10c: Comparison of responses of lower chamber pressure to shaker input.

As can be seen from Figures 5-9 and 5-10, the simulation predicts the response of the measured values exceptionaly well (within 5%). The results to these past two tests, where the amplitude and then the sweep rate were changed, indicate that the simulation will accurately predict the physical variables of interest very well, for any of these types of input. As a final check, a step bump case was run and Figures 5-11 (a and b) show the results. It can be seen from Figure 5-11a that the strut stroke is predicted within about 8% of the test data. However, the model does not correctly predict when the strut locks up, as seen by the overshoot at around 1.25 seconds. This suggests that the criteria for the strut to lock up must be improved. Otherwise, the simulation predicts the response very well.

Figure 5-11b shows the response of the upper mass to the step bump. The simulation predicted to within about 10% the values as recorded in the test data. The oscillation that can be seen in the predicted data when the strut is locked is due to tire bouncing. Since the test data does not show this behavior, the tire damping needs to be increased.
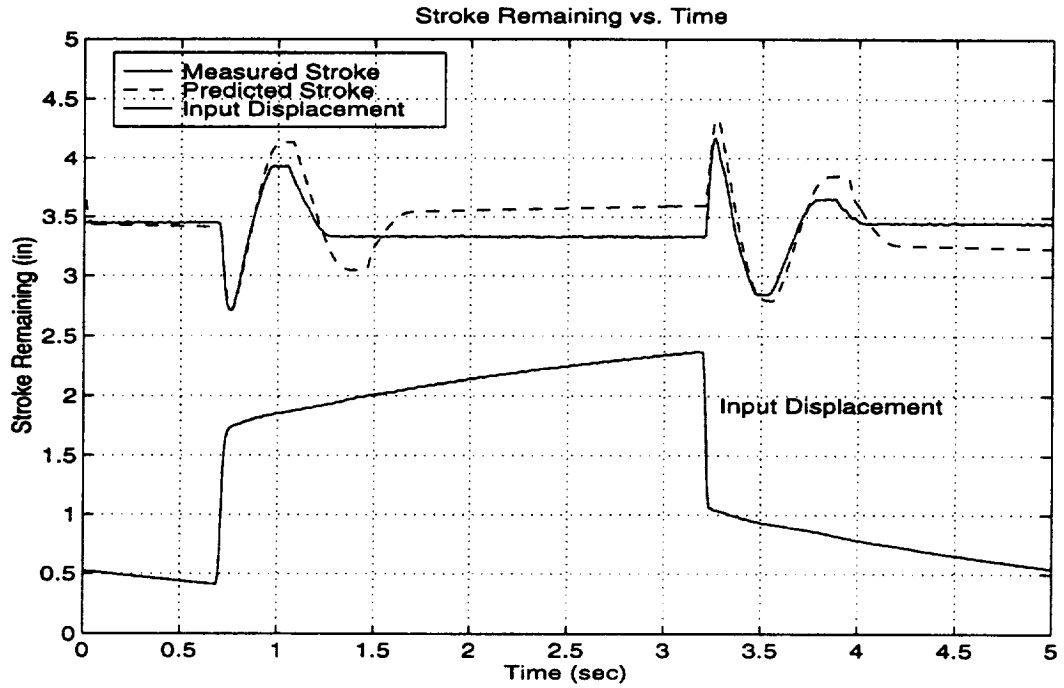
Figure 5-11a: Time history of strut position as gear encounters a step bump.
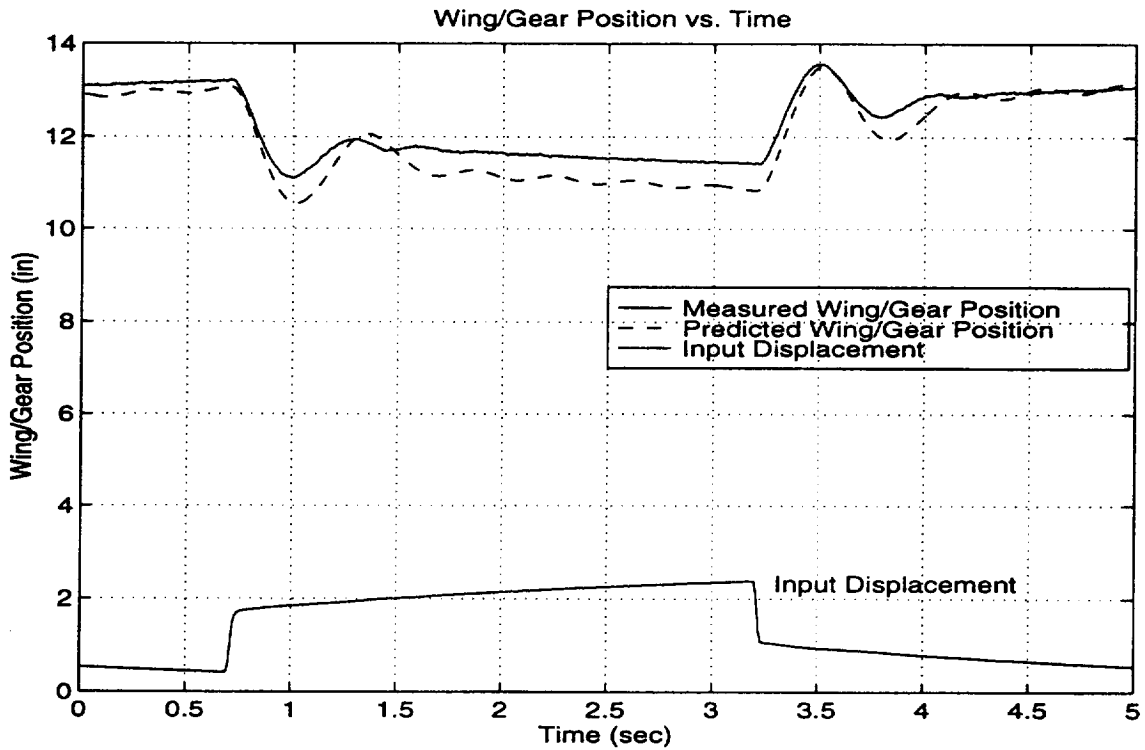
Figure 5-11b: Time history of Wing/Gear Position as gear encounters a step bump.

56

This section has shown that the parameters found by tuning the model to a 1.0 inch amplitude sine sweep from 0.75 to 3.75 Hz. in 40 seconds were also good for other cases, validating the model for other, more general types of cases that may be run.

5.5 Summary

In this chapter, the static parameters of the landing gear model such as system mass, tire load-deflection curve and pressure-stroke curve, were found from various tests performed at NASA Langley's Aircraft Landing Dynamics Facility. After the model had been updated with static data, a sine sweep test was run and the parameters of the model were, once again, updated to reflect the new knowledge of the system. Other tests were run as a check of this set of parameters and it was found that the simulation predicted the system response within the 10% range. Further changes of the model were suggested as a way to further increase the accuracy of the model. In summary, then, a fully nonlinear analytical model of a telescoping landing gear is presented here which has been tuned with test data and validated with data and which has run times of about 3 minutes per dynamic simulation second. For semi-static runs, times are much shorter, about 30 seconds real time per simulated second. This model may now be adjusted for further accuracy or it may be used as is as a tool for evaluating the effect of applying various active control schemes to the landing gear.

Chapter 6: Concluding Remarks

6.1 Conclusions

The research presented in this document brings together in one place a comprehensive development of the equations of motion, a discussion of the problems associated with integrating the equations of motion, and describes a procedure to tune the analytical model with test data. It was found that an implicit predictor-corrector routine was very efficient, but a Runga-Kutta routine was needed to integrate across discontinuities. The result of this research is a simulation tool of the A-6 Intruder main landing gear which has been validated with both static and dynamic data. This model is a contribution to the effort to study and correct vibrations that are transmitted through the landing gear into the fuselage of a plane. This tool is to be used to simulate and evaluate the effect of various active control schemes to reduce force or vibration transmission to the fuselage. Simulations based on the development presented in this document currently exist in the form of a FORTRAN program, a SIMULINK program and in a DADS format. In conclusion, then, this simulation is a powerful tool that is the result of both analytical and experimental efforts.

6.2 Future Research

This research has provided a tool which can be put to many uses. A couple of areas of future research are suggested. The first is to complete the update of the model. The model strut damping could be further tuned. A suggestion for this fine tuning is to run sensitivity studies on the variables that directly affect the model damping. An additional result may be that the friction associated with the guide roller bearings may need to be simulated. This tuning is optional, though, as acceptable measures of important parameters are currently being predicted. In addition, the stick-slip friction model needs to be tuned. Not only do the criteria of when to stick and when to slip need to be further defined, but the model that takes the dynamics from motion to the stuck phase and back again needs to be smoothed. With this change, the Runga-Kutta may not be needed at all, leaving only the Adams-Moulton, which has demonstrated excellent efficiency in solving the continuous portions of the total solution history.

The second area of future research involves actively controlled landing gear. As stated in the introduction, the ultimate goal of this research is to contribute to the process of alleviating vibrations in the HSCT. As a step toward that, this simulation is to be used to evaluate various control schemes. Three approaches to control aircraft vibrations using the landing gear are proposed. One is an active orifice concept which would allow the landing gear damping characteristics to be greatly altered in response to unacceptable ground disturbances. The second is a force actuator placed parallel to the main landing gear cylinder that acts to actively attenuate relative motion of the fuselage to the ground. A third concept uses electro-rheological fluids to actively control the damping characteristics of the landing gear. This approach may call for the replacement of the current fluid in the cylinder or perhaps be implemented as a parallel damper. The dynamics of these various concepts are to be modeled and added to the validated simulation. Control laws will then be evaluated on the basis of reducing vibrations in a simulated cockpit. These concepts are being developed by NASA engineers and are to be tested at a later date.

References

1) Tony G. Gerardi and Dr. Levon Ninnetyan ,"Status of Computer Simulations of USAF Aircraft and an Alternative Simulation Technique", AGARD CP-326, April 1982.

2) R. Freymann and W. Johnson, "Simulation of Aircraft Taxi Testing on the AGILE Shaker Test Facility" , Second International Symposium on Aeroelasticity and Structural Dynamics, sponsered by Deutsche Gesellschaft fur Luft- und Raumfahrt e.V. in Aachen, W. Germany, April 1985.

3) R. Freymann , "An Experimental-Analytical Routine for the Dynamic Qualification of Aircraft Operating on Rough Runway Surfaces", AGARD R-731, March 1987.

4) Raymond Freymann, "Actively Damped Landing Gear System", AGARD CP-484, 1990.

5) Irving Ross, Ralph Edson, "An Electronic Control for an Electrohydraulic Active Control Aircraft Landing Gear", NASA CR 3113, April 1979.

6) Alan Sheperd, Tyrone Catt, David Cowling, "The Simulation of Aircraft Landing Gear Dynamics", 18th Congress of the International Council of the Aeronautical Sciences, Beijing, People's Republic of China, Sept. 1992.

7) Tyronne Catt, David Cowling, Alan Sheperd, "Active Landing Gear Control for Improved Ride Quality During Ground Roll", AGARD Smart Structures for Aircraft and Spacecraft, Oct. 1992.

8) C.G. Mitchell, "Some Measured and Calculated Effects of Runway Unevenness on a Supersonic Transport Aircraft", Symposium on Nonlinear Dynamics, Loughborough University of Technology, England, March 1972.

9)   D. Yadav, R. P. Ramamoorthy, "Nonlinear Landing Gear Behavior at Touchdown", *Journal of Dynamic Systems, Measurement, and Control*, Vol 113, December 1991.

10) Mahinder K. Wahi, "Oleopneumatic Shock Strut Dynamic Analysis and Its Real-Time Simulation", *J. Aircraft*, Vol. 13, No. 4, April 1976.

11) Liu Li, Yang Guo-zhu, He Qing-zhi, "Optimization of Oleo-Pneumatic Shock Absorber of Aircraft", *Chinese Journal of Aeronautics*, Vol 6, No. 2, May 1993.

12) George R. Doyle Jr., "A Review of Computer Simulations for Aircraft-Surface Dynamics", *J. Aircraft*, Vol 23, No. 4, April 1986.

13) M. Moran, H. Shapiro, *Fundamentals of Engineering Thermodynamics*, John Wiley & Sons, Inc., New York, 1988.

14) B. Munson, D. Young, T. Okiishi, *Fundamentals of Fluid Mechanics*, John Wiley & Sons, Inc., New York, 1990.

15) W. Press, S. Teukolsky, W. Vetterling, B. Flannery, *Numerical Recipes in C*, Cambridge University Press, 1992.

16) C. William Gear, *Numerical Initial Value Problems in Ordinary Differential Equations*, Prentice-Hall, Inc., N.J., 1971.

17) R.W. Miller, *Flow Measurement Engineering Handbook*, McGraw-Hill Book Company, 2nd ed.,1989.

18) Dean Karnopp, "Computer Simulation of Stick-Slip Friction in Mechanical Dynamic Systems", *Journal of Dynamic Systems, Measurement, and Control*, Vol. 107, March 1985.

19) D. Haessig Jr., B. Friedland, "On the Modeling and Simulation of Friction", *Journal of Dynamic Systems, Measurement, and Control*, Vol. 113, Sept. 1991.

Appendix A

A.1 Summary of Program

As part of this reasearch, a computer program, "gearfin.f" has been written to numerically solve the equations of motion of landing gear in time. The notation used throughout the appendix is consistant with that used in the FORTRAN program, not that which is presented in the paper. Four states are used for the solution. These states are $Y(1)$ and $Y(2)$, the position and velocity, respectively of the wing/gear interface, and $Y(3)$ and $Y(4)$, the position and velocity, respectively, of the wheel axle. The program uses the Adams/Moulton predictor/corrector numerical method, and a variable step Runga-Kutta to get past discontinuities.

The program's setup is simple. There are four data files associated with it. The first, "pin.dat", lets the user define the shape of the metering pin. The first entry is the number of slope changes of the pin (n). The next n entries are the n diameters. Then the n lengths associated with the diameters. Lastly in this data file is the number defining the maximum stroke.

The next data file is called "piston.dat". This file is the entry point of the many (12) piston/cylinder associated parameters. The inputs of this file are: Xsi, the initial length at which the gear is charged, Pi, the initial charge pressure, γ, the polytropic gas constant, Du, the diameter of the upper chamber, DL, the diameter of the lower chamber, D1RC and D1RE, the diameters of one snubber hole under compression and extension conditions respectively, Dop, the diameter of the hole in the orifice plate, and Dpis, the diameter of the piston shaft, Mu, the mass of the upper system, Ml, and FSMAX, the value of the maximum sticking friction of the piston seals.

The third file is called "ic.dat". This is a file of the initial conditions. Inputs are the initial conditions of the four states in the order described above.

The last data file is a runway profile. Since various runways could be used, the name of the file is left up to the user. The user needs to locate the "Read in Runway"

section of this program and change the name. The first line of the input file should contain the length (I) of the following data. The next element of the input file is the vector: [TIME(I) ELEV(I) ELEVD(I)]. This file contains a time history of the height of the runway in meters and piecewise continuous time rate of change of the height as the wheel rolls along it. Therefore, any type of velocity or acceleration case may be investigated.

This program has six subroutines associated with it. The first is the integration routine "ddriv2.f". The next is a routing called "F". Its function is to define the derivative of the states at any time t. The third routine is called "METPIN". This subroutine returns the current value of Dpin based on the current stroke and the input data of pin.dat. The fourth is called "COEFF". In this subroutine, the C and K coefficients of the landing gear equations are calculated using the input data from "piston.dat", Dpin, and the stroke rate. The fifth is "RKF4.f", a fourth-order Runge-Kutta variable step integration routine. When the program hits a discontinuity (as when friction suddenly changes sign) it will automatically switch from the predictor corrector (ddriv2.f) to Runge-Kutta (rkf4.f). The sixth routine is really a copy of "F", and is called "FOUT". This routine is independent of the integration and can be called to record the states by the user. The current data files are for the A-6 Intruder.

The current form of the program has many outputs. These outputs are selected with the idea of validation of the model in mind. All output files are written in ASCII, and have the form of an nX4 matrix, where n is the number of times along the interval that the program writes the solutions. The first is "y.out". It contains the four states, Y(1), Y(2), Y(3), Y(4). The second file, "tfaa.out", records the time, the value of friction at each time, the accelerations, YDOT(2), and YDOT(4), of the two degrees of freedom. The third file is used to check some numerical fitness. It is called "check.out". This file writes the peak sticktion friction, the two forces that are subtracted to compare against the stiction friction, and the relative velocity of the upper and lower masses. The fourth file, "hydr.out", records the spring and damping coefficients of the functional

equations of motion. They are Pu, Pl, Ps, and Qo, the upper pressure, lower presser, snubber pressure, and flowrate through the main orifice respectively. The fifth output file, "tire.out", is used to record input information and tire coefficients. These values are U, UDOT, K_t, and C_t. These output files are used in conjunction with a MATLAB m-file "gdplta.m" and "resp.m" to calculate and plot many variables that are of interest.

The benefit of writing the program in a component form is that it makes the program much more flexible. Conceivably, many different gear configurations could be simulated, as long as they have the same basic setup. Also, this form of expressing the parameters and equations is conducive to optimization studies of various parameters. It is thought that studies will be performed to optimize the metering pin, perhaps the snubber orifices and possibly other parameters.

This program was originally written to simulate touchdown, or drop test conditions. However, it was expanded to include a rollout or taxi case in which a runway profile is defined, with bumps at various locations.

A.2 Program Listing

PROGRAM GEARFIN

```
C       This program was developed as partial satisfaction of a
C       Masters of Science from George Washington University, Joint
C       Institute for the Advancement of Flight Sciences. Work was
C       done by James Daniels. 5/15/96.
C
C       A computer program, "gearfin.f" has been written to numerically solve
C       the equations of motion of landing gear in time. Four states are used
C       for the solution. These states are Y(1) and Y(2), the position and
C       velocity, respectively of the wing/gear interface, and Y(3) and Y(4),
C       the position and velocity, respectively, of the wheel axle. The
C       program uses the Adams/Moulton predictor/corrector numerical method,
C       and a variable step Runga-Kutta to get past problem discontinuities.
C
C       The program's setup is simple. There are four data files associated
C       with it. The first, "pin.dat", lets the user define the shape of the
C       metering pin. The first entry is the number of slope changes of the
```

```
C       pin (n). The next n entries are the n diameters. Then the n lengths
C       associated with the diameters. Lastly in this data file is the number
C       defining the maximum stroke.
C
C       The next data file is called "piston.dat". This file is the entry
C       point of the many piston/cylinder associated parameters. The inputs of
C       this file are: Xsi, the initial length at which the gear is charged,
C       Pi, the initial charge pressure, gamma,the polytropic gas constant,
C       Du, the diameter of the upper chamber, DL, the diameter of the lower
C       chamber, D1RC and D1RE, the diameters of one snubber hole under
C       compression and extension conditions respectively, Dop, the diameter
C       of the hole in the orifice plate, and Dpis, the diameter of the piston
C       shaft, Mu,the mass of the upper system, Ml, the lower mass, DF, the
C       percent of the maximum friction that is active dynamically, and FSMAX,
C       the value of the maximum sticking friction of the piston seals.
C
C       The third file is called "ic.dat". This is a file of the initial
C       conditions. Its inputs are the initial conditions of the four states
C       in the order described above.
C
C       The last data file is a runway profile. Since various runways could be
C       used, The name of the file is left up to the user. The user needs to
C       locate the "Read in Runway" section of this program and change the
C       name. Its inputs are: TIME(I), ELEV(I) and ELEVD(I). This file
C       contains a time history of the height of the runway in meters as the
C       wheel rolls along it. Therefore, any type of velocity or acceleration
C       case may be investigated.
C
C       This program has six subroutines associated with it. The first is
C       the integration routine "ddriv2.f". The next is a routing called "F".
C       Its function is to define the derivative of the states at any time t.
C       The third routine is called "METPIN". Its job is to return the current
C       value of Dpin based on the current stroke and the input data of
C       pin.dat. The fourth is called "COEFF". It calculates the C and K
C       coefficients of the landing gear equations using the input data from
C       "piston.dat", Dpin, and the stroke rate. The fifth is "RKF4.f", a
C       fourth-order Runge-Kutta variable step integration routine.
C       When the program hits a discontinuous spot (as when friction suddenly
C       changes sign) it will automatically switch from the predictor
C       corrector (ddriv2.f) to Runge-Kutta (rkf4.f). The sixth routine is
C       really a copy of "F", and is called "FOUT". This routine is independent
C       of the integration and can be called to record the states by the user.
C
```

```
C       The current data files are for the A-6 Intruder.


        EXTERNAL F,COEFF,METPIN

C--------Variable Declaration----------------


C       ----Main---
        DOUBLE PRECISION Y,YDOT,WORK,DT
        DOUBLE PRECISION T,TOUT,EWT,EPS
        DOUBLE PRECISION G,STP,TMIN
        INTEGER NEQ,L,I,J,JJ
        INTEGER MSTATE,MINT,LENW,IWORK,LOUT
        INTEGER LENIW,N,NROOT,COUNT,NUMBR


C       ----Subroutine F and FOUT----
        DOUBLE PRECISION CT,KT,LIFT,TEMP
        DOUBLE PRECISION MU,GRAV,ML,U,UDOT,FRICT
        DOUBLE PRECISION XS,FT,FC,MA
        DOUBLE PRECISION DELTA,FR,MTIRE,FTC,FTK
        DOUBLE PRECISION F1,F2,FSTICK,DEL


C       --Define Type for Input Calculation--
        DOUBLE PRECISION PIE,ELVU,ELVL,ELEV,TIME
        DOUBLE PRECISION DISTL,DISTU,TAXISPD,DIS
        DOUBLE PRECISION AA,BB,HGT,LE,A0,DD,X,ELEVD
        INTEGER LN


C       ----Subroutine METPIN----
        DOUBLE PRECISION PAR,DPIN,D,LNG
        INTEGER NUM


C       ----Subroutine COEFF----
        DOUBLE PRECISION PAR1,C,K,CON,ALS
        DOUBLE PRECISION DOR,AO,RHO,CD,AL,FLW
        DOUBLE PRECISION AOP,APIN,MEW,VEL,RD,BETA,C1
        DOUBLE PRECISION ARC,ARE,CDE,CDC,E1,E2,E3,E4,AR
        DOUBLE PRECISION BETAE,BETAC,AS


C       ----Subroutine RKF4----
        DOUBLE PRECISION TOL,PD,HMIN,HMAX,H,WK
        INTEGER MTH,IERR
```

```
C       ----Define Array Size----
        PARAMETER (NEQ=4)
        DIMENSION Y(NEQ),YDOT(NEQ),WK(7*NEQ)
        DIMENSION WORK(300),IWORK(30)
        DIMENSION PAR1(12),C(2),K(2)
        DIMENSION PAR(20),D(10),LNG(10),FLW(4)
        DIMENSION TIME(5000),ELEV(5000),ELEVD(5000)

        COMMON /PARAM/PAR1,PAR,STP,TIME,ELEV,ELEVD,NUM,LN


C-----------Read in Metering Pin Info---------------
        OPEN(UNIT=4,STATUS='OLD',FILE='pin.dat')
        READ(4,*) NUM
        DO I=1,2*NUM
          READ(4,*) PAR(I)
        END DO
        READ(4,*) PAR(2*NUM+1)
        CLOSE(UNIT=4,STATUS='KEEP')
C  PAR(2*NUM+1)=[ D(N), L(N), XSMAX ]


C-----------Read in Piston Info for Coefficients------
        OPEN(UNIT=5,STATUS='OLD',FILE='piston.dat')
        DO I=1,12
          READ(5,*) PAR1(I)
        END DO
        CLOSE(UNIT=5,STATUS='KEEP')
C  PAR1(13)=[ XSI,PI,YI,DU,DL,D1RC,D1RE,DOP,DPIS MU ML FSMAX ]


C--------Read in Runway Profile--------------------
C       The data file is an ascii, three column file that
C       contains time in the first column and runway height
C       in meters in the second column and time derivative of
C       runway height in third column.
        OPEN(UNIT=6,STATUS='UNKNOWN',FILE='r211.dat')
        READ(6,*) LN
        DO I=1,LN
          READ(6,*) TIME(I), ELEV(I), ELEVD(I)
        END DO
        CLOSE(UNIT=6,STATUS='KEEP')


C--------Define Height of Stop Block in cylinder----
        STP=9.5/39.37
```

68

```
C------------Open Output Files----------------------
C These variables are strictly up to the user.  These
C are the current variables being recorded.  A MATLAB
C routine "gdplta.m" exists to plot these particular
C variables in a coherent way.  It may be altered by
C any user.
C      WRITE(11,790) (Y(J),J=1,4)
       OPEN(UNIT=11,STATUS='UNKNOWN',FILE='y.out')
C      WRITE(12,790) T,FRICT,YDOT(2),YDOT(4)
       OPEN(UNIT=12,STATUS='UNKNOWN',FILE='tfaa.out')
C      WRITE (13,790) FR,F1,F2,VEL
       OPEN(UNIT=13,STATUS='UNKNOWN',FILE='check.out')
C      WRITE(14,790) (FLW(J),J=1,4)
       OPEN(UNIT=14,STATUS='UNKNOWN',FILE='hydr.out')
C      WRITE(15,790) U,UDOT,KT,CT
       OPEN(UNIT=15,STATUS='UNKNOWN',FILE='tire.out')
C----------------------------------------------------

C----Landing or AM-2 Mat bump case or runway profile----
       LOUT=160000
       DT=0.00025
C----The amount of time one gets is = DT*LOUT


C------------------------------------
C      Re-initialize the initial conditions.
       DO I=1,NEQ
        Y(I)=0.0
        YDOT(I)=0.0
       END DO

C Read initial Conditions
C Two files are available, "landic.dat" or "static.dat".  The first
C startswith positional vector at zero and velocity vector at a given
C sink rate.  The second starts with the position vector in its
C equilibrium position and the velocity vector set to zero.
       OPEN(UNIT=10,STATUS='OLD',FILE='r211ic.dat')
       READ(10,*) (Y(I),I=1,4)
       CLOSE(UNIT=10,STATUS='KEEP')
       T=0.0

       N=NEQ
```

```
C       Call into current memory current values
C       of all the states and their accelerations.
        CALL F(N,T,Y,YDOT)

   100  TOUT=0.0


C--------Define DDRIV2 Parameters-----------
C       See the leading introduction of DDRIV2.f for further
C       explanation of these and other parameters.
        MSTATE=1
        NROOT=0
        EPS=1E-6
        EWT=1E-15
        MINT=3
        LENW=300
        LENIW=30
        COUNT=0


C----------------------------------------------------------
C      Loop entire process to get LOUT data points.
C----------------------------------------------------------
        DO L=1,LOUT

C      Increment time step.
        TOUT=DT*L


C         Call main integration routine.
     5  CALL DDRIV2(N,T,Y,F,TOUT,MSTATE,NROOT,EPS,EWT,MINT,WORK,
     *  LENW,IWORK,LENIW,G)


C         Provide a visual check of the progress of the integration.
        IF ((REAL(L)/2000.0) .EQ. INT(REAL(L)/2000.0)) THEN
          WRITE (*,889) L
        END IF

C----Check for errors from DDRIV2.
C Error (3) or (-3) indicates too much work to ge to next
C time step. Time to switch to Runga-Kutta.
        IF (MSTATE .EQ. 3 .OR. MSTATE .EQ. -3) THEN

C         Initiate backup integration method since DDRIV2 cannot
C         complete the next integration step.
```

```fortran
C--------RKF4 Parameters---------
       TOL=1E-5
       MTH=1
       HMIN=1E-15
       HMAX=1E-2
       H=HMAX
       CALL F(N,T,Y,YDOT)
2      CALL
RKF4(NEQ,T,TOUT,Y,TOL,F,PD,MTH,HMIN,HMAX,H,WK,IERR)
C Check for error from R-K. (-1) indicates that the tolerances
C are not set up correctly for this problem.
       IF (IERR .EQ. -1) THEN
              WRITE (*,889) IERR
              TOL=1E-5
              MTH=1
              HMIN=1E-15
              HMAX=1E-2
              H=HMAX
              IERR=0
              IF (COUNT .EQ. 500) GOTO 500
              COUNT=COUNT+1
              GOTO 2
       ENDIF
       IF (IERR .EQ. 0) THEN
              MSTATE=1
              GOTO 1
       ENDIF
       ENDIF
1      COUNT=0


C----Define some filtering process to record data.  Otherwise, data
C----files are VERY large.
       IF ((REAL(T/DT)/40.0) .EQ. INT(REAL(T/DT)/40.0)) THEN
       CALL FOUT(N,T,Y,YDOT)
       END IF

C    END THE L LOOP: i.e. Each integration step
       END DO

889    FORMAT(I6)
500    CLOSE(UNIT=11,STATUS='KEEP')
       CLOSE(UNIT=12,STATUS='KEEP')
```

```
        CLOSE(UNIT=13,STATUS='KEEP')
        CLOSE(UNIT=14,STATUS='KEEP')
        CLOSE(UNIT=15,STATUS='KEEP')

C--End of Main program.
        END


C_____

C===============================================================

C
C                   Subroutines
C
C===============================================================

C_____


        SUBROUTINE F(N,T,Y,YDOT)

C       Subroutine F defines the functional form of Ydot(i)=....
C       Anything changed in this subroutine needs also to be changed
C       in the FOUT routine and vise versa.

        EXTERNAL COEFF,METPIN

        DOUBLE PRECISION Y,YDOT,T,CT,KT,LIFT,MU,GRAV
        DOUBLE PRECISION ML,U,UDOT,FRICT,DPIN,TEMP
        DOUBLE PRECISION XS,VEL,FT,FC,MA,DELTA,FR
        DOUBLE PRECISION MTIRE,DEL,STP,F1,F2,FTC,FTK
        DOUBLE PRECISION FSTICK,PAR,PAR1,C,K,FLW
C       --Define Type for Input Calculation--
        DOUBLE PRECISION PIE,ELVU,ELVL,ELEV,TIME
        DOUBLE PRECISION DISTL,DISTU,TAXISPD,DIS
        DOUBLE PRECISION AA,BB,HGT,LE,A0,DD,X,ELEVD

        INTEGER N,NUM,LN

        PARAMETER (NEQ=4)

        DIMENSION Y(NEQ),YDOT(NEQ),TIME(5000),ELEV(5000),ELEVD(5000)
        DIMENSION C(2),K(2),PAR(20),PAR1(12),FLW(4)
```

72

```fortran
        COMMON /PARAM/PAR1,PAR,STP,TIME,ELEV,ELEVD,NUM,LN

        MU=PAR1(10)
        ML=PAR1(11)
        XS=PAR(2*NUM+1)+Y(3)-Y(1)

        CALL METPIN(Y,NUM,PAR,DPIN)

        CALL COEFF(Y,PAR1,DPIN,XS,C,K,FLW)


C       ----Calculate the input U into the tire from runway----
C       This section defines the ground excitation for a runway profile
C       input case.  It linearly interpolates between points of the data file.
        DO I=1,LN-1
        IF(T .GE. TIME(I) .AND. T .LT. TIME(I+1)) THEN
         ELVL=ELEV(I)
         ELVU=ELEV(I+1)
         ELLD=ELEVD(I)
         ELUD=ELEVD(I+1)
         U=(ELVU-ELVL)*(T-TIME(I))/(TIME(I+1)-TIME(I))+ELVL
C       UDOT is dU/dT, leaving only:
         UDOT=(ELUD-ELLD)*(T-TIME(I))/(TIME(I+1)-TIME(I))+ELLD
        ENDIF
        END DO
C       --------


C       ----Define Input of AM2 Repair Mat----
C       TAXISPD=20.0*.5144444
C       AA= 15.0*(.3048)
C       BB= AA+4.0*(.3048)
C       CC= BB+70.0*(.3048)
C       DD= CC+4.0*(.3048)
C       HGT= 1.5/39.37
C       -- X=TAXISPD*T --
C       X=TAXISPD*T
C       IF (X .LT. AA .OR. X .GT. DD) THEN
C        U=0.0
C        UDOT=0.0
C       ELSEIF (X .GE. AA .AND. X .LE. BB) THEN
C         U=HGT*(X-AA)/(BB-AA)
C         UDOT=HGT*TAXISPD/(BB-AA)
```

```
C       ELSEIF (X .GT. BB .AND. X .LT. CC) THEN
C         U=HGT
C         UDOT=0.0
C       ELSEIF (X .GE. CC .AND. X .LE. DD) THEN
C         U=-HGT*(X-CC)/(DD-CC)+HGT
C         UDOT=-HGT*TAXISPD/(DD-CC)
C       END IF


C----Toggle for landing/runway input case.  We want no input
C----for landing case, but DO want bumps etc. for other cases.
C       U=0.0
C       UDOT=0.0
C----------Tire Model as updated from Experimental Data----
        KT=(-252.0*(39.37*(Y(3)+U))**2.0+1397.0*(Y(3)+U)*39.37+4267.0)
   *     *(39.37*4.4482)
C       ----Tire Damping model, as observed from test data---
        MTIRE=ML
        CT=5000.0
C       ---Define the Tire Force (FT)----
        FTK=1.0*KT*(Y(3)+U) + 130.0*4.4482
        FTC=CT*(1.0)*(Y(4)+UDOT)
        IF ((Y(3)+U) .LT. 0.0) THEN
          FTK=0.0
          FTC=0.0
        END IF
        FT=FTC+FTK
C--------------------------------


        GRAV=9.81


C       ----Lift Model----
C       LIFT=9.81*MU
        LIFT=0.0


        VEL=Y(2)-Y(4)


C---------Defining relative forces before friction----
        F1=MU*GRAV-LIFT+C(1)*VEL**2.0+K(1)*(1.0/XS)**(PAR1(3))
        F2=ML*GRAV+C(2)*VEL**2.0+K(2)*(1.0/XS)**(PAR1(3))-FT


C---------------------------------------------------


C------Add the KARNOPP friction Model to the accelerations.
```

74

```
C   --DEL is how close relative velocity needs to be to zero to stick.
      DEL=.0009
      DELTA=ABS(F1-F2)
C Calculate the bearing friction of the piston in the
C cylinder.  FC is frictional coefficient, MA is moment arm.
C     FC = .05
C     MA = 10.5/39.37
C     TEMP=(FC*FT*MA/(ABS(Y(1)-Y(3)+STP))+PAR1(12))*.75


C----Future Friction Model.  Needs to be ironed out.---------
C     TEMP=(4000.0*EXP(-XS/(1.0*.0254))+1000.0*
C   *  EXP(-ABS(VEL/0.05)))*4.44822
C   * *EXP(-ABS(VEL/0.05))
C     FRICT=-TANH(VEL/.008)*TEMP
C-----Also part of future friction model.-------------
C     FR=1.0*(4000.0*EXP(-XS/(6.2*.0254))+1000.0*.4)*4.4482+PAR1(12)


C------Friction toggle for finding initial conditions----
      TEMP=400.0
      FRICT=(-0.0-TANH(VEL/.008))*TEMP*4.4482
      FR=2689.0*4.44822
C     FR=0.0
C     FRICT=0.0
C-------------


      IF (DELTA .LT. FR .AND. ABS(VEL) .LT. DEL) THEN
C Case 1, Piston Sticks in Cylinder.
      F1=MU*GRAV-LIFT+K(1)*(1.0/XS)**(PAR1(3))
      F2=ML*GRAV+K(2)*(1.0/XS)**(PAR1(3))-FT
      FSTICK=(ML*F1 - MU*F2)/(MU+ML)
      YDOT(1)=Y(2)
      YDOT(2)=F1/MU - FSTICK/MU
      YDOT(3)=Y(4)
      YDOT(4)=F2/ML + FSTICK/ML
      ELSE
C Case 2, Relative Motion between Piston
C   and Cylinder, with friction present.
      YDOT(1)=Y(2)
      YDOT(2)=F1/MU + FRICT/MU
      YDOT(3)=Y(4)
      YDOT(4)=F2/ML - FRICT/ML
      END IF
```

C Case 3, The gear and tire leave the ground.
```
        IF ((Y(3)+U) .LT. 0.0 .AND. XS .GT. PAR(2*NUM+1)) THEN
        YDOT(1)=Y(2)
        YDOT(2)=F1/MU - FSTICK/MU
        YDOT(3)=Y(2)
        YDOT(4)=F2/ML + FSTICK/ML
        END IF


        RETURN
        STOP
        END


C---------------SUBROUTINE METPIN--------------------


        SUBROUTINE METPIN(Y,NUM,PAR,DPIN)


C       This subroutine linearly interpolates in the D(n), diameter
C       array, and L(n), the length array to determine the diameter
C       of the metering pin, DPIN, at any stroke, XS.
        DOUBLE PRECISION Y,PAR,DPIN,D,LNG,XS
        INTEGER NUM,I
        PARAMETER (NEQ=4)
        DIMENSION Y(NEQ),PAR(20),D(10),LNG(10)


C  PAR(2*N+1) = [ D(N),LNG(N),XSMAX ]


        DO I=1,NUM
        D(I)=PAR(I)
        LNG(I)=PAR(NUM+I)
        END DO


        DPIN=D(NUM)
        XS=PAR(2*NUM+1)-Y(1)+Y(3)
        DO I=1,NUM-1
          IF (XS .LT. LNG(I) .AND. XS .GT. LNG(I+1)) THEN
          DPIN = D(I) + (D(I+1)-D(I))*(LNG(I)-XS)/(LNG(I)-LNG(I+1))
          ENDIF
        END DO
        RETURN


        END


C---------------SUBROUTINE COEFF--------------------
```

```
       SUBROUTINE COEFF(Y,PAR1,DPIN,XS,C,K,FLW)

C      For a thourough understanding of this subroutine, look
C      in the thesis Chapter 2, Equations (1) and (2) as they
C      are presented at the end of the chapter.  this subroutine
C      calculates the coefficients as they are defined in the paper.
C      These coefficients are only functions of geometry and flow
C      direction.
       DOUBLE PRECISION Y,PAR1,C,K,CON,ALS
       DOUBLE PRECISION DOR,AO,RHO,CD,AL,FLW
       DOUBLE PRECISION DPIN,AOP,APIN,XS
       DOUBLE PRECISION MEW,VEL,RD,BETA,C1
       DOUBLE PRECISION ARC,ARE,CDE,CDC,E1,E2,E3,E4,AR
       DOUBLE PRECISION BETAE,BETAC,AS
       INTEGER N

       PARAMETER (NEQ=4)

       DIMENSION Y(NEQ),PAR1(12),C(2),K(2),FLW(4)

C  PAR1(9)=[ XSI,PI,YI,DU,DL,D1RC,D1RE,DOP,DPIS,MU,ML FSMAX ]

C----Calculate Various areas to be used----
       CON=.7853981
       ARC=CON*PAR1(6)**2.0
       ARE=CON*PAR1(7)**2.0
       AL=CON*PAR1(5)**2.0
       AS=AL-CON*PAR1(9)**2.0
       AOP=CON*PAR1(8)**2.0
       APIN = CON*DPIN**2.0
       AO=AOP-APIN

C Define a constant (C1) to account for the annular
C nature of DOR.  It is effectively SMALLER to
C the fluid.  I'm not using this at the moment, but
C should the tests bare out the fact that something
C is not working quite right, this may be a parameter
C to tweak.
       C1=1.0
       DOR=C1*SQRT(AO/.7853981)
C RHO is fluid density.  MEW is fluid viscosity.
       RHO=912.0
```

```
        MEW=35.0*.001
        VEL=Y(2)-Y(4)
C RD is reynolds number.  An RD model of the discharge
C coefficient may want to be used in the future.
        RD=RHO*ABS(VEL)*PAR1(5)/MEW
C The various BETA's are ratios of (fluid coming from D1)/
C (fluid going through D2) ==> (D1/D2)=Beta
        BETA=DOR/PAR1(5)
        BETAC=PAR1(6)/PAR1(5)
        BETAE=PAR1(7)/(SQRT(AS/(12.0*.7853981)))
C Therefore, the discharge coefficients are now only functions
C of geometry, not Reynold's number.
        CD=1.0*BETA**2.0 - .4813*BETA + .8448
        CDC=.95*(.8*BETAC**2.0 - .4813*BETAC + .8448)
        CDE=1.0*(.8*BETAE**2.0 - .4813*BETAE + .8448)
C COMPRESSION
        IF (VEL .GT. 0.0 .OR. VEL .EQ. 0.0) THEN
C       AR is the sum of the twelve areas that comprise the snubber
C       orifices.
        AR=12.0*ARC
        E1=AO*.95*CD*SQRT((2.0)/(RHO*(1.0-BETA**4.0)))
        E2=AR*CDC*SQRT(2.0/(RHO*(1.0-BETAC**4.0)))
        ALS=AL-AS
        C(1)=((ALS/E1)**2.0-(AS/E2)**2.0)*AS-(ALS/E1)**2.0*(AL-AO)
        C(2)=((AS/E2)**2.0-(ALS/E1)**2.0)*(AS-AR)+(ALS/E1)**2.0*(AL-AR)
        K(1)=(AS-AL)*PAR1(2)*PAR1(1)**PAR1(3)
        K(2)=ALS*PAR1(2)*PAR1(1)**PAR1(3)
C--As a bonus, the pressures and flow rates are also being calculated here.
        PU=PAR1(2)*(PAR1(1)/XS)**PAR1(3)
        PL=PU+(((AL-AS)/E1)*VEL)**2.0
        PS=PL-(AS*VEL/E2)**2.0
        QO=-E1*SQRT(PL-PU)


C EXTENSION
        ELSE
C       AR is the sum of the twelve areas that comprise the snubber
C       orifices.
        AR=12.0*ARE
        E3=AO*1.1*CD*SQRT(2.0/(RHO*(1.0-BETA**4.0)))
        E4=AR*CDE*SQRT(2.0/(RHO*(1.0-BETAE**4.0)))
        ALS=AL-AS
        C(1)=(ALS/E3)**2.0*(AL-AO)+((AS/E4)**2.0-(ALS/E3)**2.0)*AS
        C(2)=((ALS/E3)**2.0-(AS/E4)**2.0)*(AS-AR)-(ALS/E3)**2.0*(AL-AR)
```

78

```fortran
      K(1)=(AS-AL)*PAR1(2)*PAR1(1)**PAR1(3)
      K(2)=ALS*PAR1(2)*PAR1(1)**PAR1(3)
C--As a bonus, the pressures and flow rates are also being calculated here.
      PU=PAR1(2)*(PAR1(1)/XS)**PAR1(3)
      PL=PU-(((AL-AS)/E3)*VEL)**2.0
      PS=PL+(AS*VEL/E4)**2.0
      QO=E3*SQRT(PU-PL)

      END IF

C--Put the pressures and flow rates into an array to pass
C--outward for recording.
      FLW(1)=PU
      FLW(2)=PL
      FLW(3)=PS
      FLW(4)=QO

      RETURN

      END
C------------------------------------------------------------

      SUBROUTINE FOUT(N,T,Y,YDOT)

C  Subroutine FOUT is the same as F and comments match until the output.
C  Anything changed in this subroutine needs also to be changed
C  in the F routine and vise versa.

      EXTERNAL COEFF,METPIN

      DOUBLE PRECISION Y,YDOT,T,CT,KT,LIFT,MU,GRAV
      DOUBLE PRECISION ML,U,UDOT,FRICT,DPIN,TEMP
      DOUBLE PRECISION XS,VEL,FT,FC,MA,DELTA,FR
      DOUBLE PRECISION MTIRE,DEL,STP,F1,F2,FTC,FTK
      DOUBLE PRECISION FSTICK,PAR,PAR1,C,K,FLW
C        --Define Type for Input Calculation--
      DOUBLE PRECISION PIE,ELVU,ELVL,ELEV,TIME
      DOUBLE PRECISION DISTL,DISTU,TAXISPD,DIS
      DOUBLE PRECISION AA,BB,HGT,LE,A0,DD,X,ELEVD

      INTEGER N,NUM,LN

      PARAMETER (NEQ=4)
```

```fortran
      DIMENSION Y(NEQ),YDOT(NEQ),TIME(5000),ELEV(5000),ELEVD(5000)
      DIMENSION C(2),K(2),PAR(20),PAR1(12),FLW(4)

      COMMON /PARAM/PAR1,PAR,STP,TIME,ELEV,ELEVD,NUM,LN

      MU=PAR1(10)
      ML=PAR1(11)
      XS=PAR(2*NUM+1)+Y(3)-Y(1)

      CALL METPIN(Y,NUM,PAR,DPIN)

      CALL COEFF(Y,PAR1,DPIN,XS,C,K,FLW)


C     ----Calculate the input U into the tire from runway----
C     This section defines the ground excitation for a runway profile
C     input case.  It linearly interpolates between points of the data file.
      DO I=1,LN-1
      IF(T .GE. TIME(I) .AND. T .LT. TIME(I+1)) THEN
       ELVL=ELEV(I)
       ELVU=ELEV(I+1)
       ELLD=ELEVD(I)
       ELUD=ELEVD(I+1)
       U=(ELVU-ELVL)*(T-TIME(I))/(TIME(I+1)-TIME(I))+ELVL
       UDOT=(ELUD-ELLD)*(T-TIME(I))/(TIME(I+1)-TIME(I))+ELLD
      ENDIF
      END DO
C     --------
C     ----Define Input of AM2 Repair Mat----
C     TAXISPD=20.0*.5144444
C     AA= 15.0*(.3048)
C     BB= AA+4.0*(.3048)
C     CC= BB+70.0*(.3048)
C     DD= CC+4.0*(.3048)
C     HGT= 1.5/39.37
C     -- X=TAXISPD*T --
C     X=TAXISPD*T
C     IF (X .LT. AA .OR. X .GT. DD) THEN
C     U=0.0
C     UDOT=0.0
C     ELSEIF (X .GE. AA .AND. X .LE. BB) THEN
C       U=HGT*(X-AA)/(BB-AA)
```

```
C        UDOT=HGT*TAXISPD/(BB-AA)
C        ELSEIF (X .GT. BB .AND. X .LT. CC) THEN
C          U=HGT
C          UDOT=0.0
C        ELSEIF (X .GE. CC .AND. X .LE. DD) THEN
C          U=-HGT*(X-CC)/(DD-CC)+HGT
C          UDOT=-HGT*TAXISPD/(DD-CC)
C        END IF
C
C----Toggle for landing/runway input case.  We want no input
C----for landing case, but DO want bumps etc. for other cases.
C        U=0.0
C        UDOT=0.0
C---------Tire Model as updated from Experimental Data----
         KT=(-252.0*(39.37*(Y(3)+U))**2.0+1397.0*(Y(3)+U)*39.37+4267.0)
     *      *(39.37*4.4482)
C        ----Tire Damping model, as observed from test data---
         MTIRE=ML
         CT=5000.0
C        ---Define the Tire Force (FT)----
         FTK=1.0*KT*(Y(3)+U) + 130.0*4.4482
         FTC=CT*(1.0)*(Y(4)+UDOT)
         IF ((Y(3)+U) .LT. 0.0) THEN
           FTK=0.0
           FTC=0.0
         END IF
         FT=FTC+FTK
C--------------------------------

         GRAV=9.81

C        ----Lift Model----
C        LIFT=9.81*MU
         LIFT=0.0

         VEL=Y(2)-Y(4)

C---------Defining relative forces before friction----
         F1=MU*GRAV-LIFT+C(1)*VEL**2.0+K(1)*(1.0/XS)**(PAR1(3))
         F2=ML*GRAV+C(2)*VEL**2.0+K(2)*(1.0/XS)**(PAR1(3))-FT

C------------------------------------------------
```

```
C------Add the KARNOPP friction Model to the accelerations.
C   --DEL is how close relative velocity needs to be to zero to stick.
        DEL=.0009
        DELTA=ABS(F1-F2)
C Calculate the bearing friction of the piston in the
C cylinder.  FC is frictional coefficient, MA is moment arm.
C      FC = .05
C      MA = 10.5/39.37
C      TEMP=(FC*FT*MA/(ABS(Y(1)-Y(3)+STP))+PAR1(12))*.75


C----Future Friction Model.  Needs to be ironed out.---------
C      TEMP=(4000.0*EXP(-XS/(1.0*.0254))+1000.0*
C    *  EXP(-ABS(VEL/0.05)))*4.44822
C    **EXP(-ABS(VEL/0.05))
C      FRICT=-TANH(VEL/.008)*TEMP
C-----Also part of future friction model.--------------
C      FR=1.0*(4000.0*EXP(-XS/(6.2*.0254))+1000.0*.4)*4.4482+PAR1(12)


C------Friction toggle for finding initial conditions----
        TEMP=400.0
        FRICT=(-0.0-TANH(VEL/.008))*TEMP*4.4482
        FR=2740.0*4.44822
C      FR=0.0
C      FRICT=0.0
C-------------

        IF (DELTA .LT. FR .AND. ABS(VEL) .LT. DEL) THEN
C Case 1, Piston Sticks in Cylinder.
        F1=MU*GRAV-LIFT+K(1)*(1.0/XS)**(PAR1(3))
        F2=ML*GRAV+K(2)*(1.0/XS)**(PAR1(3))-FT
        FSTICK=(ML*F1 - MU*F2)/(MU+ML)
        YDOT(1)=Y(2)
        YDOT(2)=F1/MU - FSTICK/MU
        YDOT(3)=Y(4)
        YDOT(4)=F2/ML + FSTICK/ML
        ELSE
C Case 2, Relative Motion between Piston
C  and Cylinder, with friction present.
        YDOT(1)=Y(2)
        YDOT(2)=F1/MU + FRICT/MU
        YDOT(3)=Y(4)
        YDOT(4)=F2/ML - FRICT/ML
        END IF
```

C Case 3, The gear and tire leave the ground.

```
      IF ((Y(3)+U) .LT. 0.0 .AND. XS .GT. PAR(2*NUM+1)) THEN
      YDOT(1)=Y(2)
      YDOT(2)=F1/MU - FSTICK/MU
      YDOT(3)=Y(2)
      YDOT(4)=F2/ML + FSTICK/ML
      END IF

      WRITE(11,790) (Y(J),J=1,4)
      WRITE(12,790) T,FRICT,YDOT(2),YDOT(4)
      WRITE(13,790) FR,F1,F2,VEL
      WRITE(14,790) (FLW(J),J=1,4)
      WRITE(15,790) U,UDOT,KT,CT

 790  FORMAT(E14.4,1X,E14.4,1X,E14.4,1X,E14.4)

      RETURN
 600  CLOSE(UNIT=11,STATUS='KEEP')
      CLOSE(UNIT=12,STATUS='KEEP')
      CLOSE(UNIT=13,STATUS='KEEP')
      CLOSE(UNIT=14,STATUS='KEEP')
      CLOSE(UNIT=15,STATUS='KEEP')
      STOP
      END
```

A.3 Sample Input Files

Pin.dat:

```
6
.0133604
.021844
.022352
.022352
.026162
.026162
0.4461
0.353314
0.277114
0.112014
0.035814
-0.0254
.383286
```

This file describes a metering pin of an A-6 intruder. There are six slope changes on the pin, and the diameters are listed from top of pin (not piston head end) to the piston end. Following these six diameters are the six stroke lengths associated with each diameter.

Piston.dat: This file contains the twelve parameters as described in the program summary section.

.0889
2571744.47
1.1
.1524
.1524
3.98781e-3
1.587503e-3
.0285877
.1397
4139.8841
145.1
511.5455

Ic.dat: This file contains the initial conditions of the state vector.

0.3164
0.0
0.04045
0.0

Test.dat: This file contains a sample runway. Only a few of the 1640 entries are shown.

1640
  0.0000000e+00 -2.1399094e-02   2.7217370e-01
  2.5000000e-02 -1.8608421e-02   2.7906726e-01
  5.0000000e-02 -1.5748813e-02   2.8596082e-01
  7.5000000e-02 -1.2598451e-02   3.1503620e-01
  1.0000000e-01 -9.1933014e-03   3.4051494e-01
  1.2500000e-01 -5.8510932e-03   3.3422082e-01
  1.5000000e-01 -2.4309578e-03   3.4201354e-01
etc.

A.4 Output Manipulation File

```
% This file loads, manipulates and plots the
% output data from the simulation.  This is
% a MATLAB .m file and is consistant with
%  MATLAB release 4.2c.


load y.out
load tfaa.out
load check.out
load hydr.out
load tire.out


t=tfaa(:,1);
fr=check(:,1)*.2248089;
fl=check(:,2);
f2=check(:,3);
delta=.5*abs(fl-f2)*.2248089;
vel=check(:,4);
xsmax=.383286;
MU=4139.8841;
ML=145.1;
fwg=MU*(-tfaa(:,3)+9.81)*.2248;
ges=-tfaa(:,3);
s=date;
xwg=y(:,1);
xa=y(:,3);
vwg=y(:,2);
va=y(:,4);
xs=(xsmax-(xwg-xa))*39.37;
kt=tire(:,2);
ct=tire(:,3);
k=hydr(:,1);
c1=hydr(:,3);
c2=hydr(:,4);
frict=tfaa(:,2);
u=tire(:,1);
relvel=(vwg-va)*3.28084;


pu=hydr(:,1)*1.450377e-4;
pl=hydr(:,2)*1.450377e-4;
ps=hydr(:,3)*1.450377e-4;
qo=hydr(:,4)*264.172052;
```

```
% Each of the following plots are
% optional.  They are only a sample
% of the types of things that can be
% considered with the information
% available.

subplot(2,1,1),plot(t,ges,'y')
xlabel('Time (sec)')
ylabel('Awg (g)')
title('Wing/Gear Force vs. Time')
gtext(s)
grid

subplot(2,1,2),plot(t,xs,t,u*39.37,'--')
xlabel('Time (sec)')
ylabel('Stroke Remaining (in)')
title('Stroke Remaining vs. Time')
grid
legend('-','Stroke','--','Input Displacement ')


%figure
%subplot(2,1,1), plot(t,relvel,'y')
%xlabel('Time (sec)')
%ylabel('Relative Vel. (ft/s)')
%title('Relative Velocity vs. Time')
%gtext(s)
%grid
%subplot(2,1,2), plot(t,delta,'-',t,fr,'--')
%xlabel('Time (sec)')
%ylabel('Force (lbf)')
%title('Relative Force and Fr vs. Time')
%grid
%legend('-','Fwg-Fa','--','Peak Friction Force')

%figure
%plot(t,pu)
%gtext(s)
%xlabel('Time (sec)')
%ylabel('Pneumatic Press. (psi)')
%title('Nitrogen Pressure vs. Time')
%grid
```

86

```
%figure
%plot(t,pl)
%gtext(s)
%xlabel('Time (sec)')
%ylabel('Hydraulic Press. (psi)')
%title('Fluid Pressure above Piston vs. Time')
%grid

%figure
%plot(t,ps)
%gtext(s)
%xlabel('Time (sec)')
%ylabel('Hydraulic Press. (psi)')
%title('Fluid Pressure in Snubber vs. Time')
%grid

%figure
%plot(t,qo)
%gtext(s)
%xlabel('Time (sec)')
%ylabel('Flow Rate (gal/s)')
%title('Flow through Main Orifice vs. Time')
%grid
```

REPORT DOCUMENTATION PAGE

Form Approved
OMB No. 0704-0188

1. AGENCY USE ONLY (Leave blank)	2. REPORT DATE	3. REPORT TYPE AND DATES COVERED
	June 1996	Contractor Report

4. TITLE AND SUBTITLE	5. FUNDING NUMBERS
A Method for Landing Gear Modeling and Simulation with Experimental Validation	NCC1-208 WU 505-63-50-19

6. AUTHOR(S)

James N. Daniels

7. PERFORMING ORGANIZATION NAME(S) AND ADDRESS(ES)	8. PERFORMING ORGANIZATION REPORT NUMBER
George Washington University Joint Institute for the Advancement of Flight Sciences MS 269, NASA LaRC Hampton, VA 23681-0001	

9. SPONSORING / MONITORING AGENCY NAME(S) AND ADDRESS(ES)	10. SPONSORING / MONITORING AGENCY REPORT NUMBER
National Aeronautics and Space Administration Langley Research Center Hampton, VA 23681-0001	NASA CR-201601

11. SUPPLEMENTARY NOTES

Langley Technical Monitor: Lucas G. Horta (1-757-864-4352)

The information in this report was offered as a thesis in partial fulfillment of the requirements for the Degree of Master of Science, The School of Engineering and Applied Science, The George Washington University, June 1996.

12a. DISTRIBUTION / AVAILABILITY STATEMENT	12b. DISTRIBUTION CODE
Unclassified - Unlimited Subject Category 05 Availability: NASA CASI, (301) 621-0390	

13. ABSTRACT (Maximum 200 words)

This document presents an approach for modeling and simulating landing gear systems. Specifically, a nonlinear model of an A-6 Intruder Main Gear is developed, simulated, and validated against static and dynamic test data. This model includes nonlinear effects such as a polytropic gas model, velocity squared damping, a geometry governed model for the discharge coefficients, stick-slip friction effects and a nonlinear tire spring and damping model. An Adams-Moulton predictor corrector was used to integrate the equations of motion until a discontinuity caused by a stick-slip friction model was reached, at which point, a Runga-Kutta routine integrated past the discontinuity and returned the problem solution back to the predictor corrector. Run times of this software are around 2 mins. per 1 sec. of simulation under dynamic circumstances. To validate the model, engineers at the Aircraft Landing Dynamics facilities at NASA Langley Research Center installed one A-6 main gear on a drop carriage and used a hydraulic shaker table to provide simulated runway inputs to the gear. Model parameters were tuned to produce excellent agreement for many cases.

14. SUBJECT TERMS	15. NUMBER OF PAGES
Landing gear, Simulation, Vibration	97
	16. PRICE CODE
	A05

17. SECURITY CLASSIFICATION OF REPORT	18. SECURITY CLASSIFICATION OF THIS PAGE	19. SECURITY CLASSIFICATION OF ABSTRACT	20. LIMITATION OF ABSTRACT
Unclassified	Unlassified	Unclassified	

NSN 7540-01-280-5500

Standard Form 298 (Rev. 2-89)
Prescribed by ANSI Std. Z39-18
298-102